INL/EXT-19-53931

# Flexible Geothermal Power Generation utilizing Geologic Thermal Energy Storage

Daniel Wendt[1], Hai Huang[1], Guangdong Zhu[2], Prashant Sharan[2], Kevin Kitz[3], Sidney Green[4], John McLennan[5], Josh McTigue[2], and Ghanashyam Neupane[1]

[1] Idaho National Laboratory
[2] National Renewable Energy Laboratory
[3] Kitzworks, LLC
[4] Enhanced Production, Inc.
[5] University of Utah

May 2019


The INL is a U.S. Department of Energy National Laboratory
operated by Battelle Energy Alliance

INL/EXT-19-53931

# Flexible Geothermal Power Generation utilizing Geologic Thermal Energy Storage

**Daniel Wendt[1], Hai Huang[1], Guangdong Zhu[2], Prashant Sharan[2], Kevin Kitz[3], Sidney Green[4], John McLennan[5], Josh McTigue[2], and Ghanashyam Neupane[1]**

**[1] Idaho National Laboratory**
**[2] National Renewable Energy Laboratory**
**[3] Kitzworks, LLC**
**[4] Enhanced Production, Inc.**
**[5] University of Utah**

**May 2019**

**Idaho National Laboratory**
**Idaho Falls, Idaho 83415**

**http://www.inl.gov**

**Prepared for the**
**U.S. Department of Energy**
**Geothermal Technologies Office**
**Under DOE Idaho Operations Office**
**Contract DE-AC07-05ID14517**

# ABSTRACT

This report concludes that there is a cost-effective strategy for seasonal storage of heat that will provide firm, but dispatchable, electrical generating capacity in times when other renewable energy is not available to meet demand. Deployment of the technology appears to require no new technology, but instead combines solar, geothermal, and conventional oil and gas drilling technologies in a novel way. The study basis is the use of sedimentary geologic formations as a medium for thermal energy storage (TES), specifically for heat collected in concentrating solar collectors.

The study identifies methodologies that could be used to transport this heat into and out of the subsurface in order to produce dispatchable electrical power, and reports on initial optimization results. The GeoTES system (heat input, storage, heat recovery, and heat to electric conversion) described in this analysis has the potential to provide a unique pathway for increasing the grid penetration of renewable energy in large blocks of power and across many states and regions. Further, the system can be used both to meet the nation's flexible energy needs while also improving grid stability and reliability.

The present study evaluated the use of a large number of dedicated wells to store and recover the heat, essentially creating a synthetic geothermal reservoir. The use of sedimentary geology allow the wells to be drilled at low cost. Dedicated hot and cold wells are used, arranged in a five-spot well pattern with each hot or cold well surrounded at an appropriate distance by the opposite type of well. In large numbers this becomes alternating rows of hot and cold wells. Each hot and cold well is operated using a push-pull strategy. This configuration provides the ability to immediately recover stored hot fluid from a GeoTES reservoir, or to store the heat over many months for recovery at low loss when needed. This is a practical approach for managing the system's fluid inventory, and reducing parasitic load. The production and injection power requirements are reduced because the rows of wells operating in "push" mode provide help to the wells operating in "pull" mode, and vice-versa. Initial charging of a GeoTES system increases the heat recovery temperature. Increasing the duration of the charging period decreases the magnitude of the temperature fluctuations that occur following prolonged system operation.

Because of direct contact of the heated water with the reservoir formation, the production of both hot water and steam from the TES, and the temperature ranges of the recovered fluid (190 – 230°C or 375 – 445°F), conventional geothermal power cycles were used to convert the stored heat to electricity. A power cycle configuration for the GeoTES system was selected following a screening study of a number of flash, and flash/binary hybrid options. This analysis concluded that, of the configurations evaluated, a dual-stage flash steam

cycle provides the lowest capital costs per unit net power generation with an acceptable hot brine inlet fluid flow rate. The evaluation included the power plant cost estimate, the cost and number of wells and the associated parasitic loads.

Annual power generation performance was simulated to evaluate capacity factor and LCOE. The LCOE calculated for the inherently high capacity GeoTES system was $0.13/kWhe. This value was calculated for the case where the solar thermal collector was sized in such a way that the solar collectors permitted an annual power plant capacity factor of up to 97%. The power cycle was able to provide power to the grid every night of the year, and flexible base-load power during the winter, if needed. This LCOE value compares favorably with reported values for solar photovoltaic plus battery energy storage (PV+BES) systems in the open literature, i.e. $0.148/kWhe for a PV+BES system with 4 hours of electrochemical battery energy storage capacity (McTigue et al, 2018a; McTigue et al, 2018b). Addition of battery energy storage with more hours of storage would further increase PV+BES system LCOE and increase the separation between GeoTES and PV+BES. A GeoTES system would therefore provide superior economics for high capacity and long duration solar energy storage.

# CONTENTS



# FIGURES

## TABLES

# Flexible Geothermal Power Generation utilizing Geologic Thermal Energy Storage

## 1. Introduction

Variable renewable energy sources such as wind and solar photovoltaic (PV) have become increasingly prevalent sources of electrical power generation due to consistent decreases in the costs of these technologies. Although the costs of wind and solar PV can compete with conventional sources of power generation such as natural gas and coal on a $/MWh basis, the variable nature of wind and solar PV add costs to the electrical grid especially as market penetration becomes large. These technologies also currently require fossil fuel backing due to the fact that they cannot always provide the power generation required by the electrical markets that they serve. Batteries remain too expensive to provide full annual or seasonal backup to these variable sources. The objective of the research is not to displace the low-cost PV and wind generators, but instead to displace the fossil fuel and electrochemical backing of these technologies.

Electrochemical batteries are a commercially available energy storage technology that could be used to store electricity produced by variable sources and then produce electricity when demand is high. However, electrochemical batteries have high capital costs, and ongoing replacement capital and maintenance costs. Because of this and other factors, they are not considered practical for providing high capacity energy storage that could be used to store energy over longer time durations such as days, weeks, or months. The objective of the research is to provide long-duration storage where other options are not viable.

The subsurface can be heated and used as a medium for thermal energy storage (TES). The present study evaluates the use of the subsurface as a medium for the storage of heat collected in concentrated solar collectors and identifies technologies that could be used to transport this heat into and out of the subsurface as well as to reliably produce on-demand electrical power using the recovered heat. Use of subsurface energy storage would provide a unique pathway for increasing the renewable energy generation that can be used to meet the nation's around-the-clock energy needs while maintaining the levels of grid stability and reliability that are absolutely essential in today's computer-driven economy.

Sedimentary systems have characteristics that appear well suited for hosting a geologic thermal energy storage (GeoTES) system. Figure 1 illustrates the large areas of the continental US where sedimentary systems exist (Porro et al., 2012). The prevalence of sedimentary systems suggests that development of GeoTES technology could provide energy storage capacity on a magnitude sufficient to transform US energy markets.

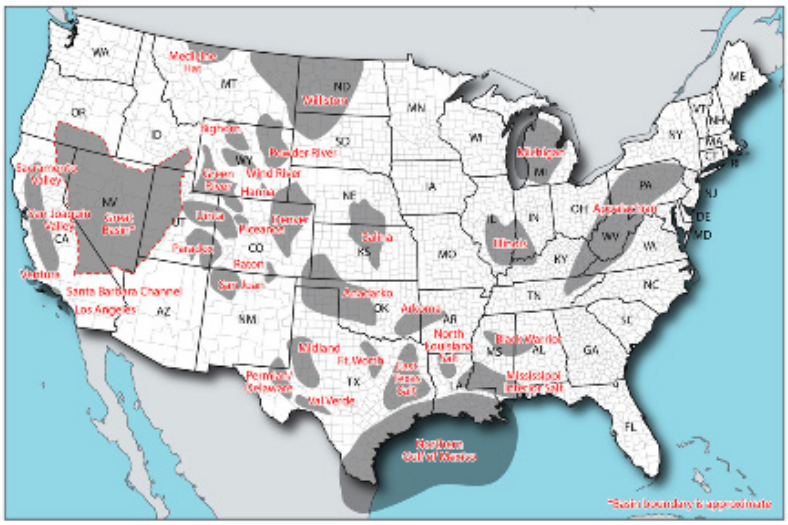


Figure 1. The shaded areas indicate the location of sedimentary formations in the United States (Porro et al., 2012).

# 2. GeoTES System Description

## 2.1 Heat Source

Any low-cost heat source could be used for a GeoTES system such as the one described here. This includes waste heat from fossil fuel combustion or unneeded nuclear power plant heat. For this study, the use of solar thermal energy is investigated.

Parabolic trough solar collectors are specified as the technology used to collect solar energy for subsequent storage and power generation using a thermoelectric power cycle. However, this choice of solar energy collector is not critical, and other forms of solar thermal collectors are also viable. Parabolic trough solar collectors focus solar radiation onto a receiver tube filled with a circulating heat transfer fluid (HTF). Heat transfer fluids such as DowTherm™ and Therminol® are commonly used for concentrated solar applications. As the HTF flows through the solar collector receivers, it is heated to a high temperature. In conventional concentrated solar power (CSP) applications the high-temperature HTF transfers heat to the power cycle via a series of heat exchangers (i.e., an economizer, vaporizer, and superheater in a conventional steam Rankine cycle based CSP plant). In the GeoTES system, heat exchangers will be used to transfer heat from the hot HTF to pressurized brine from the sedimentary formation. The hot brine will then be injected into the subsurface where it will be stored. The hot brine will be recovered and used to provide heat input to the GeoTES system's thermoelectric power plant during periods of high electricity demand.

Solar heat can be collected at temperatures of 400°C and greater. However, for the GeoTES application 250°C was selected as the baseline heat storage temperature. Although thermoelectric power plant efficiency would be greater for a higher heat recovery temperature, 250°C was selected as an intermediate value. This temperature is expected to provide acceptable power plant efficiency while minimizing potential operational issues and also avoiding the requirement for deep wells for storing liquid phase brine in formations with high hydrostatic pressure. Future studies could look both at higher storage temperatures and/or power cycles to benefit from the 400°C potential of modern solar collectors.

## 2.2 Reservoir Configuration

The reservoir configuration considered consists of sedimentary basins confined by cap rock and base rock layers. The cap rock and base rock permeabilities are significantly lower than the thermal reservoir's

permeability. Consequently, movement of fluid is confined to the reservoir zone. However, the cap and base rock can absorb/transmit a small percentage of the overall injected energy through conduction.

In the analyses carried out, the vertical permeability is assumed to be one tenth that of the horizontal permeability. This permeability anisotropy approximates the effect of different permeabilities in characteristically layered sedimentary environments. Injected fluid would preferentially flow horizontally with less tendency to flow in the vertical direction across lower permeability interbeds.

To use liquid phase water to store high-temperature solar heat in the subsurface, the formation must be at a depth where the hydrostatic pressure is sufficient to maintain the water in the liquid phase. To maintain water heated to 250°C (482°F) in the liquid phase, the fluid must be maintained at a pressure of 4 MPa (580 psi) or greater. As the hot fluid travels down the wellbore, the hydraulic head of the fluid above will cause the pressure to increase. Therefore, 4 MPa is the minimum pressure that must be maintained in the brine exiting the solar HTF / brine heat exchanger.

A reservoir depth of 1,220 meters (4,000 feet) was selected for use in subsurface simulations, as a simplifying assumption. This reservoir depth easily provides the hydrostatic pressure required to maintain liquid phase brine at a temperature of 250°C. This depth is also deep enough to avoid aquifers and to mitigate the risk of hydraulic fracturing during injection. For the injection rate selected, the initial bottomhole injection pressure for the 1,220 meters depth reservoir evaluated in the GeoTES system analysis is 12 MPa (1740 psi). Figure 2 indicates that a bottomhole injection pressure of 12 MPa at a temperature of 250°C is below a rule-of-thumb threshold in situ vertical stress gradient of 0.6 psi/ft at which hydraulic fracturing of the injection well might occur. When a particular area is studied for deployment, there is considerable potential to use shallower formations and lower-cost wells.

Other reservoir design parameters include an initial, undisturbed reservoir temperature of 50°C (122°F), and it is assumed that there is no regional flow in the formation. The formation thickness is specified as 100 meters (328 feet) with an injection interval equal to the formation thickness. Reservoir horizontal permeability is specified as $1.0 \times 10^{-13}$ meters squared (100 milliDarcies). If future work is undertaken, it could examine variations to these selected values.

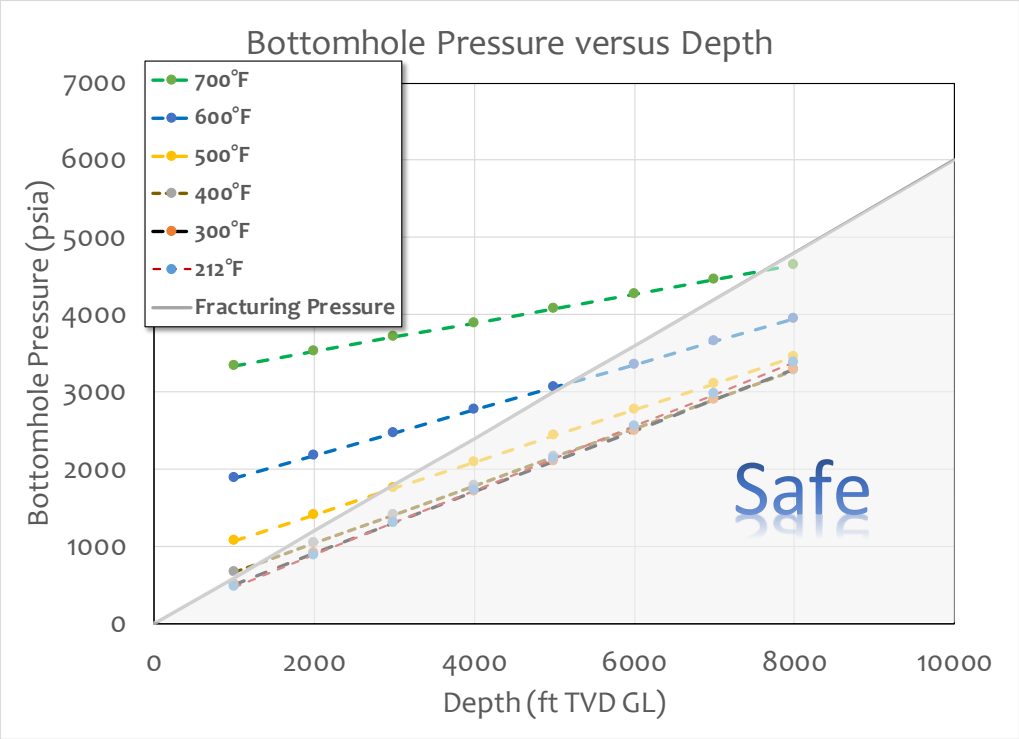


Figure 2. Bottomhole injection pressure at various depths and temperatures. The grey line indicates in situ total stress at 0.6 psi/ft. If pressures are less than this, immediate hydraulic fracturing will not occur.

## 2.3 Well configuration and operation

The GeoTES is a synthetic geothermal reservoir in which the well configuration determines how heat is added and recovered from the system, and consequently where the heat is stored in situ. The well configuration will also dictate the method by which the brine must be circulated through the formation. This configuration will determine thermal characteristics (i.e., location of the thermal front) as well as the pumping requirements to circulate and maintain fluid in the desired phase.

This analysis evaluated a 5-spot well configuration in which the center wells are designated as "hot wells" and the corner wells are designated as "cold wells" (Figure 3). The "hot wells" are operated in a push-pull operating mode and are used to store heat obtained from the solar collectors. Push-pull is sometimes also known as huff-and-puff or injection-production cycling. The "cold wells" are operated in a push-pull configuration that is complementary to the hot well operation. When the cold wells "push" (inject), the hot wells "pull" (produce) and vice versa. The so-called cold wells are used to store cool brine from the time it exits the power plant to the time it is reheated. This operating strategy allows the fluid injection to provide pressure support for the fluid production in both the heat storage and heat recovery operating modes. Since fluid is always returned to the formation, use of "hot" and "cold" wells eliminates the need to store brine in a surface vessel/reservoir between operating cycles. Storing brine in an open surface reservoir would expose it to evaporation, oxygen, and biological contaminants that would likely result in significant operational issues.

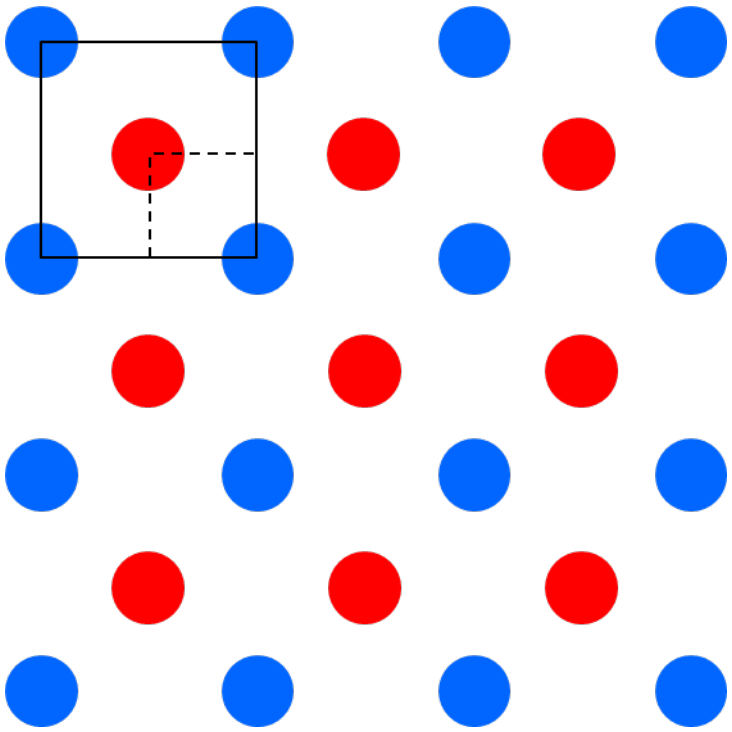

Figure 3. This shows a repeated five-spot well field configuration: Red “hot” wells denote where solar-heated hot water is injected and produced later; blue “cold” wells are where reservoir fluid is produced for solar heating and cooled water from the power generation cycle is injected back to the reservoir. The solid square represents a single five-spot “tile” in which there is a net total of one hot well and one cold well.

Figure 4 shows a schematic for a GeoTES heat storage system. The main components include the power block, solar collectors, and the GeoTES reservoir. The solar field uses parabolic trough collectors with oil (Therminol VP-1) as the heat transfer fluid. The GeoTES working fluid is water. During the charging cycle, the oil gets heated in the parabolic trough collectors and is sent to the heat exchanger to heat the brine pumped from the cold wells to the hot wells. The cooled oil is sent back to the parabolic trough collector. During the discharging cycle, heated brine from the hot wells is extracted and sent to the power block for producing power. The cooled brine exiting the power block is sent to the cold wells.

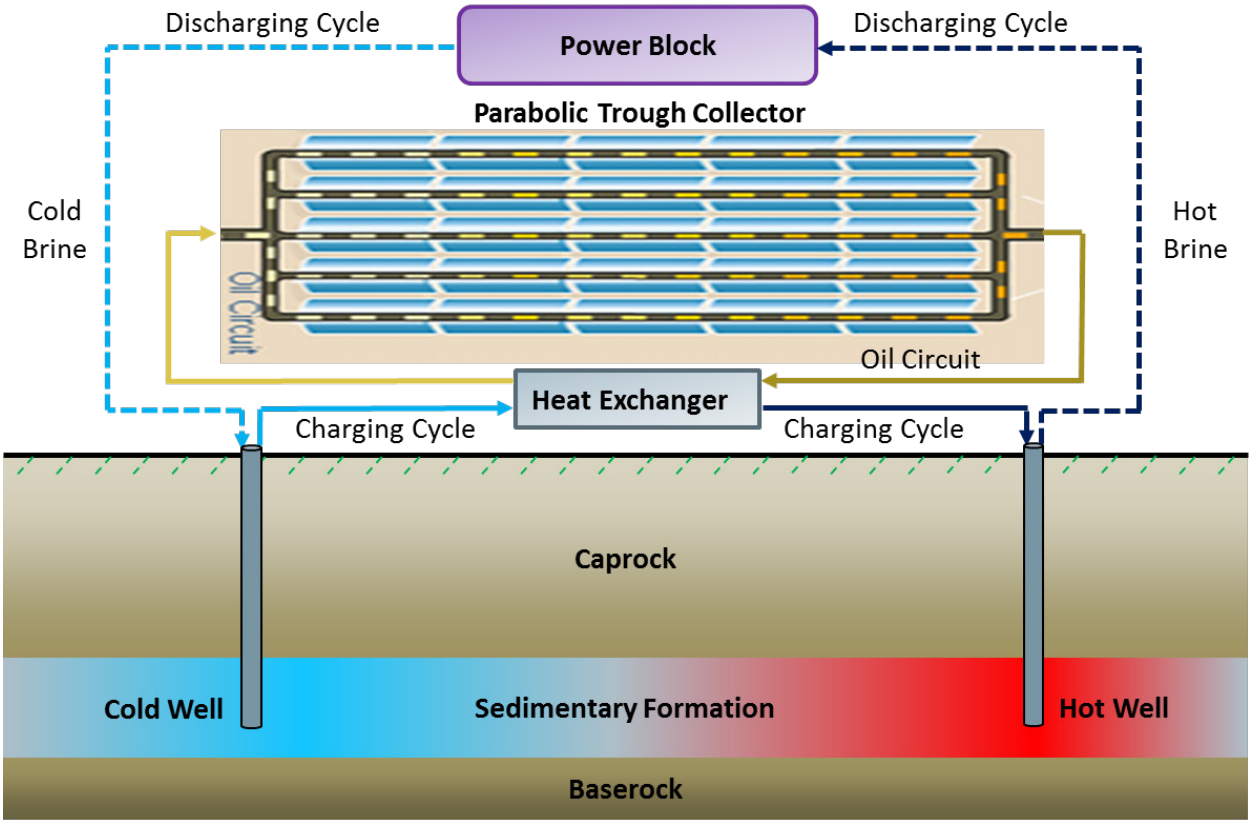


Figure 4: Schematic for the Geologic Thermal Energy Storage (Geo TES), solar collectors, and power block.

Figure 5 is a diagram of the system operating principle. In this figure, orange circles designate operations that are required to accomplish GeoTES "charging" while black circles designate operations required for GeoTES "discharging."

The fluid injection and production strategy must be compatible with the capabilities and limitations of commercially available pumps. Use of conventional injection pump technology is acceptable for the GeoTES application since the required pump can pressurize the water before it has been heated (pressurized cold fluid will be sent to the solar field HX for heating before injection). Commercially available production pumps are not capable of operating at reservoir temperatures of or even near 250°C. Therefore, the hot wells will be operated under artesian conditions, i.e., the wellhead pressure will be reduced to allow the fluid to be produced from the formation by "flashing" or boiling as it comes up the wellbore, resulting in a mix of steam and water at the surface at a lower temperature than 250°C.

In the reservoir modeling phase, the study assumed a daily injection-pumping cycle scenario in which solar-heated water is injected into the reservoir down the hot wells (red in Figure 3**)** for 8 hours at an injection rate of 40 kg/s and at 250°C. During this solar-heated water injection stage, the same volume of "cold" reservoir water is pumping out from cold wells (blue in Figure 3) at the same rate. This "cold" reservoir water will be solar-heated. After 8 hours of injection of solar heated water, a 10-hour heat production stage starts by pumping out the previously injected hot water from "hot" wells at a rate of 32 kg/s. During this heat production stage, the same amount of "exhausted" water (assumed 70°C temperature) is injected back to the reservoir into the cold wells. After this heat-production stage, all wells are shut in and the system is idle for 6 hours before the next daily cycles starts. Although 8 hours of continuous heat recovery was modeled, this "discharge" would be fully dispatchable and indifferent to a lower rate of production over the full 14 hours, or multiple high and low discharge periods. The charging

cycle in which heat is added to the reservoir is idealized at 8 hours every day. Future work will add the complexity of solar energy availability and duration including both seasonal and weather variation to the charging cycle model.

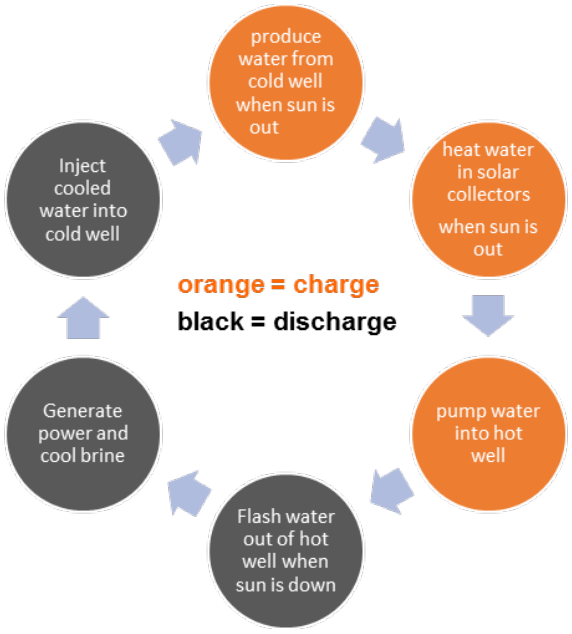


Figure 5. GeoTES system operation

## 2.4 Power cycle

A power cycle screening study was completed using proven geothermal power plant technologies and methods in which the following configurations were evaluated using a brine inlet temperature corresponding to the GeoTES brine recovery temperature at the surface after flashing:

- Single-stage flash steam cycle
- Single-stage flash steam cycle + simple ORC
- Single-stage flash steam cycle + ORC with recuperator
- Single-stage flash steam cycle + ORC with turbine inlet dryness of less than 100% in order to exit the turbine with lower superheat and no recuperator.
- Two-stage flash steam cycle

The screening study determined that the two-stage flash steam power cycle results in the lowest capital cost per unit of net power generation. Additionally, the two-stage flash steam cycle requires a mass flow rate of brine less than the single-flash steam cycle and comparable to the configurations that include an ORC bottoming cycle (per unit net power generation). Therefore, for the present study, the two-stage flash steam cycle is considered.

Figure 6 shows the schematic for the two-stage flash steam cycle. The hot water from the hot well is extracted and is flashed in the flash vessel at 210°C. This results in the production of vapor and saturated water at 210°C. The saturated water coming from the first flash vessel is flashed in the second flash vessel to produce additional vapor. The vapor produced in the flash vessels is used to run the turbines and generate electricity. The vapor exiting the steam turbines is condensed in the air cooler and pressurized to 1 MPa (10 bars) and mixed with the saturated water exiting the second flash vessel. The mixed water is then pressurized to 5 MPa (50 bars) and injected into the cold well.

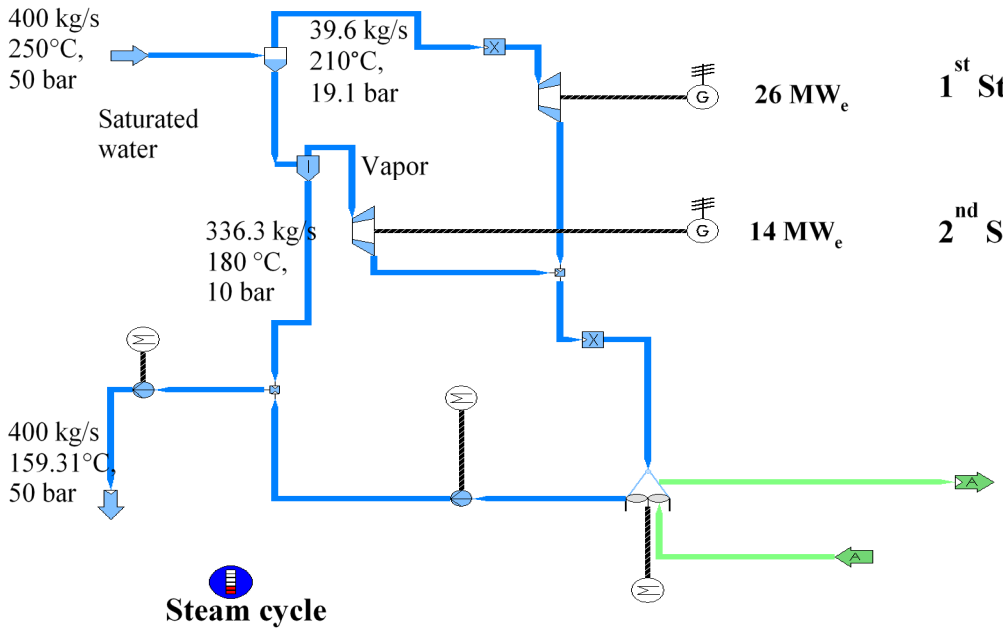


Figure 6: Schematic of double stage flash steam cycle

The power plant will utilize dry cooling technology to minimize system makeup water requirements and/or prevent pressure declines associated with depletion of the GeoTES fluid. The dry cooling technology specified for use with the GeoTES flash plant includes the use of a proven geothermal direct contact condenser (DCC) paired with an air-cooled water cooler (ACWC). The condensate will be cooled in the ACWC to provide the DCC cold liquid feed stream. This condenser design will allow air cooling technology to be used to condense the steam obtained from the Geo TES brine without non-condensable gas buildup as would occur in traditional steam power plant ACCs. Details of the DCC/ACWC condenser are included in Figure 7.

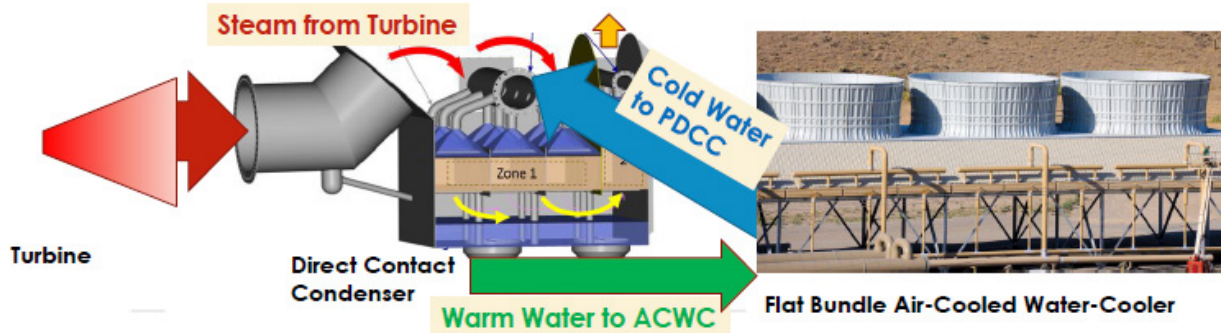


Figure 7. DCC/ACWC dry cooling technology for steam cycles: A direct contact condenser (DCC) coupled to an air-cooled water chiller (ACWC) allows dry cooling of steam cycles, including those that utilize geothermal brines containing non-condensable gases (Kitz, 2018)

## 3. Subsurface heat storage and recovery

Injection of solar-heated water and the follow on heat storage, conductive heat loss and recovered temperature of produced water were simulated using a multiphysics finite element code, FALCON, developed at INL (Podgorney et al., 2010).

As shown in Figure 8, a generic reservoir of 100-meter thickness, with low-permeability caprock and underburden layers, at a vertical depth of 1200 meters (4,000 ft) TVD GL were chosen for simulations. Table 1 summarizes the flow and transport properties of the reservoir.

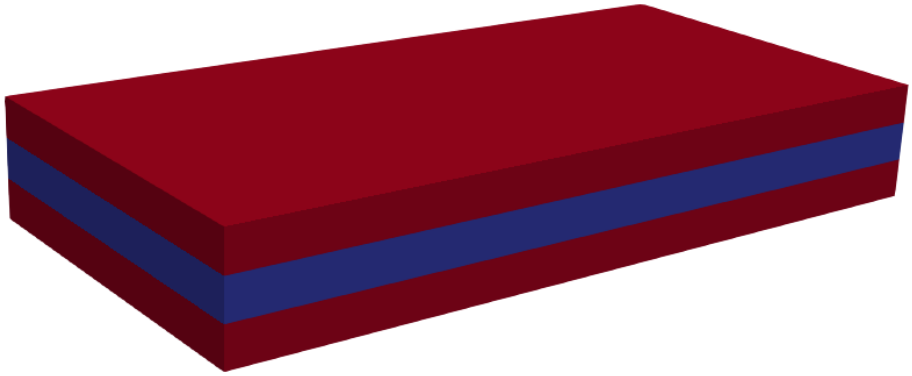

Figure 8. Conceptual 3-layer reservoir model: top and bottom layers – low-permeability barriers; middle zone – injection and storage formation

Table 1. Reservoir properties used in the simulations

| Layer | Thickness (m) | Permeability ($m^2$) | Porosity | Rock Density ($kg/m^3$) | Rock Specific Heat (J/kg K) | Thermal Conductivity ($W/m^2$ K) |
|---|---|---|---|---|---|---|
| Caprock and Bedrock | 100 | Isotropic, 1.0e-19 (i.e., 100 nanoDarcy) | 0.025 | 2500 | 770 | 1.05 |
| Injection Formation | 100 | Horizontal: 1.0e-13 (i.e., 100 millidarcy) Vertical: 1.0e-14 (i.e., 10 millidarcy) | 0.15 | 2000 | 930 | 2.50 |

The initial reservoir temperature at the middle of the injection formation was chosen to be 50°C following an average geothermal gradient of 25° per kilometer. The initial pressure at the middle of the injection formation was set to 12 MPa, according to a hydrostatic pressure distribution.

In the simulations, the model domain takes advantage of the symmetry condition of a 5-spot well pattern and only considered one hot-cold well pair, located at opposite corners of the simulation grid (Figure 3). Figure 9a shows the finite element mesh used in the simulations. The mesh is refined near the injection well. One alternative injection-pumping strategy is to thermally "charge" the reservoir for some time before the daily injection-production operation cycle starts. In such a scenario, the solar-heated water will be injected into the reservoir via hot wells for 8 hours every day without subsequent production of the heated water. Figure 9b shows the temperature field after six months of "thermal charging." After this 6-month "thermal charging," the conductive heat transfer into the over- and underburden rocks is negligible.

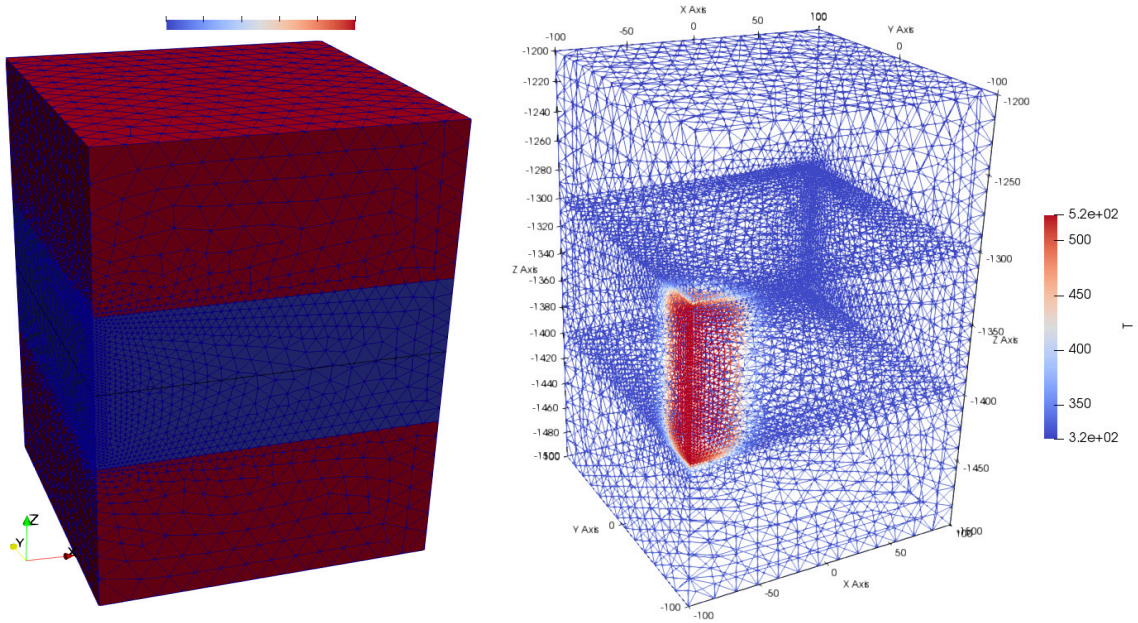


Figure 9. (a) Finite element mesh used in the simulations (left); (b) Temperature field (in Kelvin) of the reservoir after 6-month of "thermal charging" by injection of solar-heated water of 250°C at 40 kg/s for 8 hours each day (right).

One important factor for the effectiveness of subsurface heat storage is the temperature of water produced from the "hot" wells and potential temperature decline after continuous operation. Figure 10 shows the simulated temperature variations of water at a "hot" well over 30 days of continuous injection-production operation cycles for various "thermal scenarios." For the case of no "thermal charging" at all, initially large temperature oscillations are observed. This thermal oscillation starts to decrease gradually over the injection-production cycles, with an oscillation of ~50°C after 30 days and continuously decreasing. For the case of a 180-day (6-month) "thermal charging" scenario, the temperature oscillation is minimal, within ~2-3°C fluctuation over the 30-day injection-production cycles.

These initial simulation results indicate that the subsurface is a very good candidate for heat storage, and the push-pull injection/pumping strategy could be very promising for coupling underground solar heat storage with power plants.

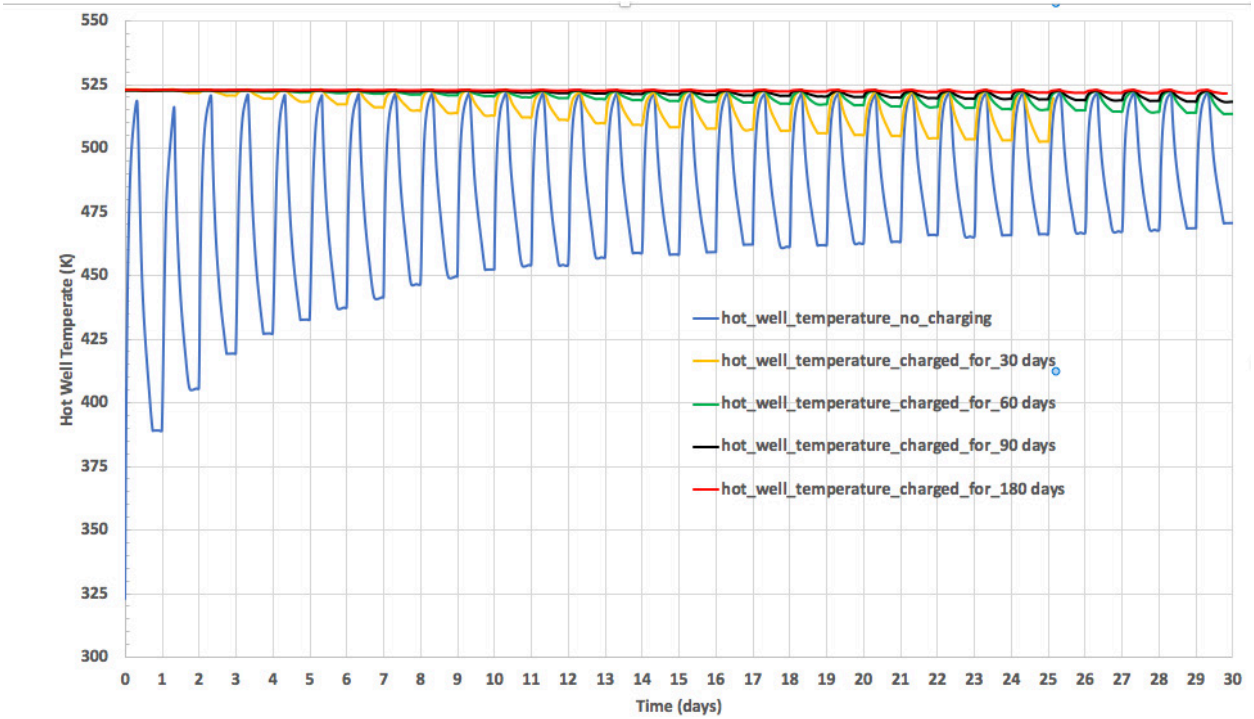


Figure 10. Simulated temperature variations of water at the "hot" well over 30-day continuous injection-production cycles for various "thermal charging" scenarios in which heat is added and recovered from the GeoTES.

# 4. Power cycle analysis

The objectives of the power cycle analysis include:

1. Optimal condenser operating pressure
2. Optimal flash temperature selection
3. Economic analysis and LCOE (levelized cost of electricity) calculation

The input parameters used for designing the power cycle are:

1. Gross power produced: 40 $MW_e$
2. Ambient air temperature: 25°C
3. Hot geothermal well condition: 250°C and 50 bar
4. HTF solar field pumping is calculated from SAM (10.3 $kW_e$/kg of HTF)
5. Condenser for the power cycle: Air-cooled condenser

The assumptions used while modeling the power cycle are:

1. Mass of water extraction from a well ($m_{well}$): 40 kg/s
2. No heat loss from the geothermal well
3. Isentropic efficiency for the turbine and pump: 85%
4. Pressure drop in air cooler: 150 Pa
5. A standard steam ACC is a reasonable representation in the model of the preferred system of a DCC and an ACWC (See Section 2.4).

To model the power cycle SimTech IPSEpro is used. The power cycle is specified to deliver a gross power output ($P_{gross}$) of 40 $MW_e$. The net power supplied from the power cycle ($P_{net}$) is:

$$P_{net} = P_{gross} - P_{pump}\left(\begin{array}{l}\text{Air Cooler} + \text{Compression of working fluid in the power cycle} \\ + \text{Geothermal Storage}\end{array}\right) \quad (1)$$

The overall efficiency ($\eta$) is given as:

$$\eta = \frac{P_{net}}{\dot{m}_{w,geo}\left(h_{in} - h_{out}\right)} \quad (2)$$

where,
$\dot{m}_{w,geo}$ = mass flow rate of water from the geothermal well(s) into the flash tank
$h_{in}$ = enthalpy of hot water entering the power cycle (250°C and 50 bar)
$h_{out}$ = enthalpy of cold water leaving the power cycle

## 4.1 Optimal condenser operating pressure

Figure 11 shows the variation in the cycle efficiency and mass flow rate of water required with condenser operating pressure. The steam flash temperature considered is fixed at 160°C. The cycle efficiency is maximum at 0.1 bar-absolute (18%) and decreases linearly with an increase in pressure. Because of higher efficiency, the net mass flow rate of geothermal water is low at a lower condenser pressure. Due to higher efficiency and lower mass flow rate, the condenser operating pressure for the steam turbine is selected to be 0.1 bar-a (1.45 psia, 3" of mercury).

IPSEpro has a built-in module for a conventional steam ACC. This module was used in place of developing a full operating model of the preferred system of a direct contact condenser (DCC) and an air cooled water cooler (ACWC) as described previously.

Future work would develop the off-design modelling capability of the preferred system of DCC+ACWC. Large cost and performance benefits may be obtained with repeating the condenser optimization analysis in future work in combination with more key parameters, including the DCC+ACWC, annual plant performance instead of single design point analysis, and the flash temperature (next section).

## 4.2 Variation in flash temperature

Figure 12 shows the variation in cycle efficiency and water mass flow rate for the two-stage flash steam cycle. With increases in flash temperature, the net heat available for power production per unit mass of water decreases and this leads to an increase in the mass flow rate of water. For 160°C (320°F), the required mass flow rate of water is 328 kg/s (2.6MMlbs/hr), and at 240°C (464°F), the net mass flow rate of water required is 600 kg/s (4.8MMlbs/hr). The consequence of this higher flow rate is that a greater number of wells is required.

As would be expected from the second law of thermodynamics, the efficiency of the cycle increases with higher turbine operating temperature. Thus higher turbine inlet temperature yields higher production of electricity per unit mass of water supplied. This both mitigates the number of new wells needed, but more importantly reduces the capital cost of the required solar thermal collectors. The effect of the increase in electricity production is more dominant compared to the increase in water flow rate, and this results in an increase in overall efficiency and lower capital cost with increasing flash temperature. The cycle efficiency increases from 18% to 23%, as the first stage flash temperature is increased from 160°C

to 240°C. For all optimization runs, the second stage flash temperature was fixed at 30°C below the first stage flash temperature as a simplifying assumption. However, as is discussed in the next section, the optimum flash temperature was shown to be between 205 and 220°C.

Future additional study scope could include the effect of injection temperature on the parasitic injection pump load and production and injection well count to further refine the effects of higher flash temperature. Deliverability and injectivity curves are also needed to truly optimize the plant design. Lastly, exploring second stage flash temperatures and pressures different than the assumed value of 30°C lower would very likely result in further reductions in LCOE.

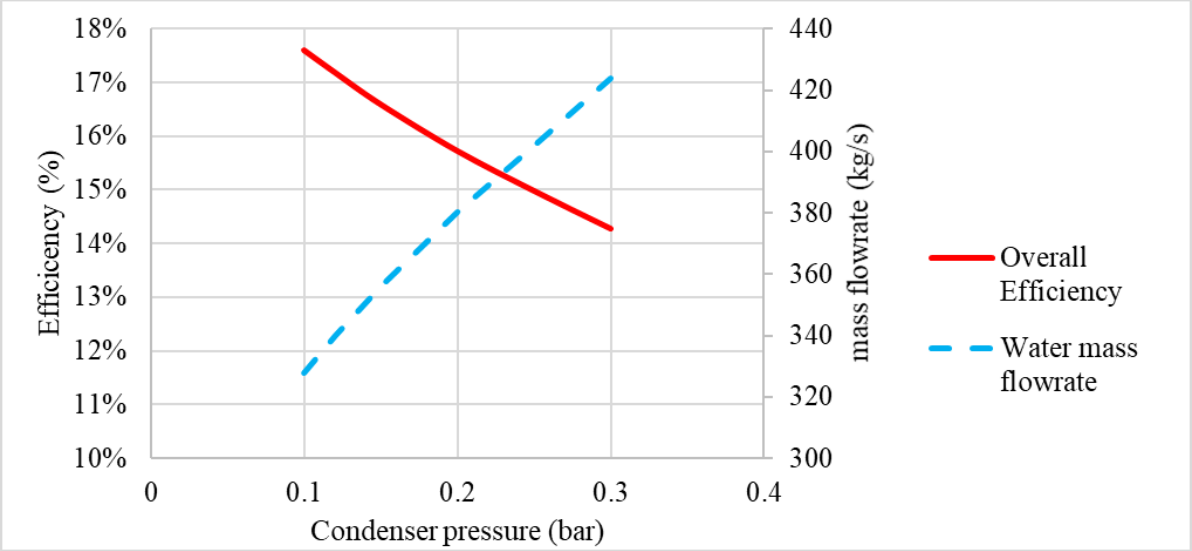


Figure 11: Variation in cycle efficiency and water mass flow rate with condenser pressure. The steam flash temperature considered is fixed at 160°C. The power plant net output is fixed at 40 $MW_e$.

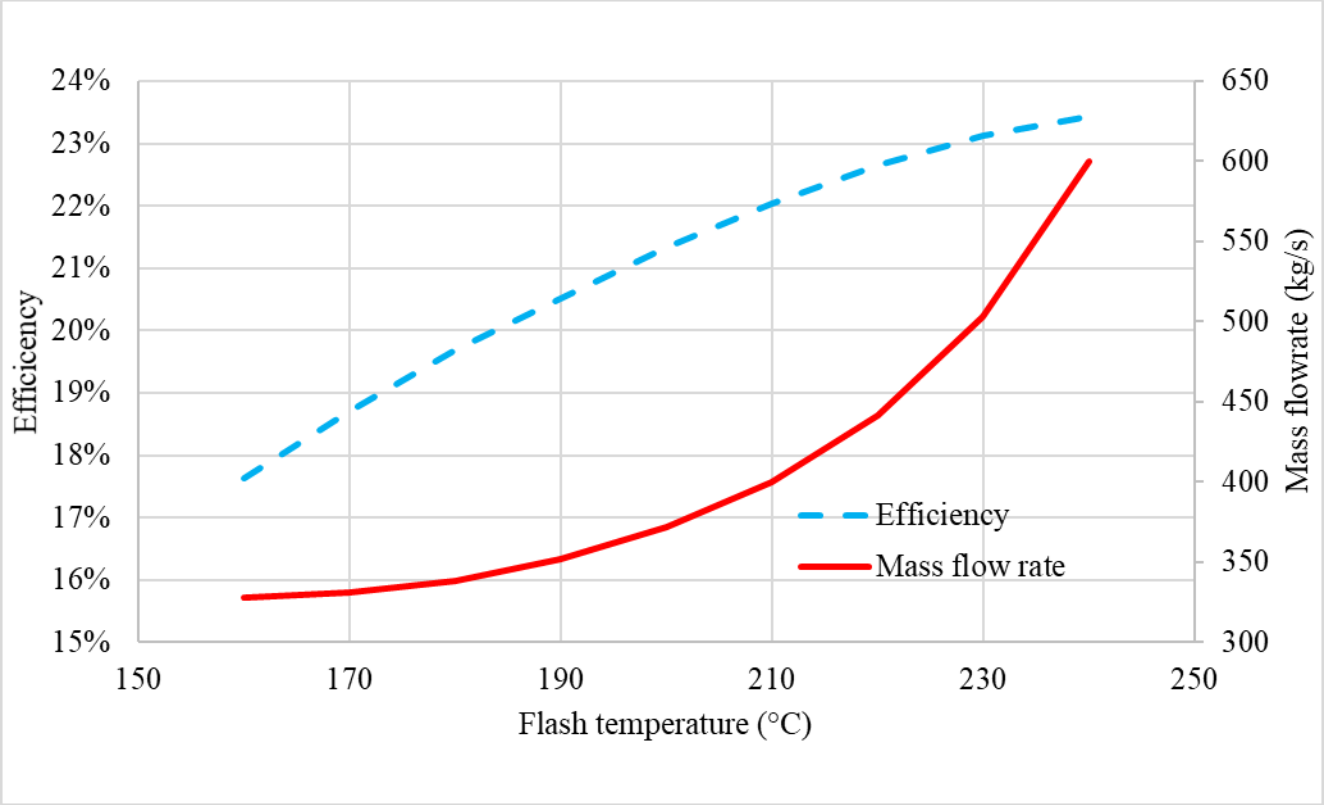


Figure 12: Variation in mass flow and overall cycle efficiency with variation in flash temperature. The power plant net output is fixed at 40 $MW_e$.

## 5. Economic analysis

To further evaluate the performance of the cycle a first order economic analysis was performed. Cost parameters used in the analysis include:

Cost of GeoTES well pair: $2 MM (hot well + cold well + cold well downhole pump).
Cost of steam power cycle: \$1.5 MM/$MW_e$
Cost of solar: \$150/m²
Land cost: \$5/m²
Water cost: \$0/kg
O&M solar: \$7.4/$kW_{th}$/year
O&M geothermal and power block: \$25/$MWh_e$

Since the GeoTES wells are being drilled in soft sedimentary formations to create a synthetic geothermal reservoir, the low drilling costs of traditional oil and gas wells are more applicable than the costs of hard rock drilling in geothermal formations.

Figure 13 shows the variation in capital cost with flash temperature. The minimum capital cost per unit electricity generation is approximately 4.2 M\$/$MW_e$ for a flash temperature of 210°C. The capital cost escalates with increases in flash temperature beyond 220°C. This increase in capital cost is because increases in flash temperature require higher water flow rates to produce the specified level of power generation, which in turn results in a greater number of wells with increased capital costs.

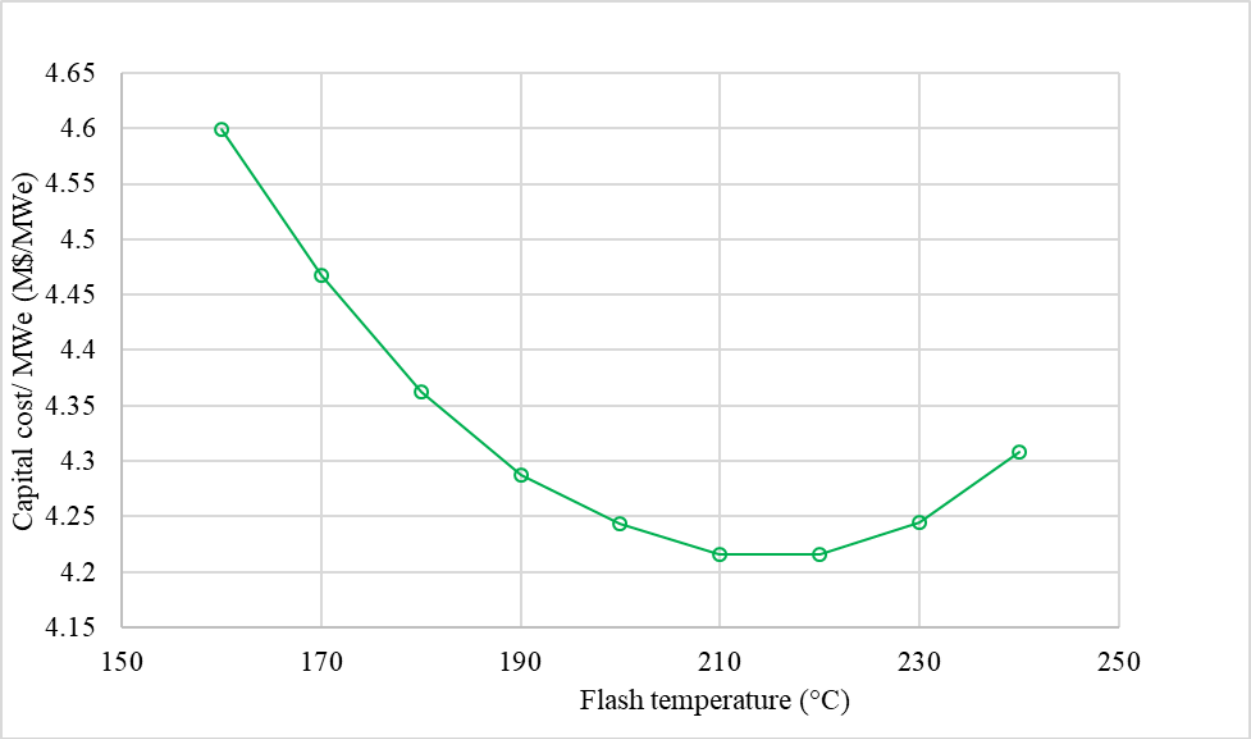

Figure 13: Variation in capital cost for unit electricity generation with flash temperature.

To calculate the levelized cost of electricity (LCOE), an annual simulation is performed using typical meteorological year (TMY) data. Minimization of the LCOE involves repeating the annual simulations with a varying solar multiple (SM) to identify the optimal SM ($SM_{opt}$). The solar multiple determines the solar field size as well as the number of wells required to accommodate the increased flow rate of hot water that must be injected into the hot wells; the capital costs are therefore affected by the SM specification. A solar multiple of 1 in this analysis produces enough solar heat at the design point irradiance onto the solar collectors to produce the required power plant design point heat input. Solar multiples above 1 are generally used in order to provide full capacity across more hours of the year, or in the case of Geo TES to increase the number of hours over which the power plant could operate.

With GeoTES, the $SM_{opt}$ was greater than would normally be selected for a solar thermal power plant. Figure 14 shows variation in the LCOE for different solar multiples. For SM = 1, the LCOE comes out to be $\$0.17/kW_e$. At a lower SM, the net heat from the sun cannot be used effectively, and this results in higher LCOE. With increase in SM, the solar collector area and the number of wells increase, and this leads to an increase in total energy stored in the Geo TES and thus the number of hours that the Geo TES can discharge to provide flexible generation on a seasonal basis. The minimum LCOE of $\$0.13/kW_e$ for the system is obtained for SM = 3.8. Any further increase in SM does not increase the heat utilization rate in the same proportion which leads to higher LCOE.

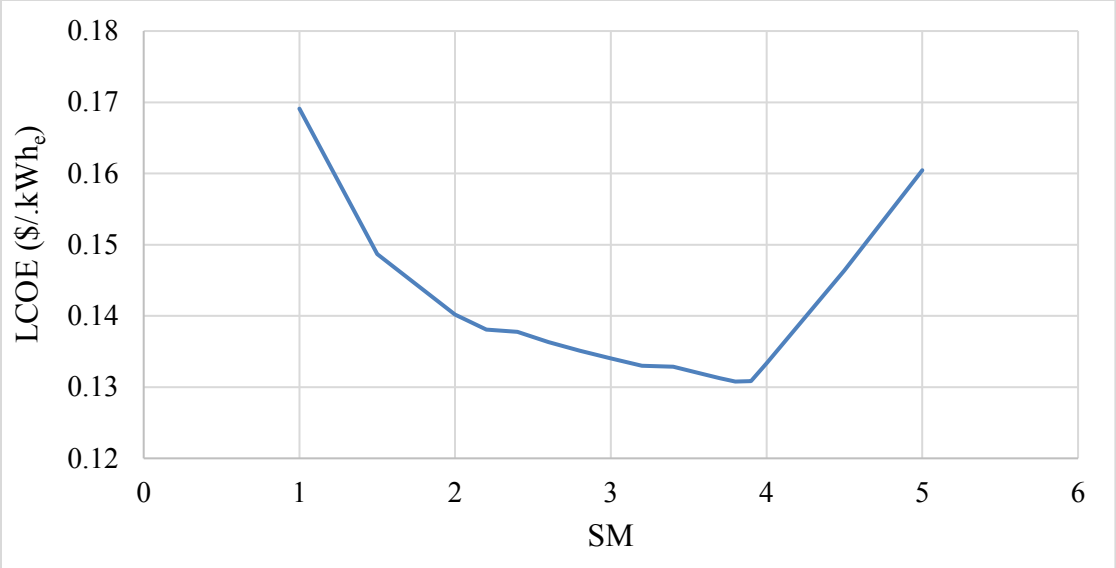

Figure 14: Variation in LCOE for double stage flash steam cycle (210°C / 180°C) with solar multiple.

## 6. Conclusions

1. Use of GeoTES for solar thermal heat storage coupled with proven geothermal power generation technology provides a unique fully dispatchable seasonal energy storage capability for both capacity (MW) and energy (MWh). The overall system provides a foundation to support grid stability, reliability, and flexibility and can provide grid ancillary services. The system has the potential to allow and integrate even larger quantities of variable wind and solar PV generation by providing non-fossil based backing at lower cost over longer durations than battery energy storage. This unique capability provides a potential pathway for the nation's energy infrastructure to evolve more quickly to renewable, carbon-free electric sources and a sustainable energy future.
2. System economics are optimized in configurations with a solar multiple greater than 1 (SM > 1). These configurations allow the GeoTES system to be charged during periods of high solar insolation. The charging provides the energy storage reserves necessary to generate power during periods of low solar insolation.
3. The minimum Levelized Cost of Energy (LCOE) obtained for the GeoTES system is \$0.13/$kW_e$ with an optimal solar multiple of 3.8.
4. The LCOE for high capacity GeoTES systems is lower than the value of \$0.148/kWh estimated by McTigue et al. (2018a, 2018b) for a low capacity (4 hr) photovoltaic plus battery energy storage (PV+BES) system. Addition of increased BES capacity would result in significant increases in PV+BES LCOE. The GeoTES system would, therefore, provide superior economics for high capacity and long duration solar energy storage.
5. A five-spot well pattern with dedicated hot and cold wells operated using a push-pull strategy provides (1) the ability to immediately recover stored hot fluid from the GeoTES reservoir, (2) a practical approach for managing the system fluid inventory, and (3) reduced parasitic load. Pressure support is provided from the wells operating in "push" mode to the wells operating in "pull" mode.

6. Initial charging of the GeoTES system increases the heat recovery temperature. Increasing the duration of the charging period decreases the magnitude of the temperature fluctuations that occur following prolonged system operation.
7. A dual-stage flash steam cycle provides lowest capital costs per unit net power generation with acceptable hot brine inlet fluid flow rate (i.e., low number of wells and associated parasitic loads). Other flash and binary cycle configurations had higher LCOE.
8. The LCOE is minimized at the optimal solar multiple ($SM_{opt}$).
    a. At $SM > SM_{opt}$ the additional capital costs associated with the solar field and GeoTES wells do not result in significant increases in annual power generation, i.e., minimal additional power sales revenue is realized from significant increases in capital cost.
    b. For $SM<SM_{opt}$ there will be greater durations of time when the GeoTES energy storage is depleted, i.e., no hot brine remains in the GeoTES reservoir, and electrical power cannot be generated to provide revenue during these times.

**Acknowledgments**

This work was supported by the United States Department of Energy through contract DE-AC07-05ID14517. Funding was supplied by the Department of Energy (DOE) Office of Energy Efficiency and Renewable Energy (EERE) Geothermal Technologies Office (GTO).

**REFERENCES**

Augustine, C. (2014) "Analysis of Sedimentary Geothermal Systems Using an Analytical Reservoir Model" GRC Transactions, Vol. 38, pp641-648.

Augustine, C. (2016) "Design Requirements for Commercial Sedimentary Geothermal Projects" Presented at Power Plays" Geothermal Energy in Oil and Gas Fields. Southern Methodist University, April 25-26.

Kirby, S. M. (2012), "Summary of Compiled Permeability with Depth Measurements for Basin Fill, Igneous, Carbonate, and Siliciclastic Rocks in the Great Basin and Adjoining Regions." Open-File Report 602. Salt Lake City, Utah. Utah Geological Survey.

Kitz, K. (2018) "A New Air-Cooled Condensing System for Both Geothermal Steam and Conventional Steam Power Plants" *GRC Transactions*, Vol. 42.

McTigue, J., Castro, J., Mungas, G., Kramer, N., King, J., Turchi, C., Zhu, G.* (2018a) "Hybridizing a geothermal power plant with concentrating solar power and thermal storage to increase power generation and dispatchability" *Applied Energy*, vol. 228, 2018

McTigue, J., Kincaid, N., Zhu, G., Wendt, D., Gunderson, J., and Kitz, K. (2018b) Solar-Driven Steam Topping Cycle for a Binary Geothermal Power Plant. 68 pp. NREL/TP-5500-71793.

Podgorney, R., H. Huang and D. Gaston (2010), Massively Parallel Fully Coupled Implicit Modeling of Coupled Thermal-Hydrological-Mechanical Processes for Enhanced Geothermal System Reservoirs, *Proceedings of 35th Workshop on Geothermal Reservoir Engineering*, Feb. 1-3, Stanford University, Stanford, California.

Porro, C., Esposito, A., Augustine, C., and Roberts, B. (2012), "An Estimate of the Geothermal Energy Resource in the Major Sedimentary Basins in the United States" *GRC Transactions*, Vol. 36.

SimTech Simulation Technology (2018). “IPSEpro Process Simulation Environment (PSE), version 7.0.” http://www.simtechnology.com/CMS/index.php/ipsepro

Zhou, M., Cho, J., Zerpa, L., and Augustine, C. (2016) “Optimization of Well Configuration for a Sedimentary Enhanced Geothermal Reservoir” GRC Transactions, Vol. 40, pp. 383-396.

# Appendix A

# Coupled Thermo-Hydro (TH) Simulations for Subsurface Geological Thermal Energy Storage (GeoTES) of Solar-Heated High-Temperature Brine

# Coupled Thermo-Hydro (TH) Simulations for Subsurface Geological Thermal Energy Storage (GeoTES) of Solar-Heated High-Temperature Water

## 1. Introduction

In order to evaluate the feasibility of subsurface geological thermal energy storage(GeoTES) of solar-heated high-temperature water and the follow on thermal recovery efficiency, injection of solar-heated high-temperature water and the follow on heat storage, conductive heat loss and recovered temperature of produced water were simulated using a multiphysics finite element code, FALCON, developed at INL[1] for various combinations of reservoir flow properties, reservoir initial temperatures, well configurations and pumping/extraction scenarios.

A very simple 3-layer hydrogeological model was used in these initial thermal-hydrological (TH) reservoir simulations. As shown in Figure 1, a generic reservoir of 100 meter thickness, with low-permeability caprock and bedrock layers, at a depth of ~1,300 meter below the ground were chosen for simulations. Initially a much smaller formation thickness of 20 meter were also chosen for initial sensitivity study, but then was quickly abandoned because the limited reservoir volume for accommodating the injection of large volume of solar-heated water. The choice of this reservoir depth is primarily for ensuring the in-situ stress would be large enough to prevent hydraulic fracturing during the injection.

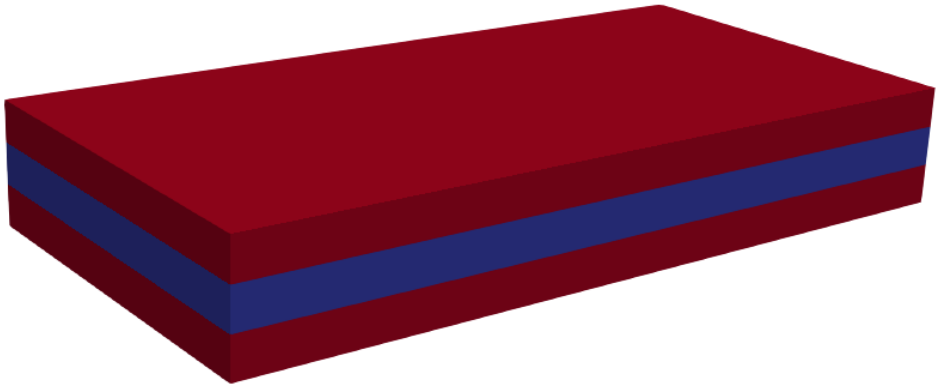

Figure A.1 Conceptual 3-layer reservoir model: top and bottom layers – low-permeability caprock and bedrock; middle – injection and storage formation

In this sensitivity study, three well configuration scenarios were considered: double well (one injection well for injected solar-heated water; one pumping well for producing hot water); single-well push/pull; and 5-spot well pattern. Table 1 summarizes the flow and transport properties of the reservoir for baseline sensitivity simulations. These parameter values were chosen largely from the literature. The permeability values of the storage formation was mainly chosen based on quick preliminary TH simulation results, in which the injection pressure at the desired injection rates of the power-plant cycle modeling team will not exceed the hydraulic fracturing pressure of the GeoTES reservoir. These permeability/porosity values correspond to "good" quality conventional sandstone reservoirs.

[1] Ref - Podgorney, R., H. Huang and D. Gaston (2010), Massively Parallel Fully Coupled Implicit Modeling of Coupled Thermal-Hydrological-Mechanical Processes for Enhanced Geothermal System Reservoirs, *Proceedings of 35th Workshop on Geothermal Reservoir Engineering*, Feb. 1-3, Stanford University, Stanford, California

Table A.1. Reservoir properties used in the baseline simulations

| Layer | Thickness (m) | Permeability ($m^2$) | porosity | Rock density ($kg/m^3$) | Rock Specific Heat ($J/kg.^0K$) | Thermal Conductivity ($W/m^2.^0K$) |
|---|---|---|---|---|---|---|
| Caprock & bedrock | 100 | Isotropic, 1.0e-19 (i.e., 100 nanoDarcy) | 0.025 | 2500 | 770.0 | 1.05 |
| Injection formation | 100 | Horizontal: 1.0e-13 (i.e., 100 millidarcy) Vertical: 1.0e-14 (i.e., 10 millidarcy) | 0.15 | 2000 | 930.0 | 2.50 |

## 2. Double-well pair configuration

Our initial GeoTES sensitivity simulations began with a double-well configuration, where one well is designed for the injection of solar-heated high-temperature water, and the other well is for pumping hot water and producing stored thermal energy. Figure 2 showed the conceptual model for the double-well pair scenario. Due to the plane symmetry condition, only half of the model domain is needed for the simulations. The domain size is chosen to be relatively large of 2 km x 2 km in the horizontal plane, in order to avoid the boundary effect.

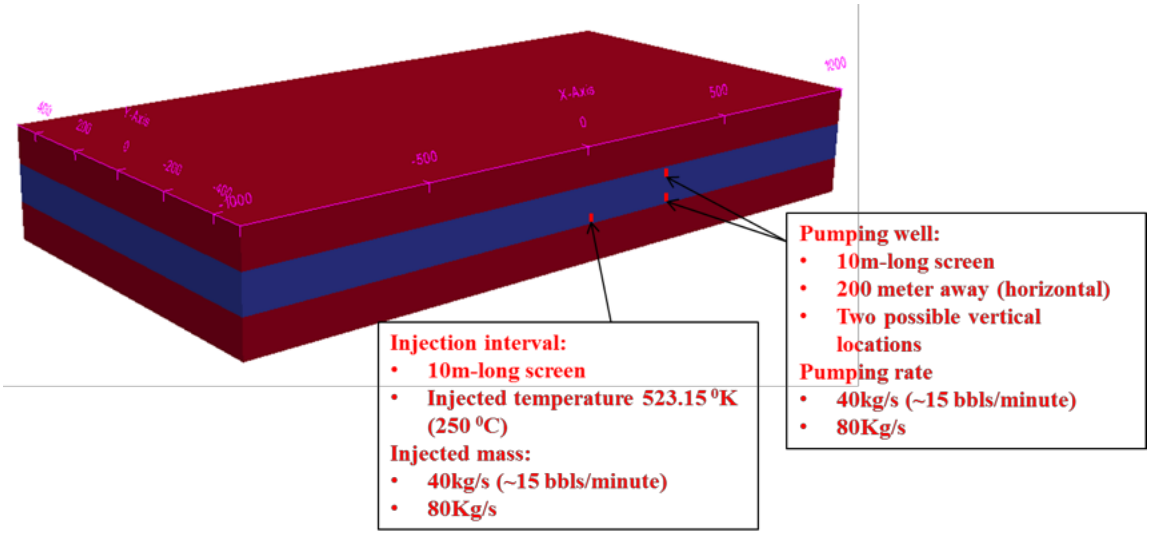


Figure A.2. Conceptual model for the double-well pair configuration. The two wells are separated by 200 meters, and the injection interval is located near the bottom of the storage formation, and two possible locations of the production well screen interval: close to the top and bottom of the storage formation, respectively.

The initial reservoir temperature at the middle of the injection formation was chosen to be 120°C., following an average geothermal gradient of ~25 degrees per 1000 meter. This relatively high initiative reservoir temperature was chosen by the power-plant cycle modeling team based on the assumption that high reservoir temperature leads to better thermal recovery efficiency and economics and the GeoTES reservoir is within an existing geothermal field. The initial pressure at the middle of the injection formation was set to 12MPa, following a hydrostatic pressure distribution above and below.

Two injection rates, 40 kg/s and 80 kg/s, at the temperature of 250°C, collectively set by the power-plant modeling team for better power generation economics, were used in these GeoTES simulations initially. It is worthy to mention in these double-well simulations, continuous constant injection and

pumping were assumed throughout the entire simulation period. Figure 3 shows the simulated temperate field and the temperature evolution of produced water through a 10-year simulation period.

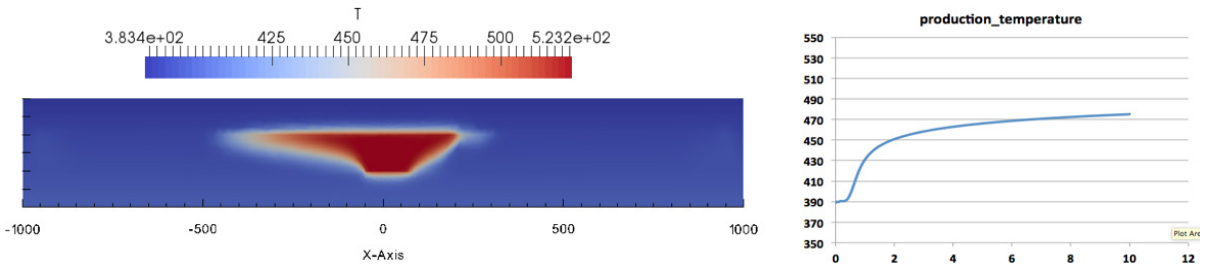


Figure A.3. The simulated temperature field at the end of 10 years of continuous injection and pumping at the rate of 40 kg/s (left); The temperature evolution of the produced water from the pumping well over a 10-year operation period (right).

The simulation results indicate significant buoyance effect during the injection, which potentially increases the additional loss of injected thermal energy. Double well configuration results in long time delays before stored heat can be recovered. Significant fluid production is required before temperature of recovered heat begins to approach the temperature at which it was stored. Some of the hot fluid that is injected into the reservoir flows away from the production well; this fluid and the thermal energy it contains will never be recovered. Such drawbacks could be alleviated by positioning the pumping well at a distance much closer the injection wells, in a ranges of 10s of meters. However, this close distance between two wells might lead to practical difficulty for injection and pumping due to strong pressure interference between two wells. Decision to pursue additional reservoir configurations was made by the team based on qualitative assessment of double-well simulation results.

## 3. Single-well push & pull configuration

Because of the potential low thermal recovery efficiency of double-well pair configuration, we performed sensitivity simulations for single-well push-pull reservoir configuration for various scenarios. We consider a daily injection-pumping cycle scenario in which solar-heated water is injected into the reservoir for 8 hours with injection rate of 40 kg/s and 250°C. After 8 hours injection of solar heated water, a 10-hour heat production stage starts by pumping out the previously injected hot water from the same well at a rate of 32 kg/s. After this heat-production stage, the well is shut off and the system relaxes for 6 hours before the next daily cycles starts. Based on the previous simulation results for double-well pair configuration, the well screen spans the entire formation thickness in order to minimize the buoyance effect and convective thermal energy loss.

Two scenarios of storage formation thickness, 20-meter and 100-meter, were considered in single-well push & pull configuration. Figure 4 shows the simulated temperature fields after 30 days of daily cyclic operations. It is very interesting to notice that for both storage formation thickness scenarios, the sizes of the thermally perturbed reservoir volume are very limited after 30 days of push-pull cyclic operations, within ~10-20 meters radial distance away from the wellbore.

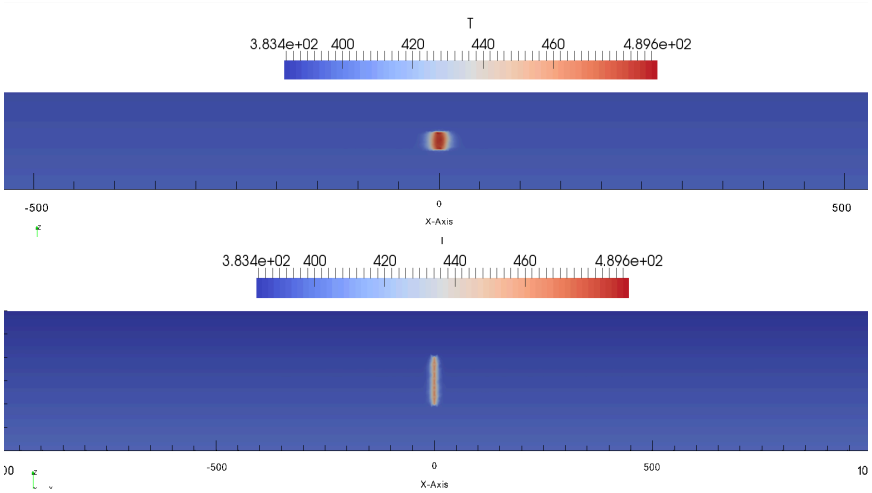

Figure A.4. The simulated temperature fields (in Kelvin) after 30-day push-pull daily cycle operations: the 20-meter thick storage formation (top); the 100-meter thick storage formation (bottom).

Figure 5 shows the simulated temperature variations of water inside the well screen interval over the 30 days of push-pull operation for two different formation thickness scenarios. During each daily cycle, the rapidly rising part of the curve represents the day time injection of solar heated water, while the declining part of the curve represents the temperature of produced water. For both scenarios, during the first a few days of push-pull operations, large daily temperature variations of produced water were observed. However, such large variations dampen out as the operation continues, but the temperature variations of the produced water is still significant after 30 days of operation, which might not be very beneficial for the power generations, where stable inlet temperatures are more desired.

Figure 6 shows the simulated wellbore pressure variations over the 30 days of single-well push-pull operation. For 20-meter thick storage formation case, the maximum wellbore injection pressure at the injection rate of 40 kg/s reaches above ~16.4 MPa, while the maximum injection pressure for the 100-meter thick storage formation case is ~12.9 MPa.

The simulations of single-well push-pull configuration clearly indicate that it is a viable solution for GeoTES concept, and a relatively thick storage formation is more preferred in order to lower the injection wellbore pressure for minimizing he hydraulic fracturing risk associated with the injection. The relatively large temperature variations of the produced water after 30 days of operations also indicate that better well configuration and production strategies would be needed.

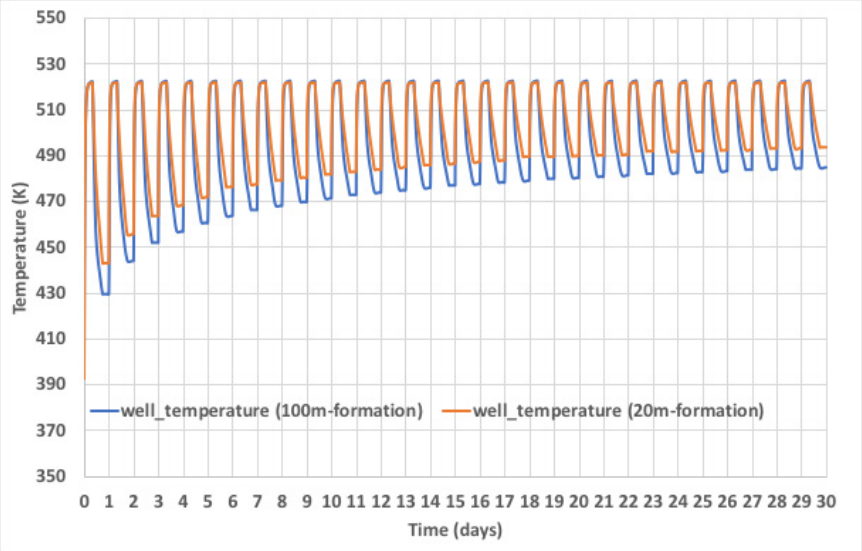


Figure A.5. The simulated water temperature variations inside the well screen interval for two formation thickness scenarios.

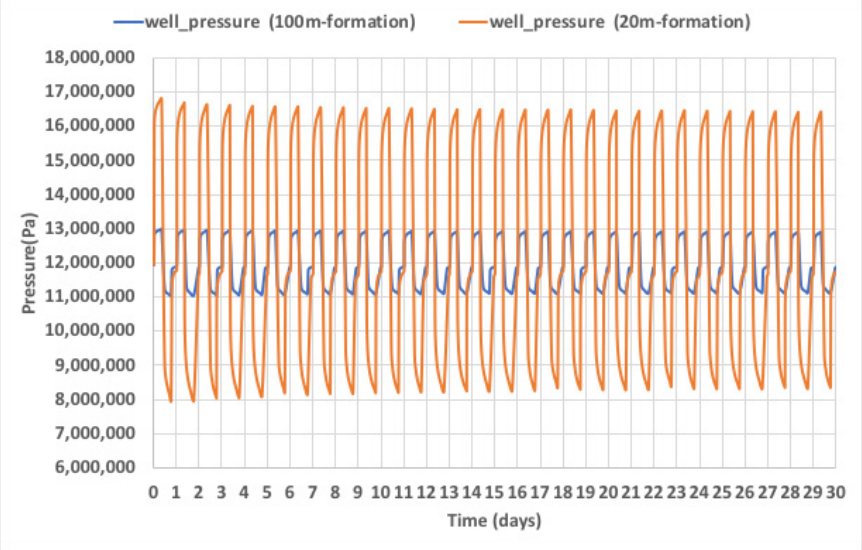


Figure A.6. The simulated wellbore pressure inside the well screen interval for two formation thickness scenarios.

## 4. Five-spot well push & pull configuration

Based on the simulation results of single-well push & pull configuration, the team designed a five-spot push & pull configuration for GeoTES operations for storing solar-heated water, as shown in Figure 7. We consider a daily injection-pumping cycle scenario in which solar-heated water is injected into the reservoir via hot wells (red in Figure 7) for 8 hours with injection rate of 40 kg/s and 250°C. During this solar-heated water injection stage, same volume of "cold" reservoir water is pumping out from cold wells (blue in Figure 7) at the same rate. This "cold" reservoir water will be solar-heated. After 8 hours injection of solar heated water, a 10-hour heat production stage starts by pumping out the previously injected hot water from "hot" wells at a rate of 32 kg/s. During this heat production stage, the same amount of "exhausted" water (assumed 70°C temperature) is injected back to the reservoir via cold wells.

After this heat-production stage, all wells are shut off and the system relaxes for 6 hours before the next daily cycles starts. The initial reservoir temperature at the middle of the injection formation was chosen to be 50°C following an average geothermal gradient of 25°C per kilometer. Unlike all previous simulations in which the initial reservoir temperature is at 120°C by assuming the reservoir is located at an existing geothermal field, we chose a lower initial reservoir temperature of 50°C in order to more realistically evaluate the thermal recovery efficiency of GeoTES reservoirs. The initial pressure at the middle of the injection formation was set to 12 MPa, according to a hydrostatic pressure distribution, similar to all previous simulations.

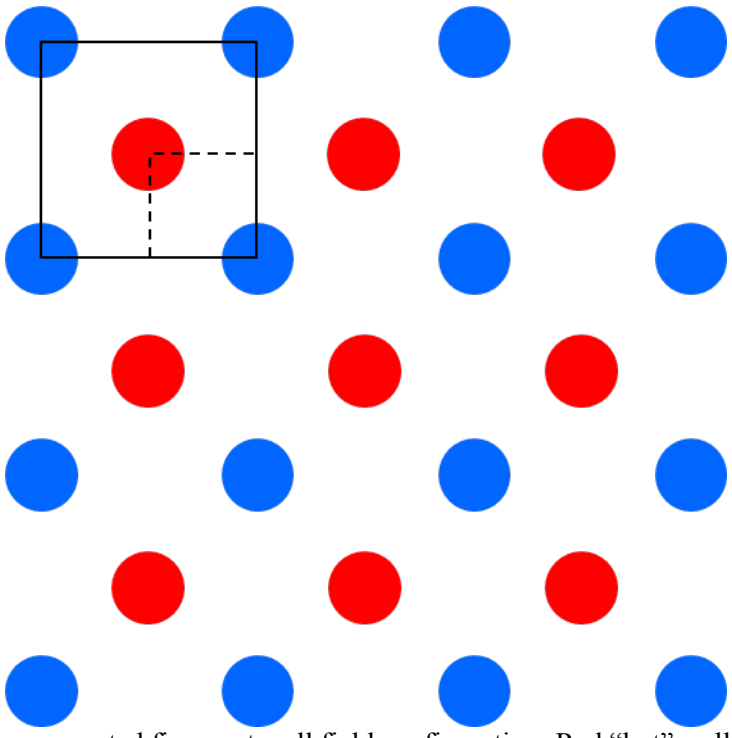

Figure A.7. This shows a repeated five-spot well field configuration: Red "hot" wells denote where solar-heated hot water is injected and produced later; blue "cold" wells are where reservoir fluid is produced for solar heating and "exhaust" water after power generation is injected back to the reservoir. The solid square represents a single five-spot "tile" in which there is a net total of one hot well and one cold well.

In the simulations, the model domain takes advantage of the symmetry condition of the 5-spot well pattern and only considered one hot-cold well pair, located at opposite corners. Figure 8 shows the finite element mesh used in the simulations. The mesh is refined near injection wells. One alternative injection-pumping strategy is to thermally "charge" the reservoir for a period of time before the daily injection-production operation cycle starts. In such scenario, the solar-heated water will be injected into the reservoir via hot wells for 8 hours every day, but no follow production of heated water. Figure 7 shows the temperature field after a 6-month 'thermal charging". It is interesting to observe after 6-month "thermal charging", the conductive heat transfer into the over- and under-burden rocks are negligible.

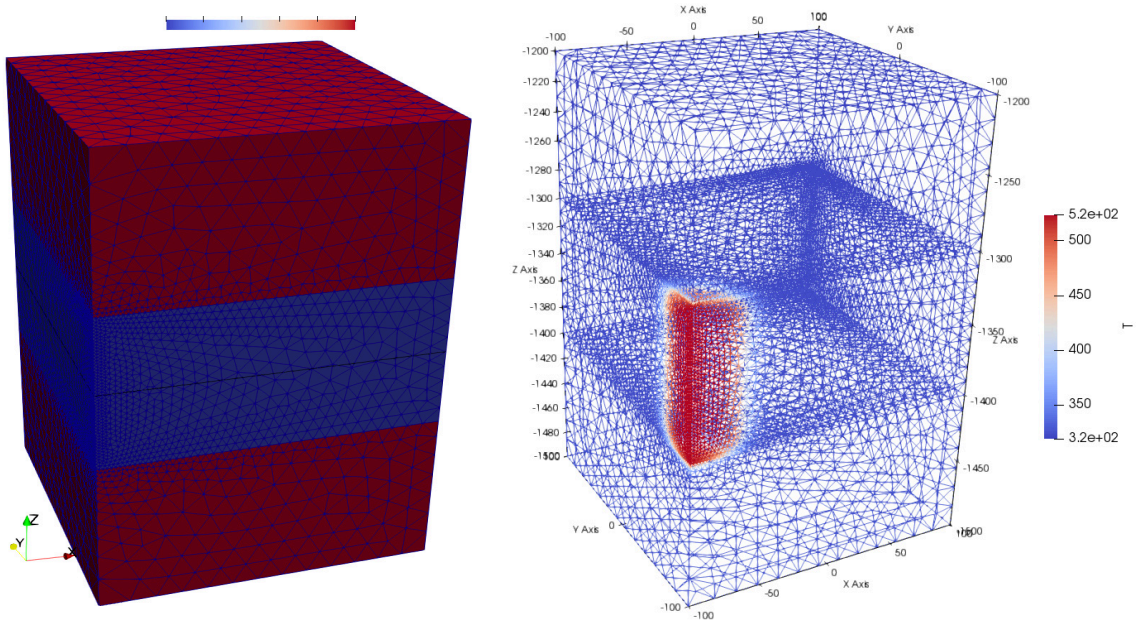


Figure A.8 Finite element mesh used in the simulations (left); Temperature field (in Kelvin) of the reservoir after 6-month of "thermal charging" by injection of solar-heated water of 250°C at 40 kg/s for 8 hours each day (right).

One important factor for the effectiveness of subsurface heat storage is the temperature of produced water from "hot" wells and potential temperature declines after continuous operation. Figure 9 shows the simulated temperature variations of water at the "hot" well over a 30-day period of continuous injection-production operation cycles for various "thermal charging" scenarios. It is interesting to observe that for the case of no "thermal charging" at all, initially large temperature oscillations are observed initially, but the oscillation starts to decrease gradually over the injection-production cycles, with oscillation of ~50 degrees after 30 days, and continuously decreasing. For the case of 180-day (6-month) "thermal charging" scenario, the temperature oscillation is minimum, within ~2-3 degrees over the 30-day injection-production cycles.

These initial simulation results clearly indicate that the subsurface could be used as a very good candidate for heat storage, and the push-pull injection/pumping strategy could be very promising for coupling underground solar heat storage with power plants.

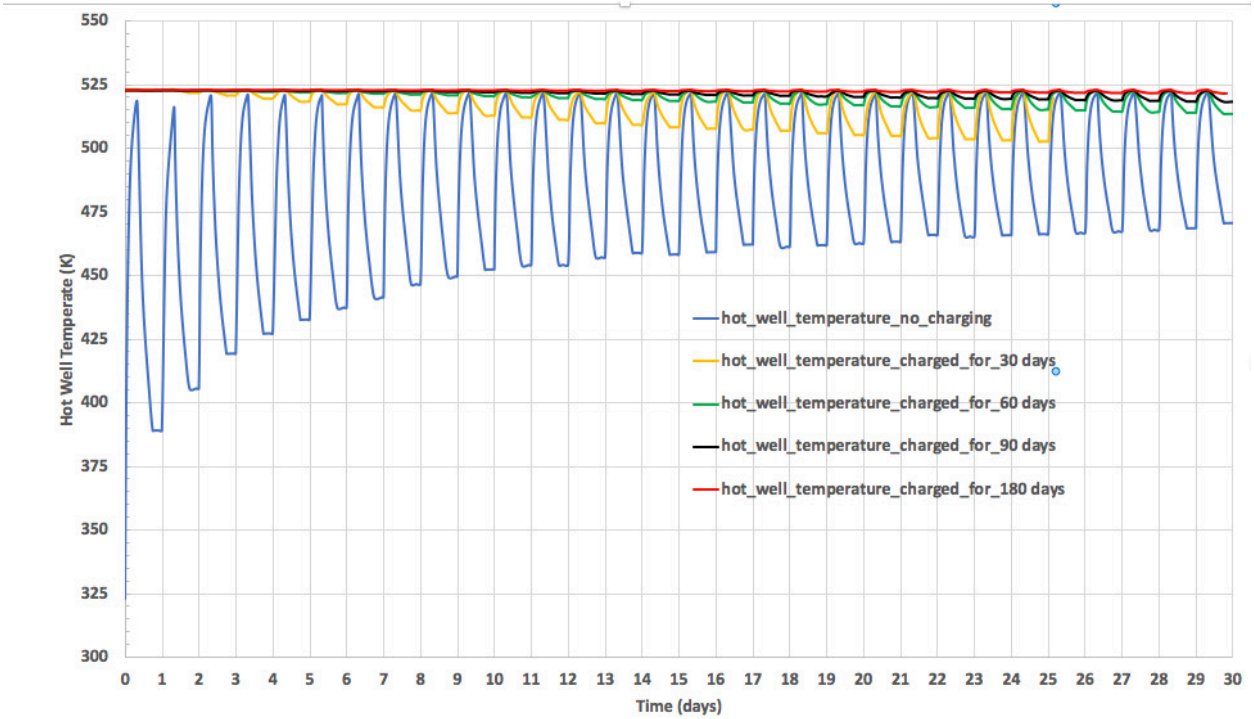

Figure A.9. Simulated temperature variations of water at the "hot" well over a 30-day period of continuous injection-production operation cycles for various "thermal charging" Scenarios.

**6. Conclusions**

- These initial simulation results clearly indicate that the subsurface could be used as a very good candidate for heat storage, assuming a "good" quality reservoir with relatively high permeability and porosity.
- A five-spot well pattern with dedicated hot and cold wells operated using a push-pull strategy provides (1) the ability to immediately recover stored hot fluid from the GeoTES reservoir, (2) a practical approach for managing the system fluid inventory, and (3) reduced parasitic load. Pressure support is provided by the wells operating in "push" mode to the wells operating in "pull" mode.
- Initial charging of the GeoTES system increases the heat recovery temperature. Increasing the duration of the charging period decreases the magnitude of the temperature fluctuations that occur following prolonged system operation.
- The current sensitivity studies didn't consider the effects of geochemistry and potential mineral precipitation and dissolutions on the wellbore injectivity and reservoir permeability/porosity.
- Current simulations didn't considere the geomechanical response and thermal stress variations during the operations of GeoTES reservoirs, which are expected to be significant.
- Fully coupled thermal-hydro-mechanic-geochemical (THMC) multiphysics simulations of GeoTES operations with more representative geological, hydrogeological settings are highly recommended for more comprehensive sensitivity studies.

# Appendix B

# Power Cycle Analysis

## 1. System description

Figure B.1 shows the schematic for geothermal energy storage (GeoTES). The main components include power block, solar collector and the geothermal storage. The solar field uses parabolic trough collector, and oil (Therminol VP-1) as the heat transfer fluid. The geothermal working fluid is water. During charging cycle the oil gets heated in the parabolic trough collector and in sent to the heat exchanger for heating the cold water coming from the cold geothermal storage, and is sent to the hot geothermal well. The cooled oil is sent back to the parabolic trough collector. During the discharging cycle, the hot water from the hot geothermal well is extracted and is sent to the power block for producing power. The water comes out cold from the power block and is sent to the cold geothermal storage.

It can be noted the power plant also operates like a normal concentrating solar thermal power plant. Where the hot water coming out from the heat exchanger is directly used to run the power cycle, and any additional hot brine is send to the GeoTES.

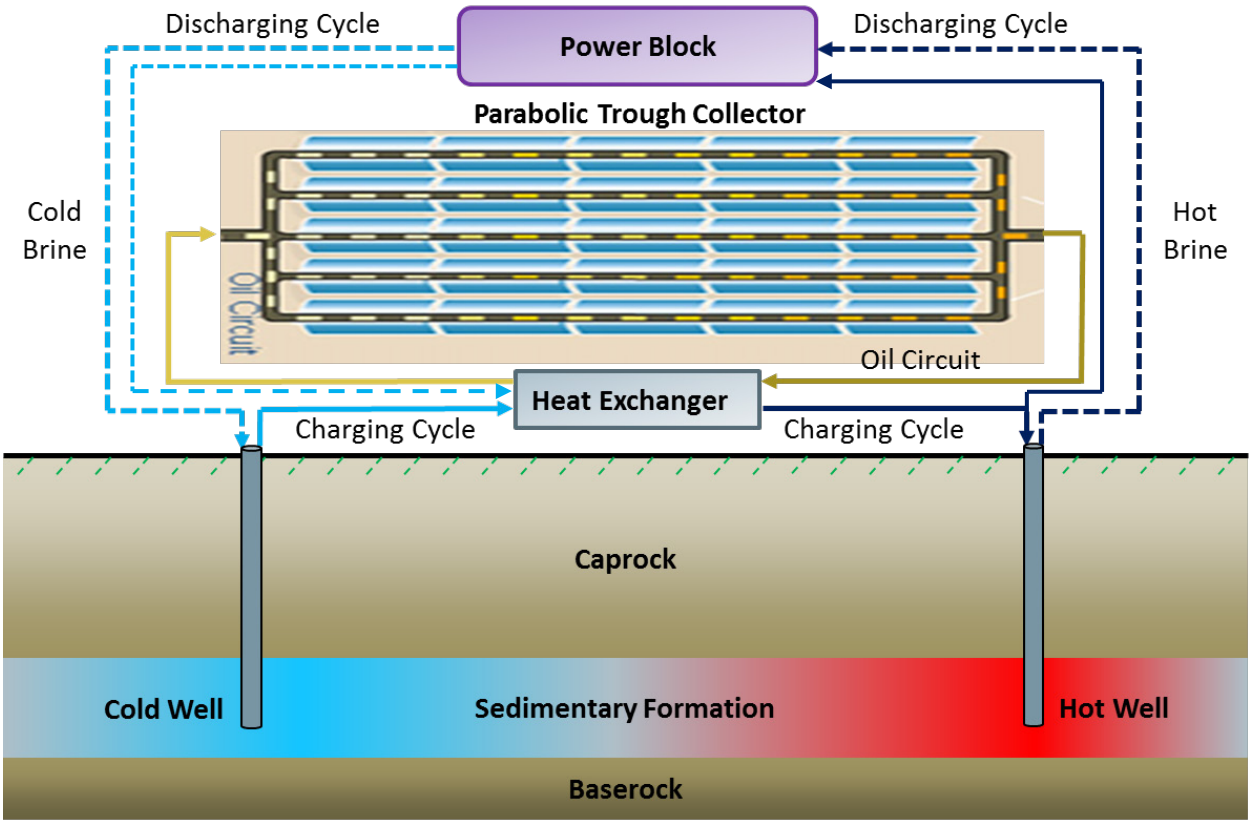


Figure B.1: Schematic for the geothermal storage

For present analysis 3 different power cycle options are considered and are as following:

- Single-stage flash steam turbine
- Single-stage flash steam turbine + simple organic Rankine cycle (ORC)
- Single-stage flash steam turbine + ORC with recuperator
- Single-stage flash steam turbine + ORC with mixing of working fluid
- Two-stage flash steam turbine

### 1.1. Single-stage flash steam turbine

Figure B.2 shows the schematic for single stage flash steam turbine integrated with the geothermal thermal storage. The hot water from the hot geothermal storage is extracted and is flashed in the flash at 160°C. This results to production of vapor and saturated water at 160 °C. The vapor produced because of flashing is used to run the turbine and generate electricity. The vapor coming out from the steam turbine is cooled in an air-cooled condenser (ACC). The cooled water at 39.5°C is pumped back the pressure corresponding to the flash tank pressure and mixed with the saturated water coming out from the flash tank. The mixed water is further pumped back at pressure of 50 bar and is sent back to the cold geothermal storage.

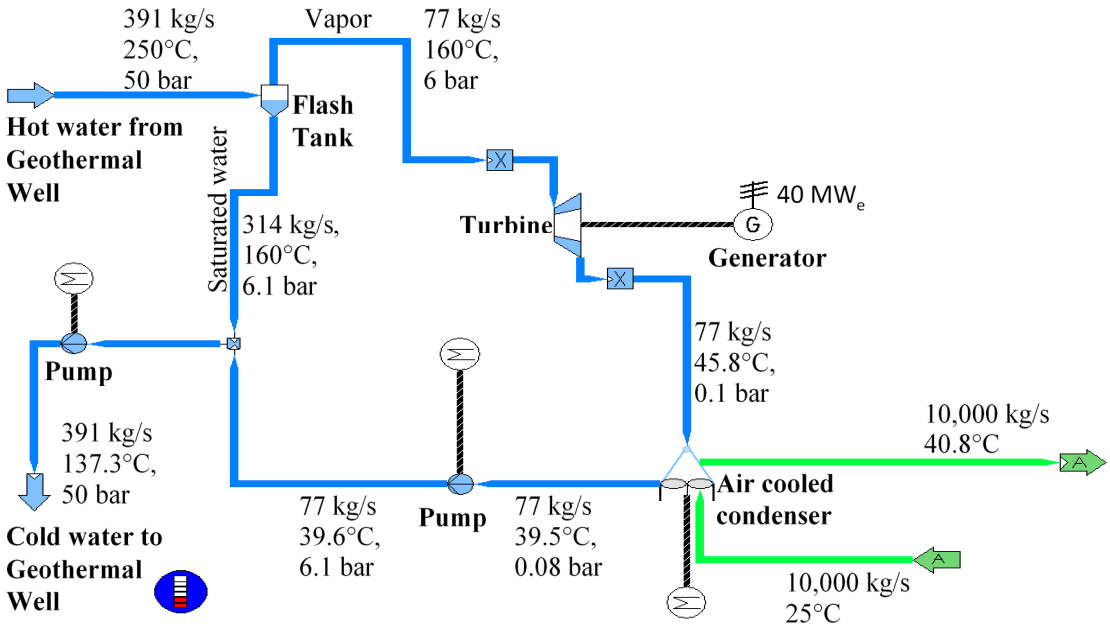


Figure B.2: Schematic of single stage flash steam cycle integrated with geothermal storage

### 1.2. Single-stage flash steam turbine + simple ORC

Figure B.3 shows the schematic for single stage flash steam cycle and simple organic cycle (ORC) integrated with the geothermal storage. The steam cycle is similar to the one explained in Figure B.2. The saturated water coming out from the flash tank acts as a heat source for the brine evaporator, where the ORC fluid gets evaporated. The working fluid used in the ORC is isopentane. The vaporized isopentane leaves the evaporator at dryness fraction of 1 and is used to run the turbine for electricity generation. The isopentane leaving the turbine is cooled in the air-cooled condenser. The cooled iso-pentane is pumped back to the ORC evaporator. The water flowing back to the geothermal storage is at significantly lower temperature compared to single stage flash steam turbine.

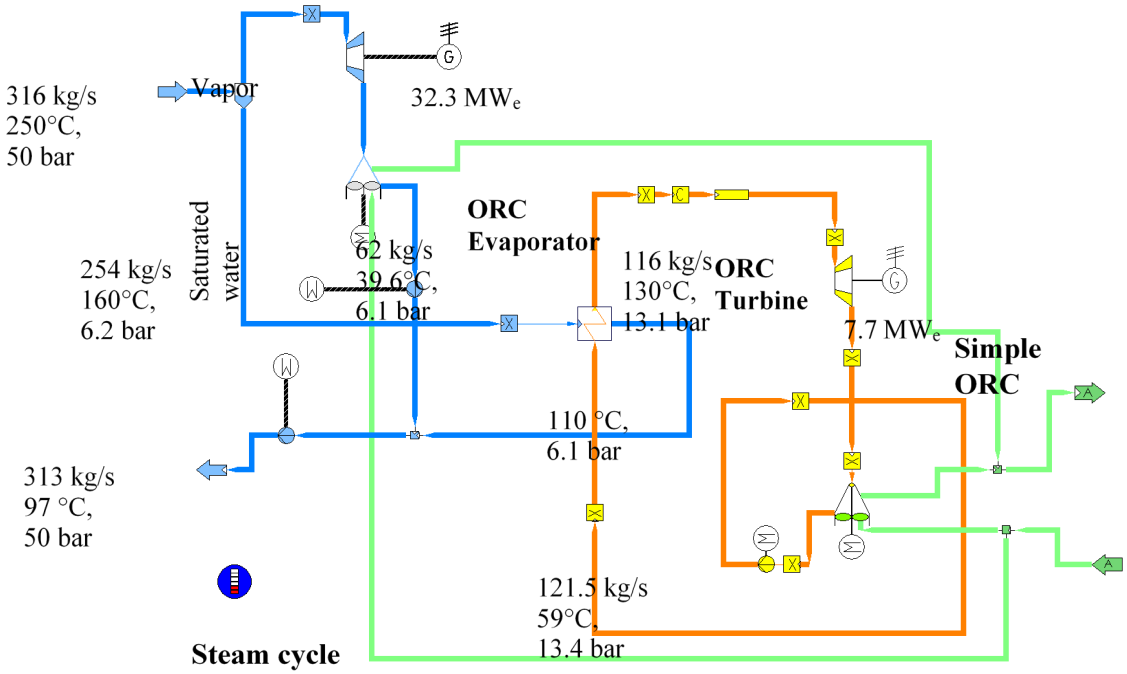


Figure B.3: Schematic of single stage flash steam cycle and simple ORC integrated with geothermal storage

### 1.3. Single-stage flash steam turbine + recuperative ORC

Figure B.4 shows the schematic for single stage flash steam cycle and recuperative organic Rankine cycle (ORC) integrated with GeoTES. To improve the performance of ORC, a recuperator is used to extract the waste heat from the working fluid exiting the turbine, and is shown in. This increases the temperature of isopentane entering the ORC evaporator.

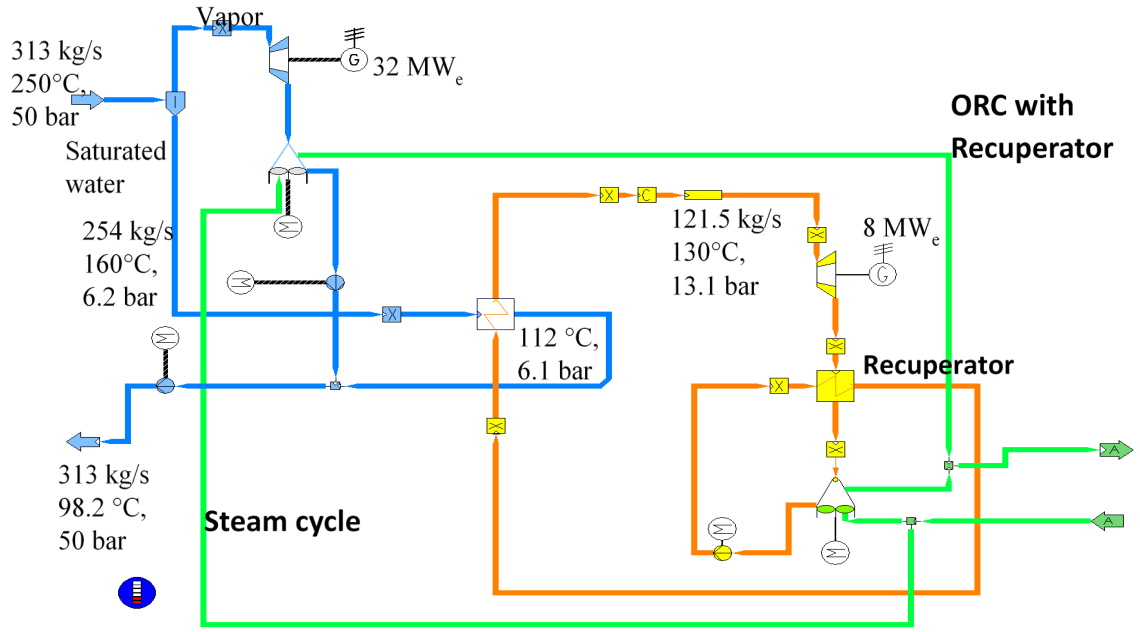


Figure B.4: Schematic of single stage flash steam cycle and recuperative ORC integrated with geothermal storage

### 1.4. Single-stage flash steam turbine + ORC with mixing of working fluid

The working fluid (isopentane) exiting the ORC turbine has significant amount of super-heating. To recover this superheat, the working fluid exiting the turbine 1 is mixed with  mixed with  working fluid (at same temperature as the turbine 1 exit, and at saturated liquid state) to produce saturated vapor with dryness fraction of 1. This in turns flows into turbine 2 to produce additional power. Please refer Figure B.5. To improve the performance of ORC, a recuperator is used to extract the waste heat from the working fluid exiting the turbine, and is shown in Figure B.4.

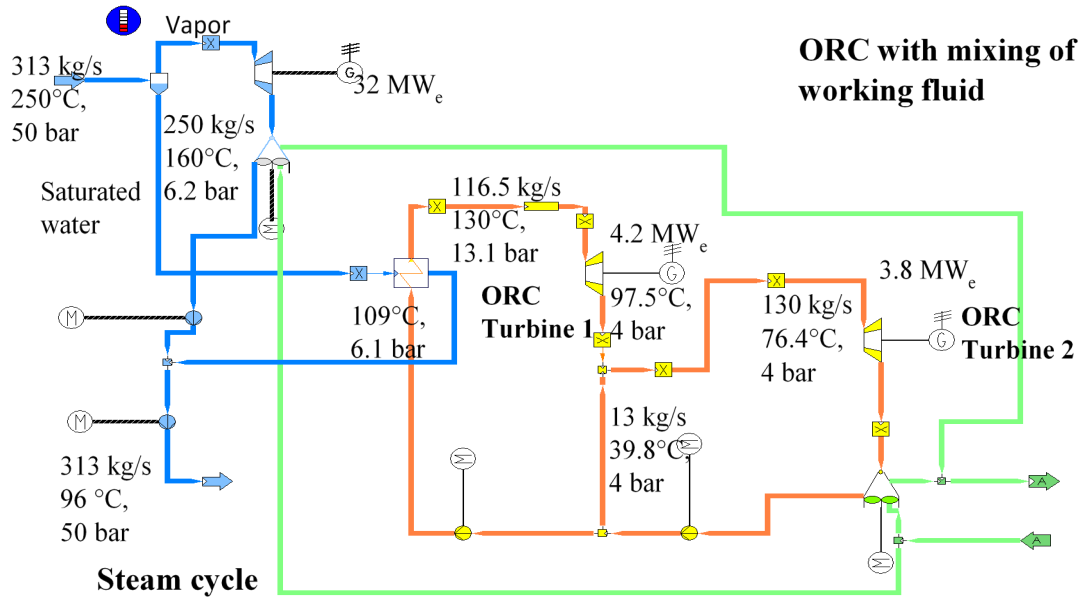


Figure B.5: Schematic of single stage flash steam cycle and ORC with mixing of working fluid integrated with geothermal storage

### 1.5. Double-stage flash steam turbine

The last cycle considered is double stage flash steam turbine. The saturated water coming out from the first stage is flashed in the second flash tank to produce additional vapor which is used to drive the second steam turbine and is shown in Figure B.6. This helps in reducing the mass flowrate of water.

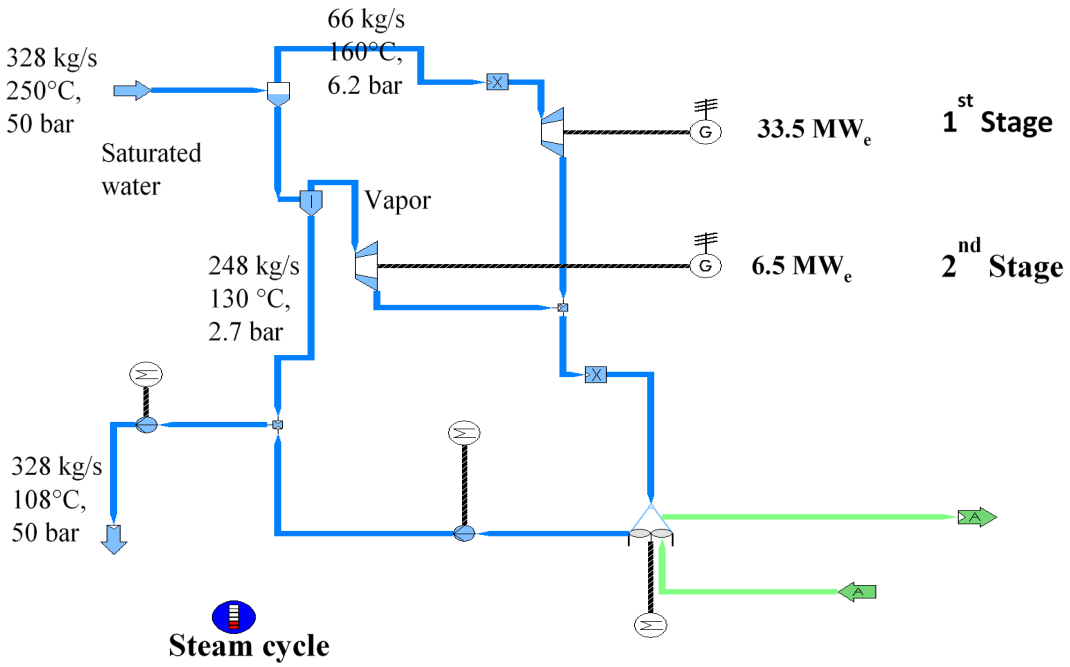


Figure B.6: Schematic of double stage flash steam cycle

## 2. Mathematical formulation

- Solar collector modelling:

The solar field uses parabolic trough collector (PTC) for heating the water. Various parameters used for modelling of PTC have been taken from NREL System Advisory Model (SAM 2017) . The optical efficiency for PTC is calculated as:

$$\eta_o = \gamma \cdot \rho \cdot \tau \cdot \alpha \cdot TE \cdot GA \cdot MC \cdot DE \cdot IAM \quad (1)$$

where $\gamma$ is the intercept factor, $\rho$ is the reflectance , $\tau$ is transmittance, $\alpha$ is the absorption, *TE* is the tracking and twist error, *GA* is the geometric accuracy, *MC* is the mirror cleanliness, *DE* is the dust on envelope, and *IAM* is the incident angle modifier and is a function of transversal and longitudinal angle. The net heat absorbed by the solar collector receiver per unit aperture reflective area ($\dot{q}_{abs}$) is:

$$\dot{q}_{abs} = \eta_o DNI \quad (2)$$

where DNI is the direct normal irradiance. The heat lost by the receiver per unit length ($\phi$) is calculated from (Burkholder and Kutscher 2009) and is given as:

$$\phi = 0.141 T_m + 6.48 \cdot 10^{-9} T_m^4 \quad (3)$$

where $T_m$ is the mean temperature and is gives as:

$$T_m = \frac{T_{oil,in} + T_{oil,in}}{2} - T_{air} \quad (4)$$

where $T_{oil}$ is the oil temperature and $T_{air}$ is the air temperature. The receiver heat loss can be converted to receiver heat loss per unit aperture reflective area ($\dot{q}_{rec}$) as:

$$\dot{q}_{l,rec} = \frac{\phi}{w} \quad (5)$$

where $w$ is aperture width for the PTC. The piping heat loss from piping are calculated from (SAM 2017) and is given as:

$$\dot{q}_{l,pipe} = 10 \cdot (0.001693 \cdot T_m - 1.683 \cdot 10^{-5} T_m^2 + 6.78 \cdot 10^{-8} T_m^3) \quad (6)$$

Net solar aperture reflective area at design point ($A_{solar,D}$) is:

$$A_{solar,D} = \frac{\dot{Q}_D}{\dot{q}_{abs} - \dot{q}_{l,rec} - \dot{q}_{l,pipe}} \quad (7)$$

where $\dot{Q}_D$ is the heat demand of the power cycle at design point. The power consumption for pumping the oil through the PTC circuit ($P_{oil}$) in $kW_e$ is:

$$P_{oil} = 5.19 \cdot \dot{m}_{oil} \quad (8)$$

In addition to prevent the oil from freezing in cold ambient condition, the oil must be circulated through the solar field. Antifreeze oil pumping power is considered to be 10% of the oil pumping power.

- Power cycle Model

The model for power cycle was developed in SimTech IPSEpro. The heated water coming out from the geothermal storage, first gets flashed in the flash tank to produce vapor and saturated water. The flash tanks are assumed to be isenthalpic with an separation efficiency of 100% (Mctigue et al. 2018). For modelling out power cycle, a design point turbine isentropic efficiency of 85% is assumed, with a generator efficiency of 98%. For off design analysis the off-design turbine efficiency profile is calculated from data atlas Copco steam turbine performance.

For air cooled condenser a pressure drop ($\Delta P$) of 150 Pa for the air side is assumed. The net pumping power for the ACC is given as:

$$P_{ACC} = \frac{\dot{m}_{air} \Delta P}{\eta_{isen} \eta_{motor}} \quad (9)$$

where $\dot{m}_{air}$ is the mass flowrate of air, $\eta_{ise}$ are the isentropic efficiency of fan and $\eta_{motor}$ is the isentropic efficiency of the motor. At design point $\eta_{ise}$ is 85% and $\eta_{motot}$ is 98%. For off-design of ACC the default fan efficiency profile in Ipsepro has been used.

- Cycle Efficiency

Let the gross power output from the power cycle be $P_{gross}$ and is defined as the power produced from the turbines in the power cycle. The net power supplied from the power cycle ($P_{net}$) is defined as the difference between $P_{gross}$ and the parasitic pumping power for the power cycle and is given as:

$$P_{net} = P_{gross} - P_{pump,ACC} - P_{pump,GeoTES} \tag{10}$$

The efficiency of the power cycle ($\eta$) is given as:

$$\eta = \frac{P_{net}}{\dot{m}_{w,f}\left(h_{in} - h_{out}\right)} \tag{11}$$

where,

$\dot{m}_{w,f}$ = mass flow rate of water into the flash tank

$h_{in}$ = enthalpy of hot water entering the power cycle (250 °C and 50 bar)

$h_{out}$ = enthalpy of cold water leaving the power cycle

- Heat Exchanger

Conductance ($UA$) of the heat exchanger is defined as the product of overall heat transfer coefficient and heat exchanger area. The commonly used correlation to predict the off-design performance of the heat exchanger is (Sharan et al. 2019):

$$\frac{UA_{design}}{UA_{off-design}} = \left(\frac{\dot{m}_{design}}{\dot{m}_{off-design}}\right)^{0.8} \tag{12}$$

where $\dot{m}$ is the mass flow rate.

- Annual simulation

An 8760 data point simulation is carried to predict the annual performance of the system. For any time interval $i$, the heat supplied from the solar field ($\dot{q}_{solar}[i]$) is given as:

$$\dot{q}_{solar}[i] = SM \cdot A_{solar,D}\left(\dot{q}_{abs}[i] - \dot{q}_{l,rec}[i] - \dot{q}_{l,pipe}[i]\right) \tag{13}$$

where $SM$ is the solar multiple and is defined the ratio of solar-field delivered power at design point ($MW_{th}$) to heat demand by the power block at design point ($MW_{th}$). Net mass of hot water produced ($\dot{m}_{w}[i]$) is given as:

$$\dot{m}_w[i] = \frac{\dot{q}_{solar}[i]}{h_{in} - h_{out}} \tag{14}$$

Amount of water flowing into the hot geothermal well ($\dot{m}_{w,geo}$) is:

$$\dot{m}_{w,geo}[i] = \dot{m}_w[i] - \dot{m}_{w,f}[i] \tag{15}$$

Volume of water stored in the hot GeoTES, $V_w[i]$ is:

$$V_w[i] = V_w[i-1] + \frac{3600 \cdot \dot{m}_{w,geo}[i]}{\rho_w} \tag{16}$$

where $\rho_w$ is the density of the water and term 3600 is used to convert kg/s to kg/h. The power delivered by the power cycle is a function of $\dot{m}_{w,f}$ and $T_a$. Annual electricity generation from the system ($E$) is given as:

$$E = \sum_{i=1}^{i=8760} \left( P_{gross,\text{annual}}[\text{i}] - P_{pump,ACC}[i] - P_{pump,GeoTES}[i] - P_{oil}[i] \right)$$

Number of hot geothermal wells required ($N_{\text{hot well}}$) is:

$$N_{hot\,well} = \frac{\max\left(\dot{m}_{w,geo}[i]_{i=1}^{8760}\right)}{\dot{m}_{w,well,max}} \tag{17}$$

where $\dot{m}_{w,well,max}$ is the maximum allowable mass flow rate of water per well. Since the present model considers a two-tank hot geothermal storage, an equivalent number of cold well will be required. The other important parameter term commonly used while designing of CSP power plant is the hours of storage ($H$) and is defined as number of hours the power plant can be operated during non-solar period at full load, and is given as:

$$H = \frac{max(V_w[i]_{i=1}^{8760})}{\frac{3600 \cdot \dot{m}_{w,f,D}}{\rho_w}} \tag{18}$$

- Economic Analysis

The total capital cost ($C_{capex}$) for the system includes solar field cost, power block cost, geothermal well cost, contingency cost and indirect cost. The operation and maintenance cost (O&M) for the system includes solar O&M, replacement cost geothermal pump and maintenance/replacement for the well. For $E$ annual electricity generation, the levelized cost of electricity (LCOE) is:

$$LCOE = \frac{FCR \cdot C_{capex} + O\&M}{E} \tag{19}$$

where FCR is the fixed charge rate and is defined as the revenue per unit of investment that must be collected annually to pay for the carrying charges of the investment (Mctigue et al. 2018).

## 3. Illustration

Table 1 shows the input parameters for the system design. For present analysis, Las Vegas, Nevada is selected as potential site for colocation of CSP-GeoTES plant, as it has good solar resource (annual average beam radiation of 7.17 kWh/$m^2$/day) and sedimentary basin ideal for GeoTES system. The power cycle is designed to generate a gross electricity of 40 $MW_e$. Table 2 shows the various cost parameter used in the analysis.

Table B.1: Input parameter for system design

| | |
|---|---|
| Location | Las Vegas, Nervada |
| Gross electricity generation | 40 $MW_e$ |
| Hot water temperature leaving the solar field | 250 °C |
| Pressure of hot water leaving the solar field | 50 bar |
| Ambient air temperature at design point | 25 °C |
| Maximum injection mass flow rate | 40 kg/s |
| Isentropic efficiency for the turbine and pump | 85% |
| Air pressure drop in ACC | 150 Pa |

Table B.2: Input parameter for system design

| Component | Cost |
|---|---|
| Geothermal well cost | 0.75 M$/well |
| Cost of geothermal pump | 0.5 M$/pump |
| Cost of steam power block | 1.5 M$/$MW_e$ |
| Cost of ORC power block | 2 M$/$MW_e$ |
| O&M for solar | 7.4 $/$kW_{th}$/year |
| O&M geothermal and power block | 131 $/$kW_e$/year |
| O&M geothermal pump | 40,000 $/year |
| Maintenance/replacement of pump | 5% of capital cost for 25 years |
| Discount rate | 5.5 % |
| Analysis period | 25 years |

- **Off Design performance curve**

Figure B.7 shows the gross electricity generation and the mass of water required with ambient temperature. The power cycle is modelled in such a way that the temperature of water leaving the system remains constant irrespective of the ambient temperature. The design point ambient temperature of 25 °C is assumed. For low ambient temperature, the condenser operating pressure decreases, and this reduces the mass flowrate of water required and increases the system efficiency. For higher ambient temperature, the condenser operating pressure decreases, resulting in decrease in efficiency and decrease in power production the power cycle. It is interesting to note the decrease in mass flowrate for ambient temperature greater than 25 °C, this is because the water temperature leaving the power cycle is maintained constant.

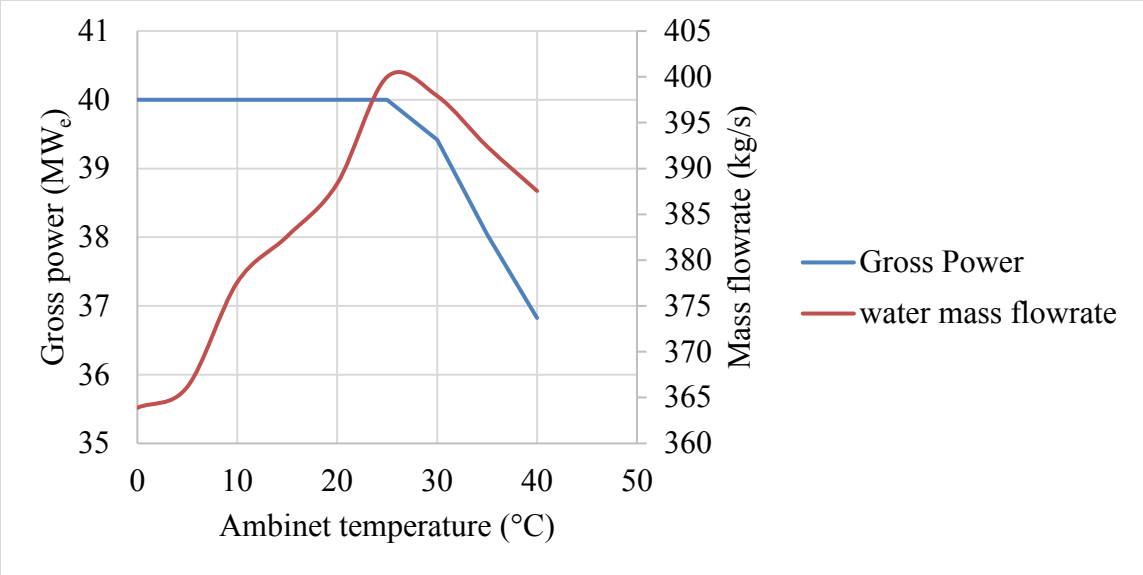

Figure B.7: Variation in water mass flowrate and gross power with ambient temperature

- **Flash temperature**

The power cycle performance is directly dependent on the flash temperature. Higher the flash temperature higher the power production from the power cycle (based on second law of thermodynamics). Figure B.8 shows variation in cycle efficiency and mass of water required with different flash temperature. The cycle efficiency for 1-stage flash cycle increases as the flash temperature is increased, this is due to efficient cycle performance at higher temperature. However, with increase in flash temperature the net temperature difference for vapor flashing decreases and this increases the mass flowrate of water required. For flash temperature ($T_{f1}$ = 160 °C), the mass flowrate of water flowing into the steam turbine is 390 kg/s whereas $T_{f1}$ = 240 °C, the mass flowrate of water required is around 2040 kg/s. With increase in flash temperature the water pumping power requirement for the cycle increases proportionally to the water flow rate and this reduces the net power generation. The cycle attains a maximum efficiency of around 24% with water mass flowrate of 1085 kg/sec for 1-stage flash cycle for $T_{f1}$ = 230 °C.

In 2-stage flash cycle because of presence of second flash tank, the water coming out from the first flash tank can be further flashed to produce additional power, and this curtails the rate of increases in water flow. For 2-stage flash tank the water flow increases from 328 kg/s to 600 kg/s. The maximum cycle efficiency is achieved at 240 °C. While modelling 2-stage flash cycle, the second flash tank was operated at 30 °C temperature lower than the first flash tank.

For 1-stage flash + recuperative ORC cycle, the water mass flowrate requirement is somewhat similar to 2-satge flash cycle for $T_{f,1}$, but cycle efficiency is on the lower side. The ORC cycle needs an additional pump to compress the working fluid, which is a parasitic load for the power cycle. So, the efficiency for ORC turbine is lower than the 2$^{nd}$ stage flash steam turbine. With increase in flash temperature, the ORC operating temperature also increases, resulting to increase in cycle efficiency till $T_{f1}$ = 220°C and then starts to decrease. The ORC uses isopentane as the working fluid for the ORC cycle, and it has a critical temperature of 187 °C and the maximum temperature the ORC cycle can operate is 185 °C. Therefore, for any further increase in flash temperature the ORC performance does not improve, but the mass flowrate of water required increases and this results to reduction in cycle efficiency. The mass flowrate of water required for 1-stage flash + recuperative ORC cycle is higher than 2-stage flash cycle, because of lower

thermal efficiency of the power cycle. It can be noted while modelling of 1-stage flash + recuperative ORC cycle, the temperature of water leaving the ORC was 30 °C lower than the flash tank temperature.

The efficiency trend for 1-stage flash steam cycle + simple ORC and 1-stage flash + ORC with isopentane mixing follow a trend exactly similar to recuperative ORC one, but there efficiency in on the lower side, resulting in higher mass flowrate of water required compared to recuperative cycle.

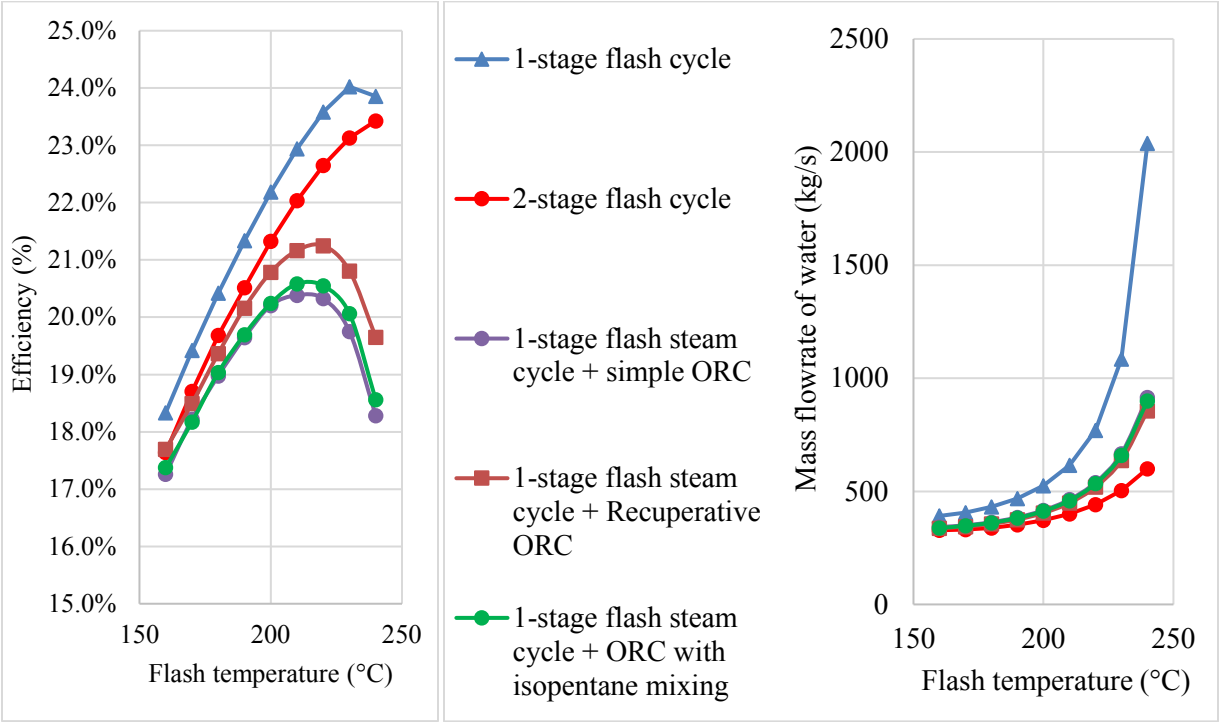


Figure B.8: Variation in cycle efficiency and mass flowrate with flash temperature

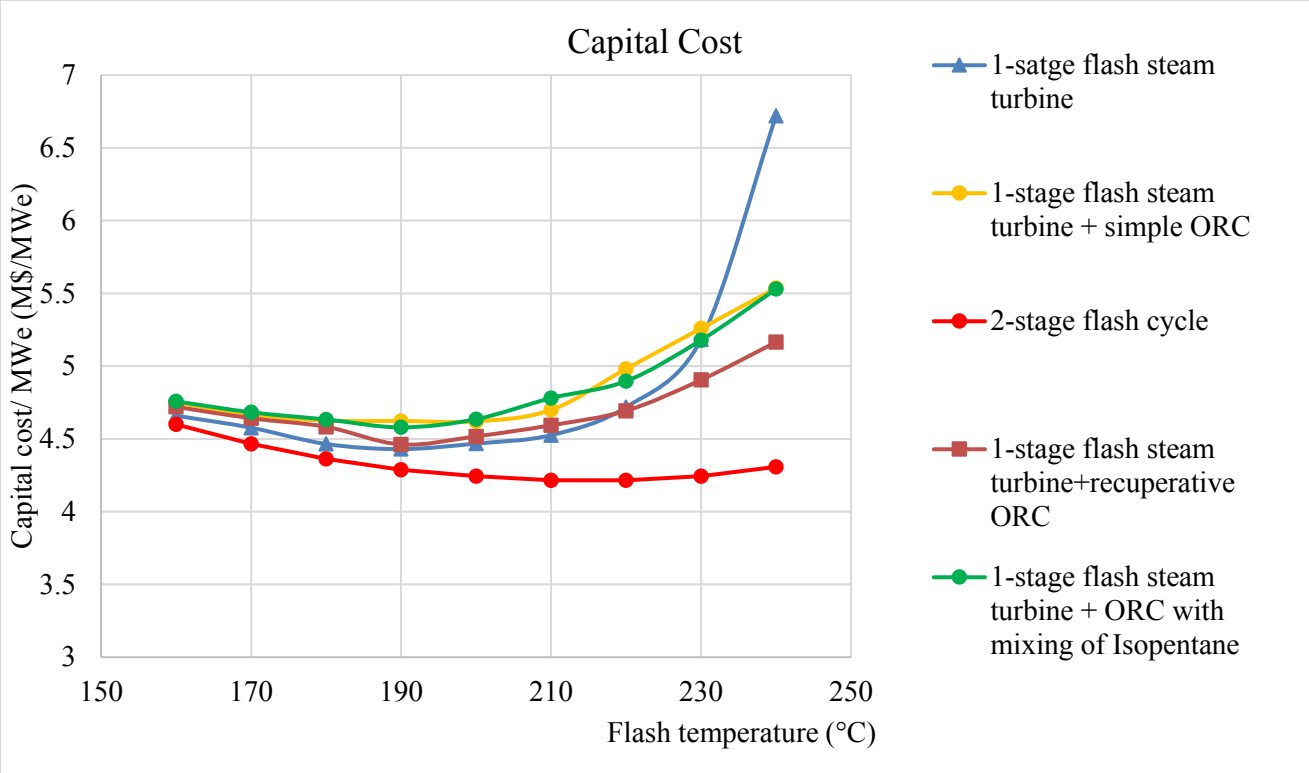

Figure B.9: Variation in capital cost for unit electricity generation

Figure B.9 shows variation in the capital cost for unit electricity generation with first stage flash temperature. The temperature of water leaving the 2nd flash tank (2-stage flash cycle) or water leaving the ORC heat exchanger (1-stage flash + recuperative ORC) is optimized to minimize the capital cost for unit electricity generation. The capital cost has been optimized assuming $SM$ = 2. The capital cost for the 2-stage flash cycle is lowest among the three-cycle considered. The optimal values for flash temperature for 2-stage flash cycle comes out to be 210°C and 180°C, with a capital cost of 4.2 M$/MW$_e$. Table 2 summarizes the optimal working parameters for the different power cycle for minimum capital cost for unit electricity generation. An interesting thing to note here is the temperature of water entering the cold geothermal well is significantly higher when compared to traditional geothermal power cycle (which is around 60°C). This is because in present GeoTES system the cold water entering the cold geothermal well is reused in comparison to traditionally used geothermal power cycle where it is rejected as waste heat.

Table B.3: Optimal system parameters for different power cycle

| | Flash Temperature (°C) | Capital cost/$MW_e$ (M$/$MW_e$) | Number of wells | $T_{cold\ well}$ (°C) | $A_{solar}$ (x$10^5$ $m^2$) | $\eta$ (%) | Net Power ($MW_e$) |
|---|---|---|---|---|---|---|---|
| 1-stage flash cycle | 190 | 4.4 | 12 | 171 | 5.7 | 21.3 | 36.1 |
| 2-stage flash cycle | 210, 180 | 4.2 | 10 | 159.3 | 4.9 | 22.2 | 36.5 |
| 1-stage flash cycle + simple ORC | 190, 166 | 4.6 | 10 | 149.2 | 5.4 | 19.8 | 36.0 |
| 1-stage flash cycle + Recuperative ORC | 190, 155 | 4.5 | 9 | 140.1 | 5.2 | 20.3 | 36 |
| 1-stage flash cycle + Recuperative ORC | 190, 167 | 4.6 | 10 | 150.4 | 5.3 | 19.6 | 35.6 |

From henceforth only 2-stage flash cycle will be analyzed since it has minimum capital cost for unit power generation.

- **Optimal Solar multiple**

Figure B.10 shows the variation in LCOE, capacity factor and number of operating wells with *SM*. As the solar multiple is increased from 1 to 2, the net mass of hot water coming out from the solar field increase and this increases the number of wells required from 1 to 12. Due to increase in thermal storage size the capacity factor for the power plant increases from 24% to 50% and this decreases the LCOE for the system from 16.9 cents/$kWh_e$ to 14 cents/$kWh_e$. The capacity factor for the power plant is defined as the ratio of net annual electricity generation to design point electricity generation. With increase in *SM* the capacity factor increases almost linearly up to *SM* = 3.8 to 97%. With further increase in *SM,* the capacity factor can reach 100 % but this is bot as the additional solar area will not be utilized throughout the year, whereas the number of hot wells required keeps on increasing due to increase in heat supplied from the solar field. This results in a minimum LCOE of 13.1 cents/$kWh_e$. The number of hot wells required is 32.

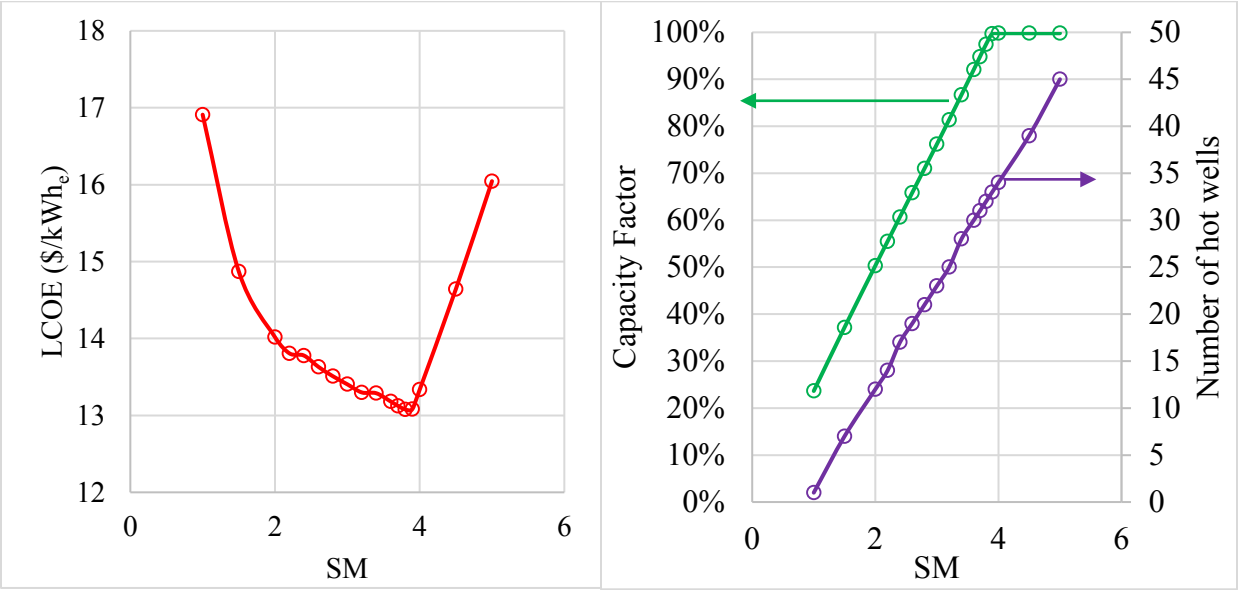

Figure B.10: Variation in LCOE, capacity factor and number of wells with solar multiple

- **Variation in hours of storage**:

The objective of this section is to calculate the optimal hours of storage (quantity of water) which would minimize the cost of electricity generation. Assuming the storage size is only 8 h, the capacity for the system is 46% with optimal solar multiple of 1.9 and number of wells required is 11 (as shown in Figure B.11), and has a LOCE of 14.9 cents/kWh$_e$. It can be noted for each hours of storage the LCOE is minimized to calculate optimal *SM*, *CF* and $N_{wells}$. As the hours of storage is increased, the amount of solar energy required to charge the system increases, resulting in higher solar multiple (3.8 for 2000 hours of storage). With higher hours of storage, the system moves from diurnal storage to seasonal storage and the excess energy available during summer can be utilized for winter. Because of availability of energy during winter, and the electricity generation during winter increases significantly and leading a higher capacity factor of 95% for 1000 hours of storage. Because of higher capacity factor the LCOE for the system reduces to a minimum value of 13.4 cents/kWh$_e$, for 1100 hours of storage. Any further increase in hours of storage does not give any additional reduction in LCOE because the additional solar area required to charge the system to increase the capacity factor remain un-utilized for maximum duration of the year, and hence solar multiple is fixed at 3.8 with minimum LCOE of 13.4 cents/kWh$_e$.

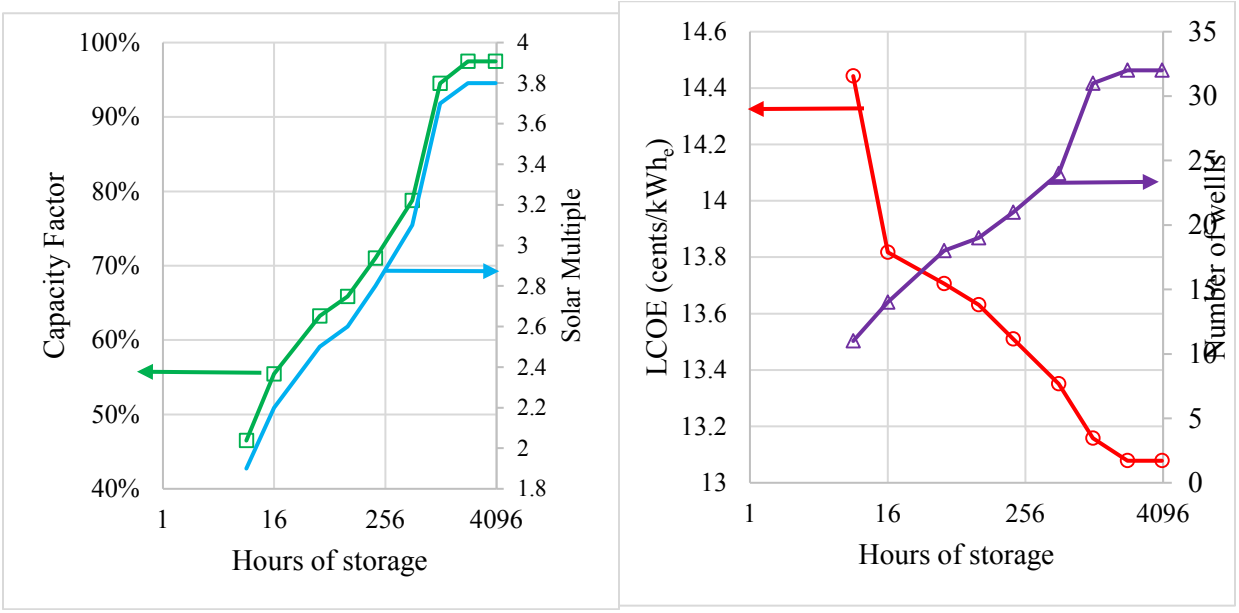


Figure B.11: Variation in capacity factor, solar multiple, LCOE and number of wells with hours of storage

- Hours of hot storage in winter and summer

Figure B.12 shows the storage and electricity generation for a week in summer. It is interesting to note that in peak summer condition the system can have more than 1000 hours of storage. This excessive storage is a seasonal storage and acts as a heat source during peak winter condition. The maximum hours of storage the system can have is 1100 hours and any further increase is solar multiple is not economical for electricity production. It can be noted that the electricity generation in peak summer can be slightly lower than design condition of 40 MW$_e$. This is because the high ambient weather conditions can deteriorate the performance of the power cycle and more over for operation and maintenance issue, the

turbine is not made to have higher mass flowrate of vapor than design condition and this further reduces the power cycle performance in peak summer.

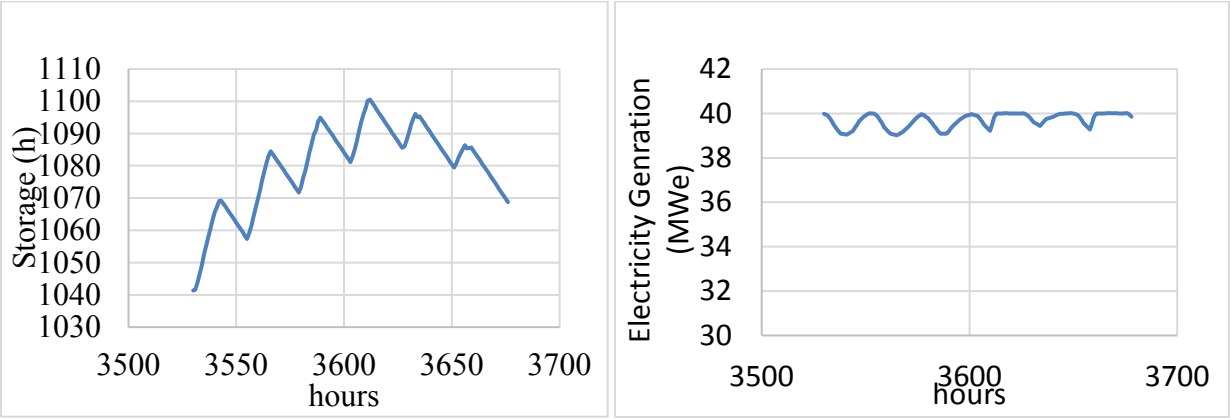


Figure B.12: Variation in net hot water storage capacity and electricity in peak summer

Figure B.13 shows the variation in hours of hot storage and electricity generation for a week duration in winter starting from mid of January. In winter due to poor solar radiation the hot storage can be charged maximum up to 15 hours and it discharges to a minimum value of zero hours. The electricity generation profile is kind of a histogram, where the system charges and discharges daily. In peak winter as well, the system generates electricity at full load for more than 80 %.

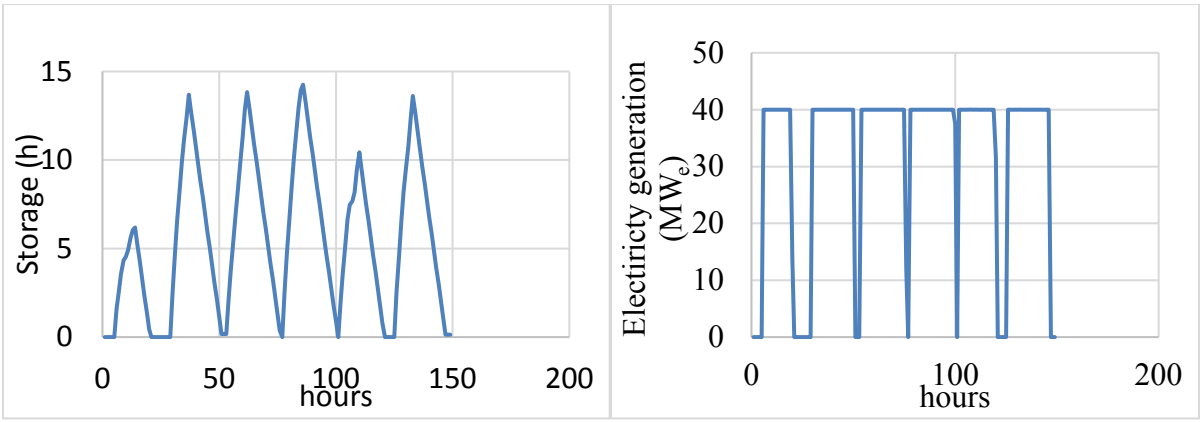


Figure B.13: Variation in net hot water storage capacity and electricity in peak winter

- Capital cost and LCOE

Figure B.14 shows the variation in capital cost and LCOE with 1100 hours of storage. The solar constitute about 53% of the total capital cost, followed by well cost (24 %) and power block cost (23 %). The minimum LCOE for the system is 13.4 cents/$kWh_e$. In LCOE the O&M cost constitute about 27% of the total cost. The reason for higher O&M cost is the low efficiency of the power cycle, due to lower operating temperature. The other two important cost parameters are solar cost (27%) and parasitic cost (22%). The reason for higher parasitic cost is also lower operating temperature which increases the air cooled condenser parasitic per unit power generation and higher mass flowrate of water required increases the GeoTES cost.

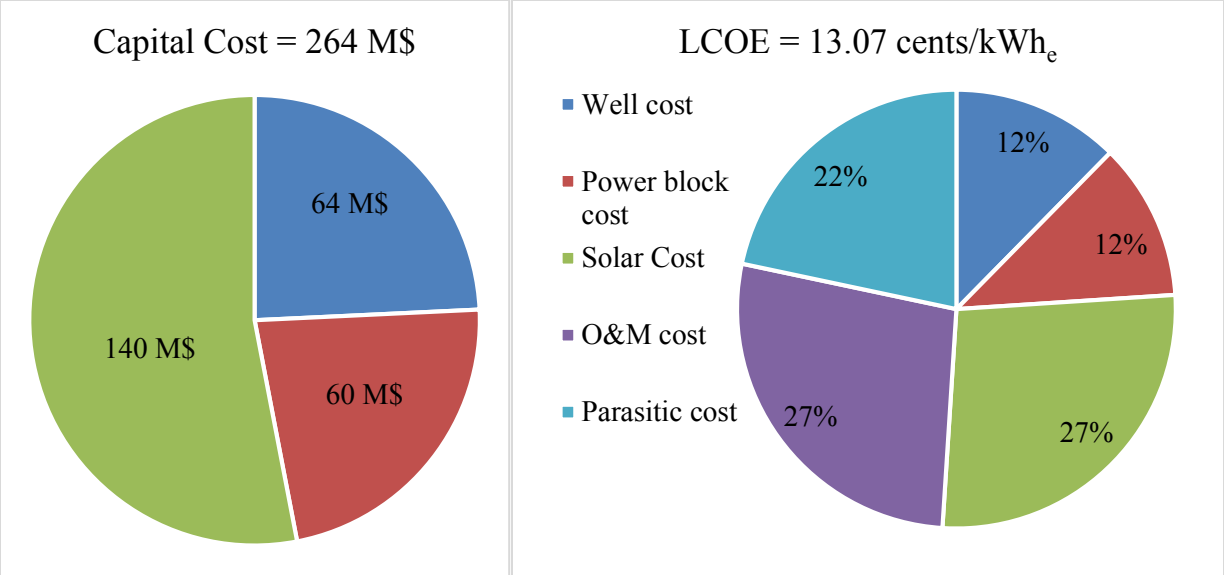

Figure B.14: Capital cost and LCOE bifurcation for the GeoTES system

- Non-solar period of operation

The LCOE for the system is on the higher side as compared to other renewable energy source (photovoltaics, concentrating solar power or wind energy). However, these technologies have very low capacity factor, whereas the proposed GeoTES can have about 100% capacity factor. One of the viable solutions can be produce electricity during day time using the commercially available renewable technology and during non-solar hours the electricity can be generated using GeoTES system.

Since in such a situation the GeoTES will be operated only for non-solar period, the capacity factor the power plant can achieve is around 64%. Moreover, in this case the entire heated water is first sent to the geothermal well, so this increases the number of wells required as well. The optimal solar multiple required is 2.5, as the power plant is operating during non-solar period. The minimum LCOE the system can achieve is 15.4 cents/kWh$_e$, with a capacity factor of around 64%.

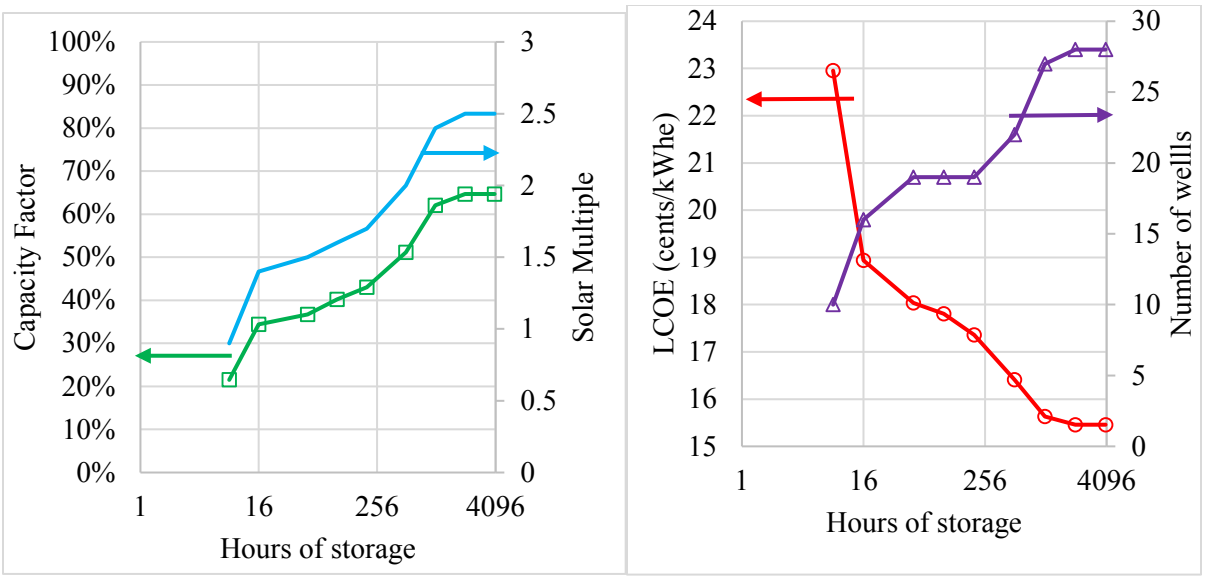

Figure B.15: Variation in capacity factor, solar multiple, LCOE and number of wells with hours of storage for non-solar period of operation

## 4. Sensitivity analysis

In this section the sensitivity of the GeoTES system to solar cost, power block cost, well cost, daytime pumping using photovoltaics for parasitic is considered.

### ○ Solar cost

As already discussed, the solar cost constitutes about 53% of the total capital cost. Figure B.16a shows the effect of variation in solar cost on LCOE. The solar cost is varied from 200 $/m$^2$ to 60 $/m$^2$ with a base price of 150 $/m$^2$. For 'X%' change in solar price, the LCOE changes by approximated 0.37X%. Recently U.S department of energy released a funding announcement expecting the solar cost to go as down as 60 $/m$^2$. For collector cost of 60 $/m$^2$ the LCOE can be reduced to 10.2 cents/kWh$_e$

### ○ Power block cost

The power block constituted about 24% of the total capital cost. It can be noted a capital cost of 1.5 M$/MW$_e$ is on higher side because of lower efficiency of the power cycle. It can be easily right down to 1.1 M$/MW$_e$ by increasing the efficiency of the power cycle (SAM 2017). As shown in Figure B.16b, the power block cost is not as sensitive to the LCOE as the solar cost. For X % change in power block price the LCOE changes by 0.16X %, and at 1.1 M$/MW$_e$ the LCOE for the system is 12.5 cents/kWh$_e$.

### ○ Well cost

Figure B.16c, the variation in well cost sensitivity is similar to power block cost, and for X % variation in well cost the LCOE changes by 0.17 X%. However, it can be noted it might be difficult to bring down the cost of well below 0.75 M$/well.

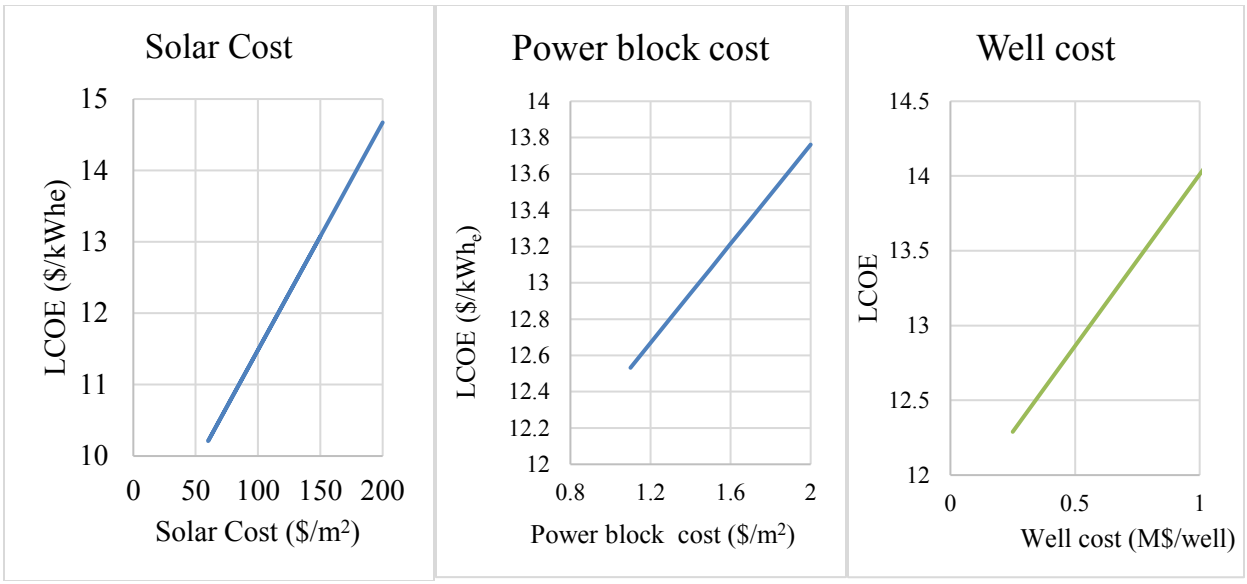


(a) (b) (c)

Figure B.16: Sensitivity of solar prices, power block cost and well cost on LCOE

- **Using electricity generated by PV or CSP to drive the parasitic load**

Parasitic load constitute about 22% of the LCOE cost. The day time parasitic cost can be reduced by using PV when the sunlight is available with an LCOE of 4.1 cents/. The LCOE for the system can be reduced to 12.4 cent/$kWh_e$ around 4.6 % lower than the base price. If the parasitic were driven using the electricity produced from CSP plant at 8 cents/$kWh_e$ and 65% capacity factor the LCOE for the system can be reduced to 12.7 cents/$kWh_e$ which is around 3.2 % cheaper compared to the base case.

# Appendix C

# Safe Bottomhole Injection Pressure in an Injection Well

## Safe Bottomhole Injection Pressure in an Injection Well

Figure 1 is an indication of the bottomhole pressure for various depths and temperatures, with enough pressure to suppress boiling in the tubulars. This was part of an early evaluation to determine what depth of injection would be "optimum" – below aquifers, at a depth where hydraulic fracturing is avoided, but not so deep that parasitic losses associated with compression (to ensure this pressure) are too large to bear. Figure 2 shows the bottomhole pressure for radial flow (likely an underestimate). The surface pressure can also be estimated by subtracting the hydrostatic pressure from these numbers and adding an estimate of the friction pressure for 40 kg/s pumped down 4-1/2-in tubing. Figure 2 shows a safe (from hydraulic fracturing) shaded region. This assumes a conservatively low frac gradient of 0.6 psi/ft. These two figures are a combination of plots from Wendt, 2018 (Figure 3) that show the saturation pressure and the density of the associated liquid at various temperatures.

In Figure 2, any combination of depth and temperature in the gray shded area will be safe from hydraulic fracturing, presuming a frac gradient (minimum total horizontal stress divided by the true vertical depth) of 0.6 psi/ft.

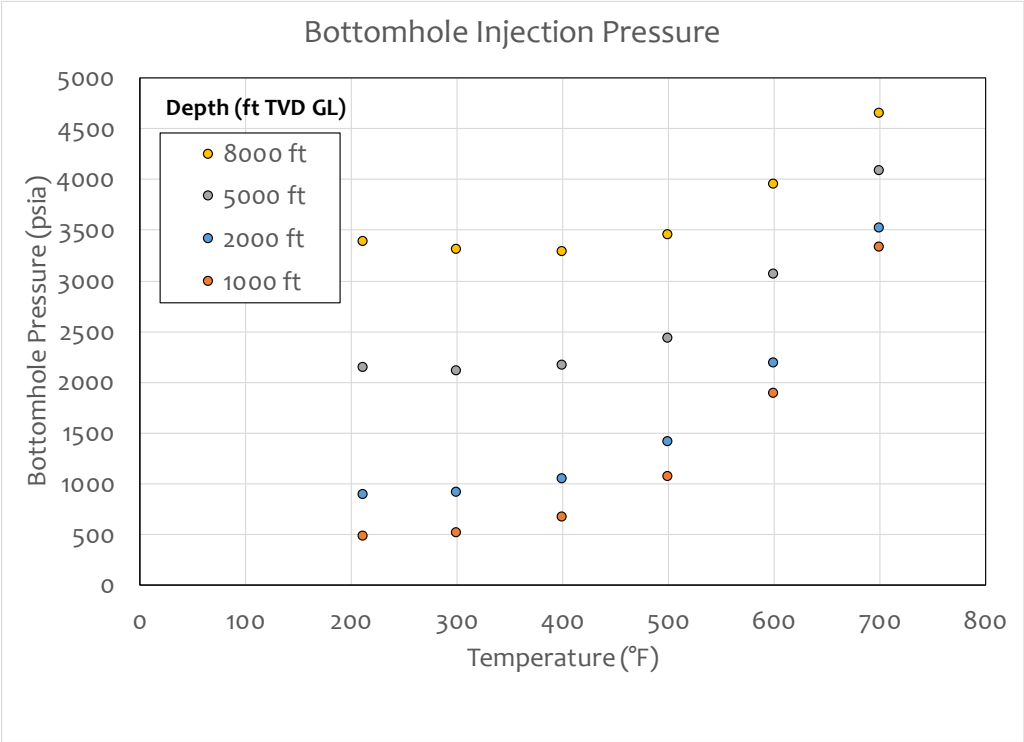


Figure C.1. Bottomhole pressure versus surface injection temperature (maintaining a liquid phase).

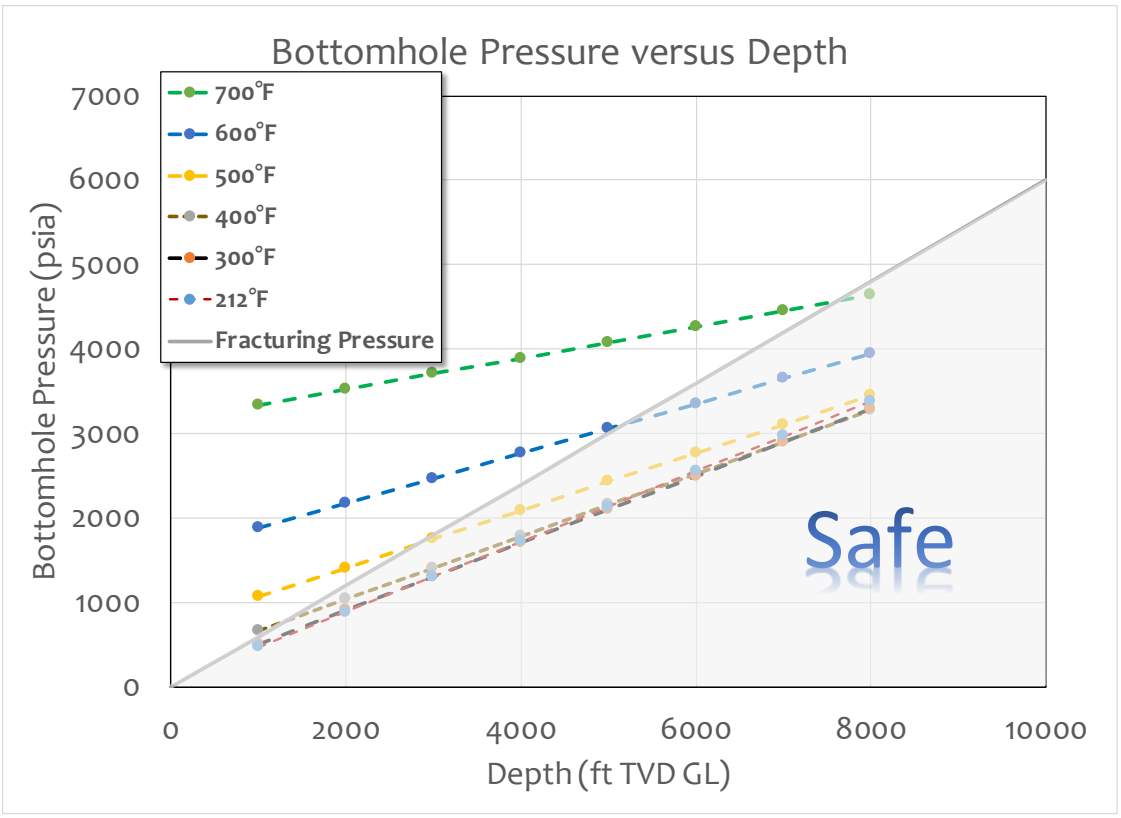


Figure C.2. Bottomhole injection pressure at various depths and temperatures. The grey line indicates in situ total stress at 0.6 psi/ft. If pressures are less than this, hydraulic fracturing will not occur "immediately."

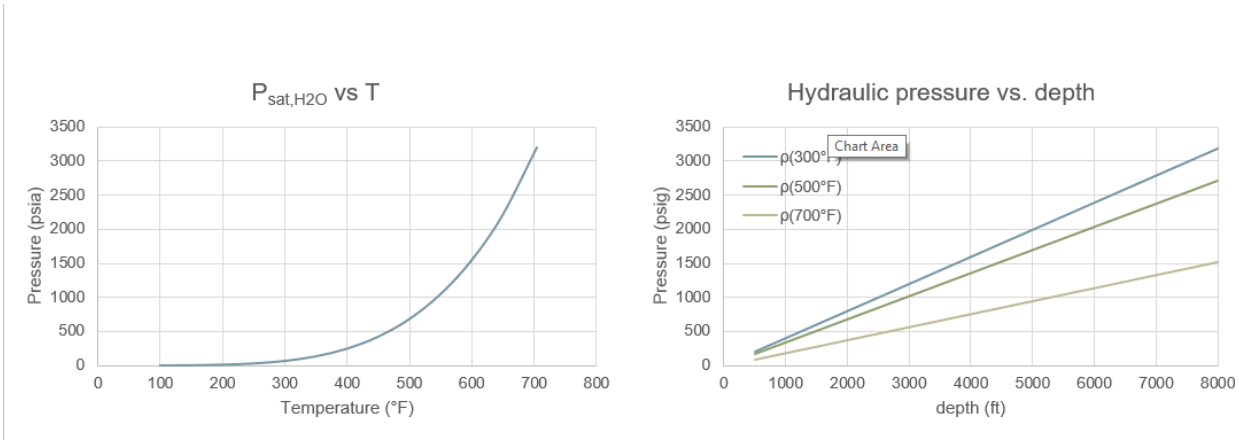


Figure C.3. Plots after Wendt, 2018.

# Appendix D

# Evaluation of Wellbore Pressure Using Steady State Radial Flow Equation

# Evaluation of Wellbore Pressure Using Steady State Radial Flow Equation

Table 1 is an example input table. The goal is to evaluate rate dependence and the potential for fracturing. It is desirable to inject at a rate that is below the pressure that would cause hydraulic fracturing. The basis of the calculations was to compare the pressure at the wellbore that would result from steady state radial flow with a generic pressure that would be required for hydraulic fracturing to occur. The radial flow equation was for a single phase, slightly compressible liquid, at steady state and with no skin. All of those restrictions can be removed and more complicated calculations carried out analytically or numerically. Table 1 shows the input for the baseline radial flow calculations.

Table D.1. Sample Input

| | | |
|---|---|---|
| **Wellbore radius** | ft | 0.33 |
| $Q_w$ | BWPD | -21737 |
| $\mu$ | cP | 0.1 |
| **k** | md | 100 |
| **h** | ft | 330 |
| $\phi$ | | 0.15 |
| $c_t$ | $psi^{-1}$ | 1.01E-05 |
| **t** | hours | 8 |
| $p_i$ | psi | 1740 |

$Q_w$ ..... volumetric flow rate (injection is negative)
$\mu$ ..... dynamic viscosity
k ..... permeability
h ..... reservoir thickness
$\phi$ ..... porosity
$c_t$ ..... total compressibility
t ..... injection time
$p_i$ ..... initial reservoir pressure

Figure 1 shows steady state predictions (isothermal) for bottomhole injection pressure after eight hours for reservoirs with 10 and 100 md permeability. Superimposed are the virgin reservoir pressure (12 MPa) and an assumed frac gradient of 0.7 psi/ft TVD (true vertical depth), assuming a depth of 4000 ft. A frac gradient can be interpreted as the gradient in wellbore pressure to break down the well and cause a fracture to initiate. This is a driller's definition. Alternatively, it can be viewed as the gradient of the pressure required to propagate the fracture. We are assuming the former definition here. In a real situation, the breakdown pressure and the propagation pressure are calculated, and we would compare those with the pressure that would arise from injecting into an unfractured wellbore.

Two permeability scenarios were considered. It can be seen for a reservoir this thick (100 m), and with a permeability of 100 md, nearly any injection is theoretically possible without hydraulic fracturing (assuming a fracturing pressure of 19.31 MPa which results from a typical frac gradient of 0.7 psi/ft or 16.16 kPa/m). Of course, it is more complicated in reality where progressive plugging with fines will lead to cyclical increases in pressure, generation of a small fracture, reduction in pressure and a repeat of this sporadic propagation cycle.

For lower permeability and thinner reservoirs, the predictive relationship has a linear dependency. In Figure 1, it can be seen that 10 md is a riskier long-term proposition, although usually, injectivity will be self-sustaining with periodic episodes of small fracture growth and associated pressure increase, decrease. In the figure, for the 10 md permeability reservoir, injection at a rate of about 60 kg/s will reach a situation where hydraulic fracturing could occur.

The value used for fracturing is a rule of thumb only. It can be higher or lower on a case by case basis and breakdown of the formation (to initiate a fracture) can be higher still. Regardless, **the message is that reservoir permeability likely needs to be significantly higher than 10 md. This guided the selection of the value of 100 md, used in other simulations.**

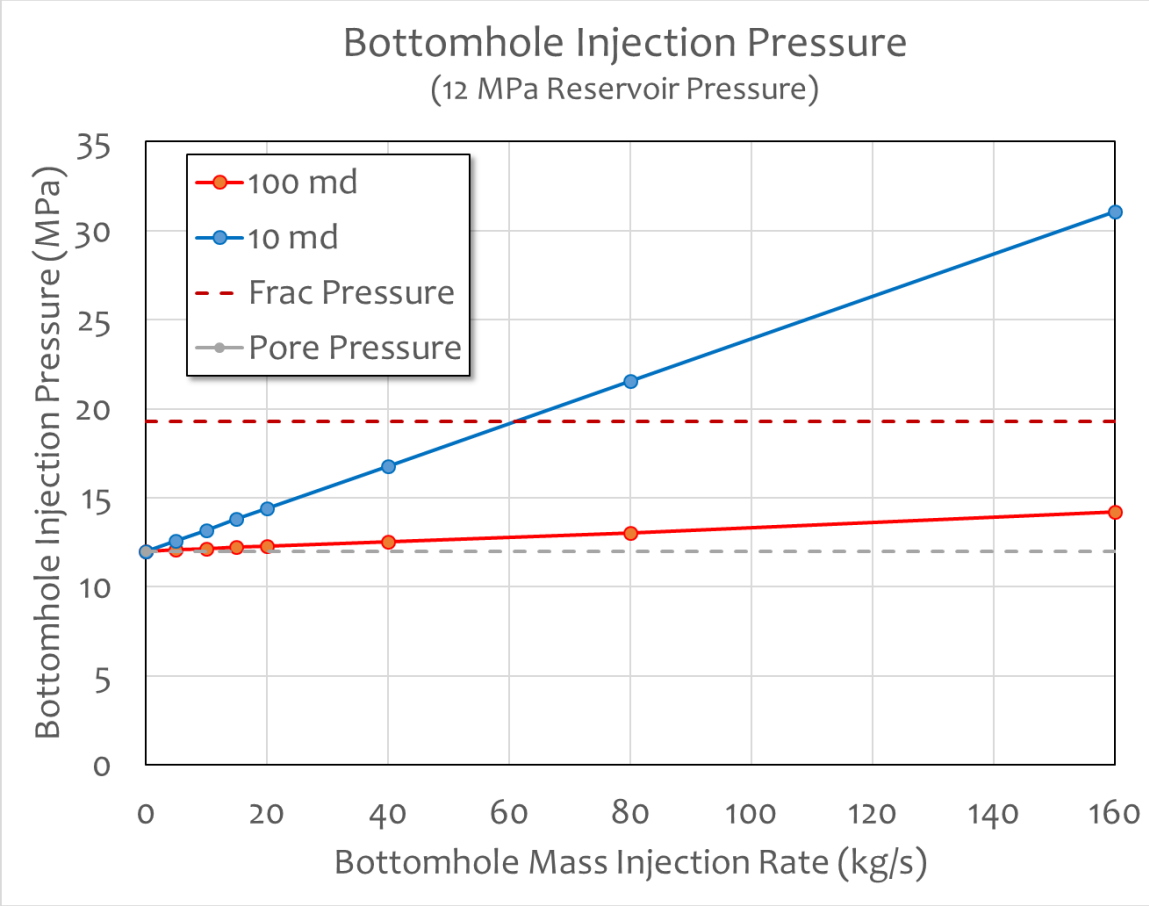


Figure D.1. Steady state solution for wellbore pressure (bottomhole) for a slightly compressible fluid (water) under isothermal conditions.

# Appendix E

# Thermoelastic Stress in Barriers

## Thermoelastic Stress

This work is based on numerical solutions and curve fitting through data developed by Perkins and Gonzalez, 1984.2 Solutions were provided for a cylindrical or disk-shaped region of altered temperature that surrounds the well. "The solution for the thermoelastic stresses interior or exterior to the disk-shaped region can be obtained by adapting a solution for a semi-infinite cylinder embedded in an infinite elastic medium, which is given by Myklestad." Compression is taken as positive. Figure 2 shows the calculated internal stresses (from the original publication).

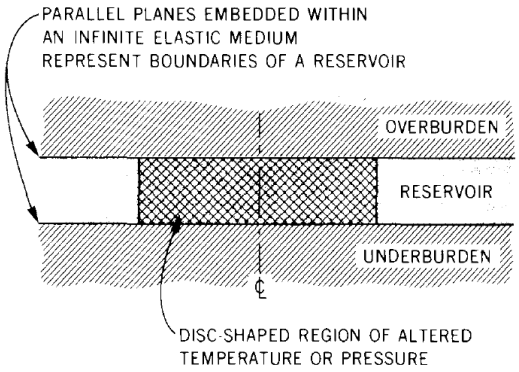


Figure E.1. Heated Geometry

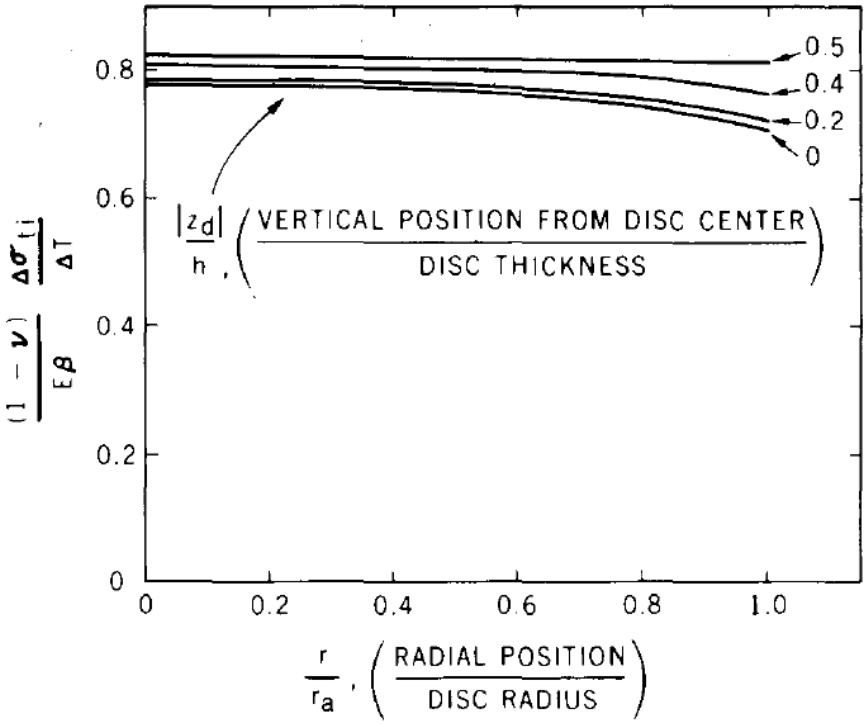


Figure E.2. Nondimensionalized tangential stress in the heated reservoir (interior).

[2] Perkins, T.K. and Gonzalez, J.A. 1984. Changes in Earth sTresses Around a Wellbore Casued by Radially Synnetrical Pressure and Temperature Gradients, SPEJ, April.

Recognizing the relative constancy of the stresses shown in Figure 2, an average tangential total stress in the interior of the heated disk is:

$$\bar{\sigma}_t = \frac{4}{hd}\int_0^{h/2}\int_0^{d/2}\sigma_t dr dz \qquad (1)$$

where:

h ..... reservoir vertical thickness,
d ..... extent of the radially heated zone,
$\sigma_t$ ..... total local tangential stress,
r ..... radial coordinate, and,
z ..... vertical coordinate.

An approximation of the tangential[3] interior stress is:

$$\frac{(1-\nu)}{E\beta}\frac{\Delta\bar{\sigma}_t}{\Delta T} = 0.5\left[1 + \frac{1}{1 + 1.45(h/d)^{0.9} + 0.35(h/d)^2}\right] \qquad (2)$$

where:

$\nu$ ..... Poisson's ratio
$\Delta T$ ..... change in temperature
E ..... Young's modulus
$\beta$ ..... coefficient of linear thermal expansion

Exterior to the disk, the tangential stresses are a function of the radius but do not vary as much vertically. A single integrated average value between the bounding planes is determined.

Figure 3 shows the circumferential (tangential stresses) They have been normalized by the term that is in the denominator of the LHS of Equation (9) which follows. The x-axis is the ratio of the vertical distance from the center of the heated zone (disk) the thickness of the disk (this means that you are just inside the overburden of underburden when the x-axis has a value of 0.5. r is the radial distance from the well and $r_a$ is the radius of the uniformly heated or colled disk.

Above and below the bounding planes ($|z_d| \geq 0.5h$) have been calculated for d/h, $r/r_a$, and $z_d/h$. Approximate values were provided.

$$F_2 = 1 \; if \; r < r_a \quad F_2 = r/r_a \; if \; r > r_a \qquad (3)$$

$$n_1 = 3 \; if \; r > 2r_a \; and \; n_1 = 1 + 2\left|\frac{r}{r_a} - 1\right|^{1/3} \; if \; r < 2r_a \qquad (4)$$

[3] In cylindrical coordinates. This is the tangential or circumferential or hoop stress.

$$F_3 = 2 \; if \; r = 0 \quad F_3 = \left\{ 0.5 + \frac{1.5}{exp\left[4\left|ln\left(\frac{r}{r_a}\right)\right|^{0.472}\right]} \right\}^{-1} \; if \; r > 0 \tag{5}$$

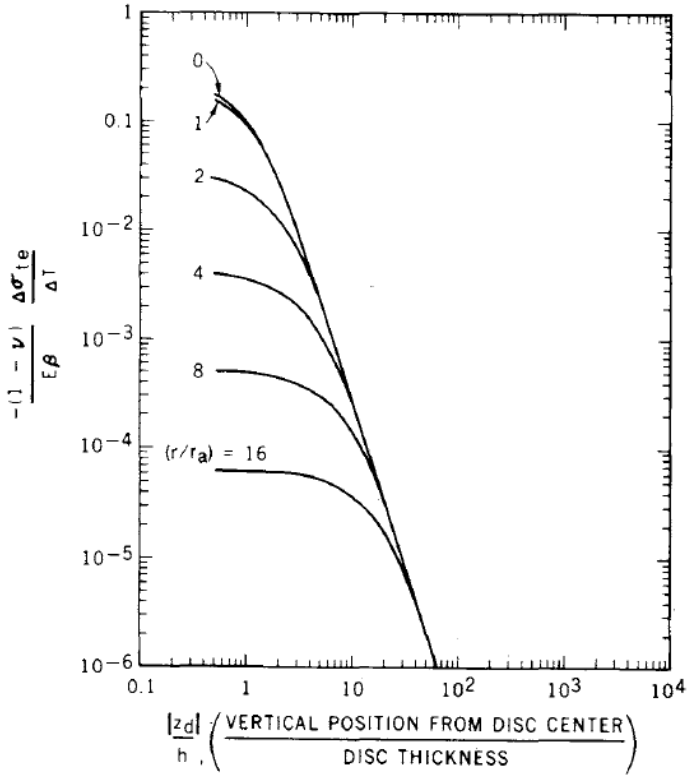


Figure E.3. This figure shows the thermoelastic stresses above and below planes that bound a disk-shaped region of changed temperature. This example is for the case where $r_a/h - 1$ (the heated distance is equal to the heated thickness). That is analagous to the numerical solutions carried out.

$$F_4 = \left( \left\{ (F_3)^{n_1} + \left[ 4.5 \left( \frac{|z_d|}{r_a F_2} \right)^{0.778} \right]^{n_1} \right\}^{10/n_1} + \left( \frac{4|z_d|}{r_a F_2} \right)^{10} \right)^{1/10} \tag{6}$$

$$F_5 = 0.5 + \frac{0.2}{\left(\frac{2|z_d|}{h} - 1\right)^{1.699}} \; if \; |z_d| > 0.55h$$
$$F_5 = 0.5 + \frac{0.1}{\left(\frac{2|z_d|}{h} - 1\right)^{2}} \; if \; 0.5h < |z_d| \leq 0.55h \tag{7}$$

$$F_6 = 0 \; if \; |z_d| = 0.5h \; and \; F_6 = \frac{\left(\frac{|z_d|}{r_a F_2}\right)^3}{F_5} \; if \; |z_d| > 0.5h \tag{8}$$

$$n_2 = 1 + \left[1 + \frac{1}{\left(\frac{2|z_d|}{h} - 1\right)}\right]^{-1} \quad (9)$$

$$-\frac{\Delta\bar{\sigma}_{te}}{\left(\frac{E\beta\Delta T}{1-\nu}\right)} = \frac{1}{[(F_4)^{n_2} + (F_6)^{n_2}]^{1/n_2}\left(\frac{d}{h}\right)F_2^3} \quad (9)$$

An example is given below. The parameters for solving equation (9) are given in Table 1. Figure 2 is a graphical prediction of the stresses.

Table E.1. Parameters for Analytical Prediction of Thermoelastic Stress

| Parameter | Symbol | Value | Units |
|---|---|---|---|
| Radius of Disk | $r_a$ | 100 | m |
| Thickness of Disk | h | 20 | m |
| Vertical Position | z | 10.1 | m |
| Young's Modulus | E | 2.00E+06 | psi |
| Young's Modulus | E | 1.38E+10 | Pa |
| Poisson's ratio | □ | 0.25 | - |
| Temperature Change | □T | 100 | °C |
| CTE | □ | 5.00E-06 | 1/°C |
| Coefficient[4] | | 9195402.3 | Pa |

Figure 4 shows the tangential stresses related to a uniform, radial thermal front extending radially away from a wellbore for a distance of 100 m. The initial observations are that the superimposed stresses are low. Follow on evaluations can be done analytically and numerically. **For example, this is suggesting an elevation (compression) of the tangential stress immediately inside the barriers of approximately 0.73 MPa (just over 100 psi). Further evaluations are required to look at different reservoir geometries, longer-term heating, cycling of the hot injectate and higher changes in temperature.**

[4] Denominator on LHS of Equation (9).

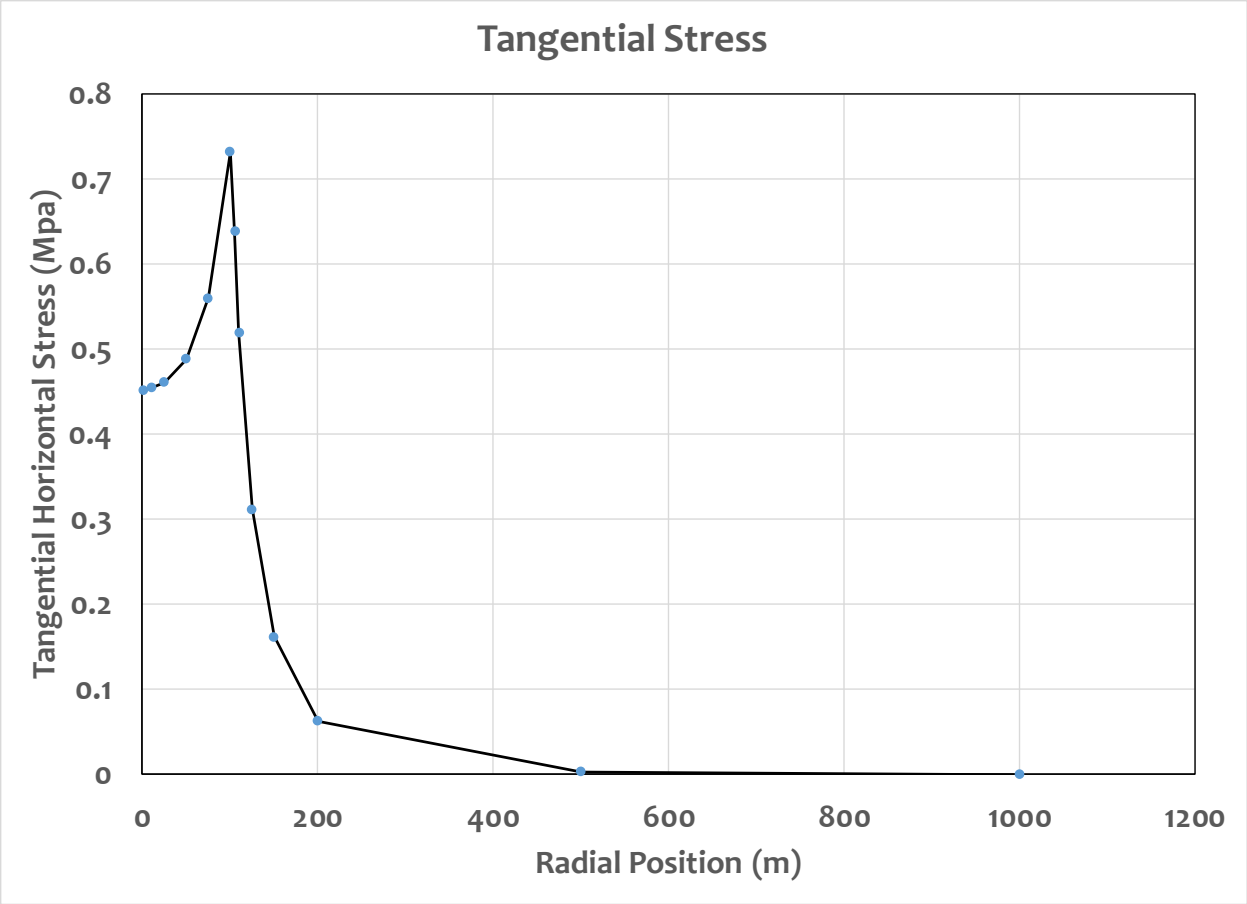

Figure E.4. Radial profile of tangential stress immediately inside over- and underburden.

# Appendix F

# Phase and Temperature Distribution in the Wellbore

## Phase and Temperature Distribution in the Wellbore

Three simulation codes were evaluated to assess where phase changes could be occurring in a production well, and to confirm that phase change was not occurring in the reservoir itself. None of the simulators is completely acceptable for this purpose. In order of increasing usefulness, the simulators evaluated were:

1. Prosper – this is a petroleum industry code that carefully deals with wellbore and surface facility flows. It did not adequately deal with water in the vapor phase during production.
2. WellSim – this is a geothermal code. It was awkward to use for the problem at hand but may be worth revisiting. An example is shown in Figure 1.
3. ProMax – this turns out to have been the most effective code that has been currently used. The wellbore was discretized in 20 sections and the head was specified as 4000 ft.

The remainder of this write up summarizes the work in ProMax. Figure 2 shows a schematic of how the reservoir and the wellbore and the surface were represented. Figure 2 shows the following:

**Stream 1:** This is the feed from the reservoir. Typical properties are shown in Figure 3 (along with results). The inlet rate from the formation is specified, as is the temperature and pressure. It is uncertain if this is not overspecifying the problem. In the case shown (Figures 2 and 3), the reservoir pressure at the production wellbore (bottomhole) was 14 MPa[5], the inflow temperature was 250°C, and the mass flow rate was 40 kg/s.

**Wellbore (Pipe 1):** The 4000 ft vertical wellbore is shown schematically in Figure 4, and its properties are shown in Figure 5. The inner diameter was set at 10.25 inches. Larger diameters could be simulated and might be preferable based on geothermal experience.[6] The average ground temperature was set at 75°C – one might be able to represent a gradient by specifying this for pipe lengths in series, but the 75°C value was taken to be an average of the native temperature along the length of the pipe.

**Stream 3:** This is simply a connection from the pipe to the separator.

**Separator:** This is shown in Figure 6. The separator can be specified with a pressure drop – varied from 0 to 250 psi, based on the surface pressure of the upflow from the wellbore.

**Streams 2 and 4:** These are outflows from the separator – one is vapor and the other is liquid.

[5] From INL simulations.

[6] Kevin Kitz, personal communication.

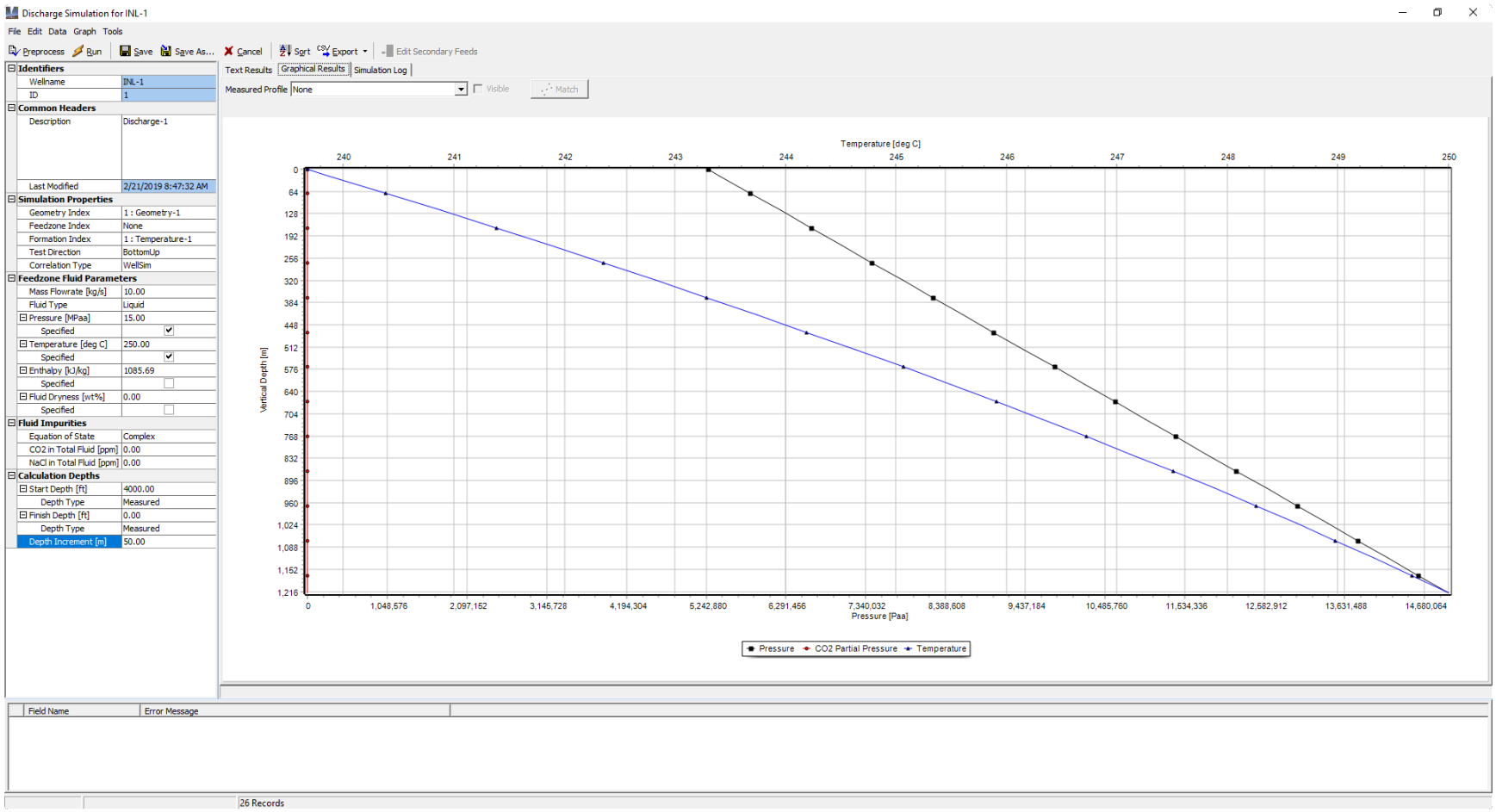


Figure F.1. This shows one example of a WellSim run where the bottomhole pressure, rate, and temperature were specified as 15 MPa, 10 kg/s (low end) and 250°C. Nothing very remarkable – similar temperature and pressure profiles to the data in ProMax – providing confidence there.

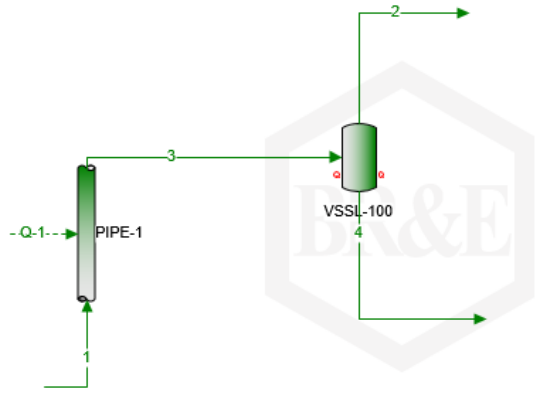


Figure F.2. Schematic of the formation and the wellbore.

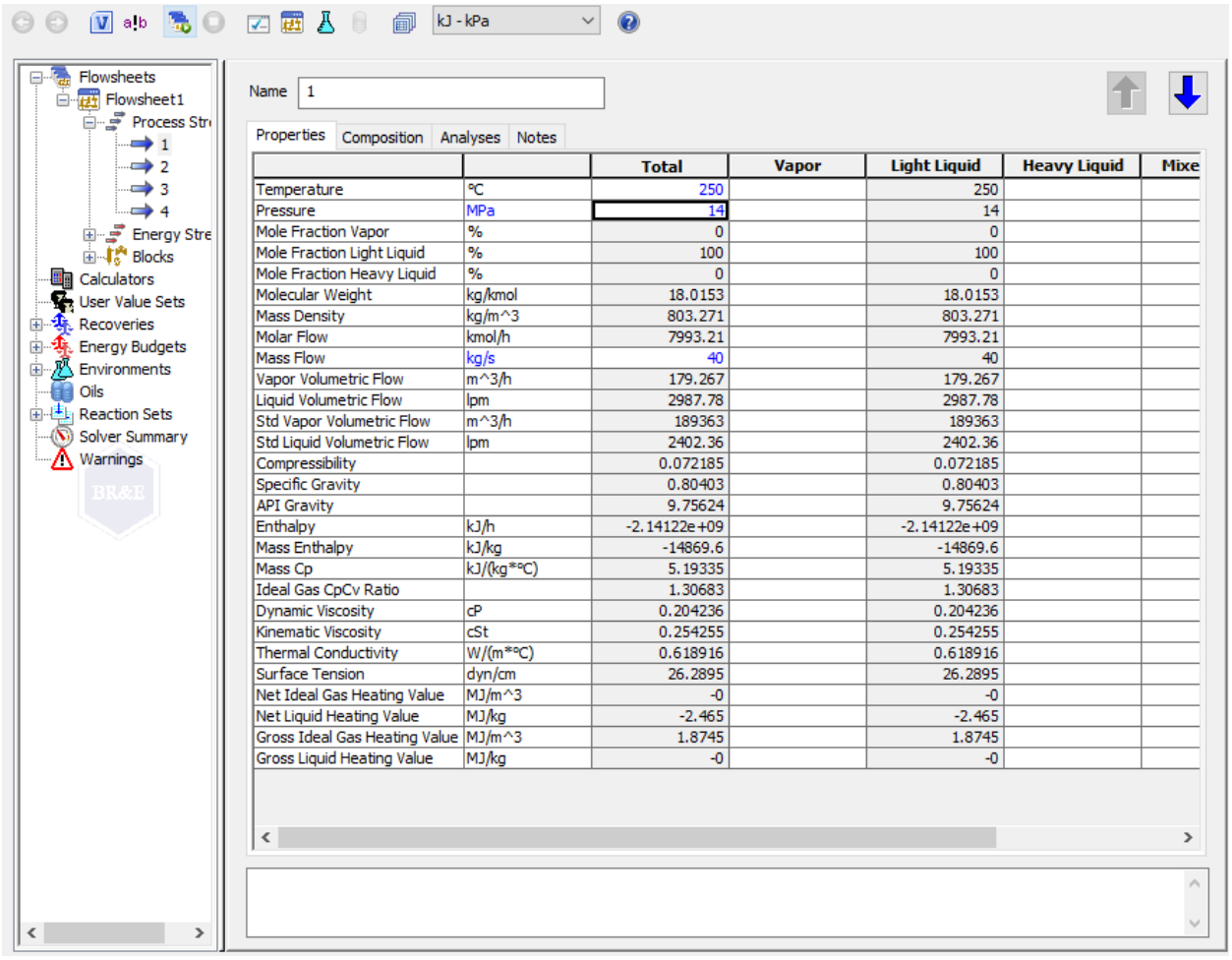


| | | Total | Vapor | Light Liquid | Heavy Liquid | Mixe |
|---|---|---|---|---|---|---|
| Temperature | °C | 250 | | 250 | | |
| Pressure | MPa | 14 | | 14 | | |
| Mole Fraction Vapor | % | 0 | | 0 | | |
| Mole Fraction Light Liquid | % | 100 | | 100 | | |
| Mole Fraction Heavy Liquid | % | 0 | | 0 | | |
| Molecular Weight | kg/kmol | 18.0153 | | 18.0153 | | |
| Mass Density | kg/m^3 | 803.271 | | 803.271 | | |
| Molar Flow | kmol/h | 7993.21 | | 7993.21 | | |
| Mass Flow | kg/s | 40 | | 40 | | |
| Vapor Volumetric Flow | m^3/h | 179.267 | | 179.267 | | |
| Liquid Volumetric Flow | lpm | 2987.78 | | 2987.78 | | |
| Std Vapor Volumetric Flow | m^3/h | 189363 | | 189363 | | |
| Std Liquid Volumetric Flow | lpm | 2402.36 | | 2402.36 | | |
| Compressibility | | 0.072185 | | 0.072185 | | |
| Specific Gravity | | 0.80403 | | 0.80403 | | |
| API Gravity | | 9.75624 | | 9.75624 | | |
| Enthalpy | kJ/h | -2.14122e+09 | | -2.14122e+09 | | |
| Mass Enthalpy | kJ/kg | -14869.6 | | -14869.6 | | |
| Mass Cp | kJ/(kg*°C) | 5.19335 | | 5.19335 | | |
| Ideal Gas CpCv Ratio | | 1.30683 | | 1.30683 | | |
| Dynamic Viscosity | cP | 0.204236 | | 0.204236 | | |
| Kinematic Viscosity | cSt | 0.254255 | | 0.254255 | | |
| Thermal Conductivity | W/(m*°C) | 0.618916 | | 0.618916 | | |
| Surface Tension | dyn/cm | 26.2895 | | 26.2895 | | |
| Net Ideal Gas Heating Value | MJ/m^3 | -0 | | -0 | | |
| Net Liquid Heating Value | MJ/kg | -2.465 | | -2.465 | | |
| Gross Ideal Gas Heating Value | MJ/m^3 | 1.8745 | | 1.8745 | | |
| Gross Liquid Heating Value | MJ/kg | -0 | | -0 | | |

Figure F.3. Inflow stream representing production from the reservoir.

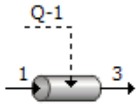


Figure F.4. Schematic of the wellbore. In reality, it is rotated 90° so that there is a head of 4000 ft. The outlet stream at the surface feeds arbitrarily to the surface.

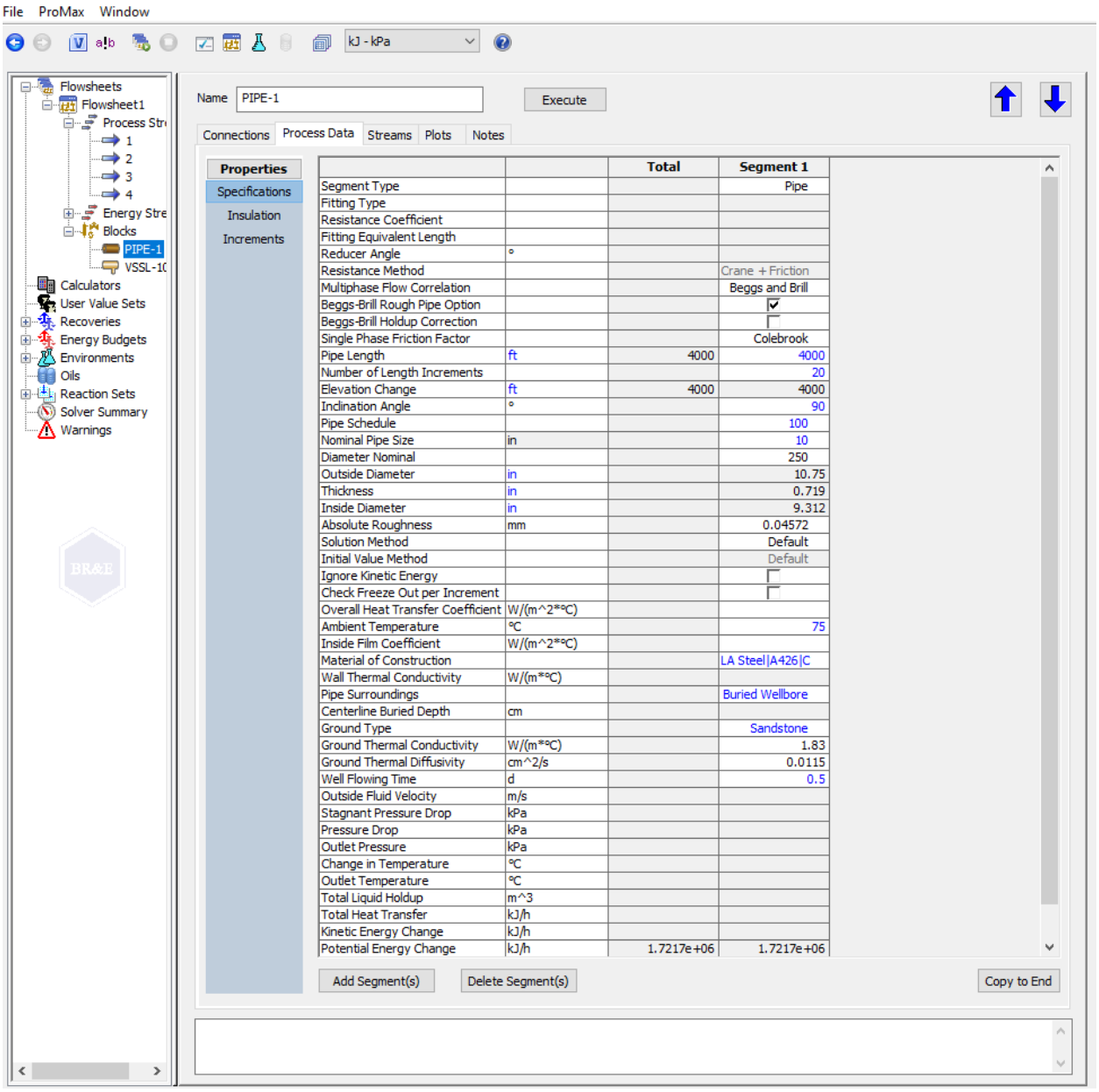


| | | Total | Segment 1 |
|---|---|---|---|
| Segment Type | | | Pipe |
| Fitting Type | | | |
| Resistance Coefficient | | | |
| Fitting Equivalent Length | | | |
| Reducer Angle | ° | | |
| Resistance Method | | | Crane + Friction |
| Multiphase Flow Correlation | | | Beggs and Brill |
| Beggs-Brill Rough Pipe Option | | | ☑ |
| Beggs-Brill Holdup Correction | | | ☐ |
| Single Phase Friction Factor | | | Colebrook |
| Pipe Length | ft | 4000 | 4000 |
| Number of Length Increments | | | 20 |
| Elevation Change | ft | 4000 | 4000 |
| Inclination Angle | ° | | 90 |
| Pipe Schedule | | | 100 |
| Nominal Pipe Size | in | | 10 |
| Diameter Nominal | | | 250 |
| Outside Diameter | in | | 10.75 |
| Thickness | in | | 0.719 |
| Inside Diameter | in | | 9.312 |
| Absolute Roughness | mm | | 0.04572 |
| Solution Method | | | Default |
| Initial Value Method | | | Default |
| Ignore Kinetic Energy | | | ☐ |
| Check Freeze Out per Increment | | | ☐ |
| Overall Heat Transfer Coefficient | W/(m^2*°C) | | |
| Ambient Temperature | °C | | 75 |
| Inside Film Coefficient | W/(m^2*°C) | | |
| Material of Construction | | | LA Steel\|A426\|C |
| Wall Thermal Conductivity | W/(m*°C) | | |
| Pipe Surroundings | | | Buried Wellbore |
| Centerline Buried Depth | cm | | |
| Ground Type | | | Sandstone |
| Ground Thermal Conductivity | W/(m*°C) | | 1.83 |
| Ground Thermal Diffusivity | cm^2/s | | 0.0115 |
| Well Flowing Time | d | | 0.5 |
| Outside Fluid Velocity | m/s | | |
| Stagnant Pressure Drop | kPa | | |
| Pressure Drop | kPa | | |
| Outlet Pressure | kPa | | |
| Change in Temperature | °C | | |
| Outlet Temperature | °C | | |
| Total Liquid Holdup | m^3 | | |
| Total Heat Transfer | kJ/h | | |
| Kinetic Energy Change | kJ/h | | |
| Potential Energy Change | kJ/h | 1.7217e+06 | 1.7217e+06 |

Figure F.5. The wellbore.

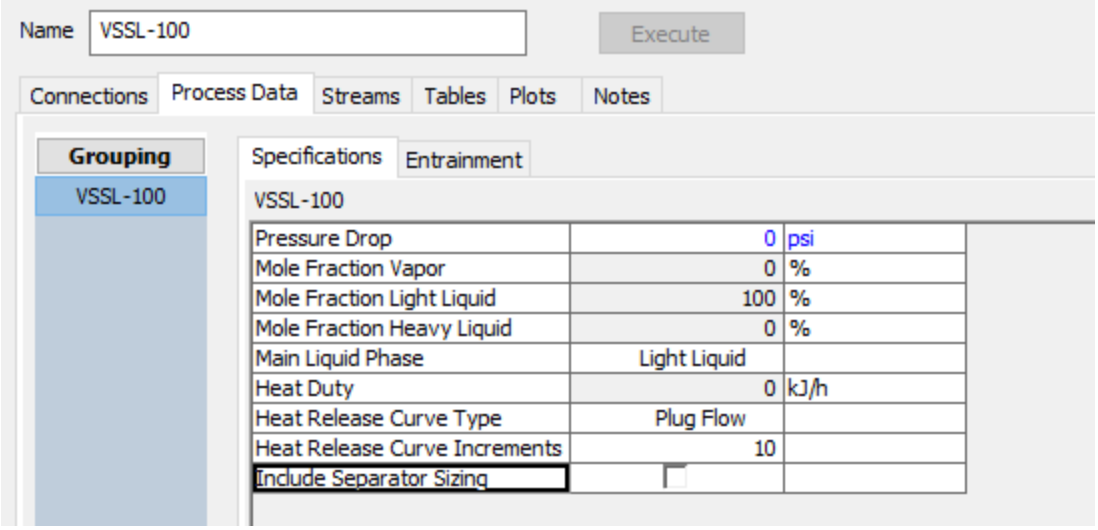

Figure F.6: Separator. This case, for illustration only specifies no pressure drop.

## Results:

The main simulations reported here are for 40 kg/s inflow at the reservoir exit and bottomhole pressures of 10 and 14 MPa. Hydrostatic pressure at 4000 ft for a fluid with a specific gravity of 0.8 is about 9.6 MPa. Figure 7 shows outflows for a BHP of 10 MPa and a 250 psi pressure drop through the separator. Figure 8 shows outflows for a BHP of 14 MPa.

Additional simulations are required for detailed engineering and design. The observation from the simulations carried out is some steam is present but that the bulk of the transport up the production wellbore will be in a liquid phase and **because of the specified bottomhole pressure, the water will only be liquid in the wellbore and formation.**

Name VSSL-100 Execute

Connections | Process Data | Streams | Tables | Plots | Notes

Streams | Properties | Composition

| | | 3 | 2 | 4 |
|---|---|---|---|---|
| Temperature | °C | 210.826 | 122.356 | 122.356 |
| Pressure | psia | 280.992 | 30.9916 | 30.9916 |
| Mole Fraction Vapor | % | 6.95894 | 100 | 0 |
| Mole Fraction Light Liquid | % | 93.0411 | 0 | 100 |
| Mole Fraction Heavy Liquid | % | 0 | 0 | 0 |
| Molecular Weight | kg/kmol | 18.0153 | 18.0153 | 18.0153 |
| Mass Density | kg/m^3 | 118.715 | 1.1893 | 941.753 |
| Molar Flow | kmol/h | 7993.21 | 1918.96 | 6074.25 |
| Mass Flow | kg/h | 144000 | 34570.6 | 109429 |
| Vapor Volumetric Flow | m^3/h | 1212.99 | 29068 | 116.198 |
| Liquid Volumetric Flow | m^3/h | 1212.99 | 29068 | 116.198 |
| Std Vapor Volumetric Flow | m^3/h | 189363 | 45461 | 143902 |
| Std Liquid Volumetric Flow | lpm | 2402.36 | 576.744 | 1825.62 |
| Compressibility | | 0.0730616 | 0.984296 | 0.00124303 |
| Specific Gravity | | | 0.622021 | 0.942643 |
| API Gravity | | | | 9.99691 |
| Enthalpy | kJ/h | -2.15e+09 | -4.57934e+08 | -1.69206e+09 |
| Mass Enthalpy | kJ/kg | -14930.5 | -13246.3 | -15462.6 |
| Mass Cp | kJ/(kg*°C) | 4.63664 | 1.94212 | 4.24105 |
| Ideal Gas CpCv Ratio | | 1.31046 | 1.31765 | 1.31765 |
| Dynamic Viscosity | cP | | 0.0134096 | 0.223826 |
| Kinematic Viscosity | cSt | | 11.2752 | 0.237669 |
| Thermal Conductivity | W/(m*°C) | | 0.0292281 | 0.684003 |
| Surface Tension | dyn/cm | | | 53.8841 |
| Net Ideal Gas Heating Value | MJ/m^3 | -0 | -0 | -0 |
| Net Liquid Heating Value | MJ/kg | -2.465 | -2.465 | -2.465 |
| Gross Ideal Gas Heating Value | MJ/m^3 | 1.8745 | 1.8745 | 1.8745 |
| Gross Liquid Heating Value | MJ/kg | -0 | -0 | -0 |

Figure F.7. This shows outflows for a BHP of 10 MPa and a 250 psi pressure drop through the separator. The key values to look at are the mole fraction of vapor and liquid in the surface flow line to the separator (stream 3). There is some steam but the fluid is still largely liquid in the wellbore.

Name VSSL-100 Execute

Connections | Process Data | Streams | Tables | Plots | Notes

Streams | Properties | Composition

| | | 3 | 2 | 4 |
|---|---|---|---|---|
| Temperature | °C | 237.432 | 225.038 | 225.038 |
| Pressure | psia | 619.849 | 369.849 | 369.849 |
| Mole Fraction Vapor | % | 0 | 100 | 0 |
| Mole Fraction Light Liquid | % | 100 | 0 | 100 |
| Mole Fraction Heavy Liquid | % | 0 | 0 | 0 |
| Molecular Weight | kg/kmol | 18.0153 | 18.0153 | 18.0153 |
| Mass Density | kg/m^3 | 816.991 | 12.4076 | 833.264 |
| Molar Flow | kmol/h | 7993.21 | 266.605 | 7726.61 |
| Mass Flow | kg/h | 144000 | 4802.96 | 139197 |
| Vapor Volumetric Flow | m^3/h | 176.256 | 387.099 | 167.05 |
| Liquid Volumetric Flow | m^3/h | 176.256 | 387.099 | 167.05 |
| Std Vapor Volumetric Flow | m^3/h | 189363 | 6315.98 | 183047 |
| Std Liquid Volumetric Flow | lpm | 2402.36 | 80.1281 | 2322.23 |
| Compressibility | | 0.0221988 | 0.893862 | 0.0133099 |
| Specific Gravity | | 0.817764 | 0.622021 | 0.834051 |
| API Gravity | | 9.9256 | | 9.95583 |
| Enthalpy | kJ/h | -2.15036e+09 | -6.29723e+07 | -2.08738e+09 |
| Mass Enthalpy | kJ/kg | -14933 | -13111.1 | -14995.9 |
| Mass Cp | kJ/(kg*°C) | 5.16187 | 2.21489 | 4.99753 |
| Ideal Gas CpCv Ratio | | 1.30803 | 1.30918 | 1.30918 |
| Dynamic Viscosity | cP | 0.214446 | 0.0174896 | 0.231513 |
| Kinematic Viscosity | cSt | 0.262482 | 1.40959 | 0.277839 |
| Thermal Conductivity | W/(m*°C) | 0.633161 | 0.0415283 | 0.645591 |
| Surface Tension | dyn/cm | 29.2262 | | 32.0837 |
| Net Ideal Gas Heating Value | MJ/m^3 | -0 | -0 | -0 |
| Net Liquid Heating Value | MJ/kg | -2.465 | -2.465 | -2.465 |
| Gross Ideal Gas Heating Value | MJ/m^3 | 1.8745 | 1.8745 | 1.8745 |
| Gross Liquid Heating Value | MJ/kg | -0 | -0 | -0 |

Figure F.8. This shows outflows for a BHP of 14 MPa and a 250 psi pressure drop through the separator.

# Appendix G

# Preliminary Results on Geochemical Implications of Injection of Hot Water into the Sedimentary Reservoir

## Preliminary Results on Geochemical Implications of Injection of Hot Water into the Sedimentary Reservoir

### 1. Introduction

This project envisions injection of surface heated hot water (250°C) into the reservoir (originally at 50°C) to store excess heat energy during period of low energy demand. During the period of high energy demand, the stored heat can be withdrawn and used for generation of additional dispatchable power. In this document, we report our preliminary results on potential geochemical implications of injection of hot water into the reservoir and withdrawal of reservoir-interacted hot water for heat extraction.

### 2. Model Reservoir Rock Type

As a model/generic reservoir, we selected a sedimentary basin in Las Vegas Valley. This is a structural basin located in southeastern part of Nevada, around the city of Las Vegas (Figure G.1A). The basin is formed in the basement rocks of Precambrian metamorphic rocks; Precambrian and Paleozoic carbonate rocks; Permian, Triassic, and Jurassic clastic rocks; and Miocene igneous rocks (Plume, 1984). The basin is filled with 3,000 to 5,000 ft of Miocene-Holocene valley-fill clastic sedimentary deposits (Plume, 1984, Dettinger, 1987). The basin fill sedimentary deposits can be divided into two units- Muddy Creek Formation (Miocene and Pliocene), and Younger deposits. The Muddy Creek Formation consists of coarse grained sediments near the mountains that progressively become finer grained towards center of the valley. In general, sandstone, siltstone, clays, with intercalated gravel beds define this formation in various locations (Dettinger, 1987).

The Muddy Creek Formation is used as a generic reservoir rock type for this simplified geochemical modeling exercise. General lithology of this unit is further simplified to calcareous sandstone with quartz and calcite as the two principal rock forming minerals. The ambient reservoir temperature is assumed to be 50°C. More detailed geochemical modeling, however, requires a more representative modal composition of the reservoir rock that includes both major rock forming minerals as well as accessory minerals that can be geochemically significant, such as gypsum, oxides of iron, sulfides, and so on.

### 3. Composition of Initial Water

Dettinger (1987) provides ground water compositions for 40 wells in Las Vegas Valley (Figure G.1B). None of the wells reported by Dettinger (1987) penetrate to the deeper parts of the basin. For this work, we selected a composition of water from Well No. 25 to formulate initial water chemistry of the reservoir for the geochemical modeling work. Well No. 25 is a 1000-ft deep well located at the central part of the Las Vegas Valley. The screen depth in the well ranges from 517 ft and 964 ft. The reported temperature of water is 23 °C. This is a near neutral (pH = 7.5) Ca-$HCO_3$ type water. Besides Ca and $HCO_3$, other major ions in this water are Mg and $SO_4$. General chemistry of this water is illustrated in Figure G.2.

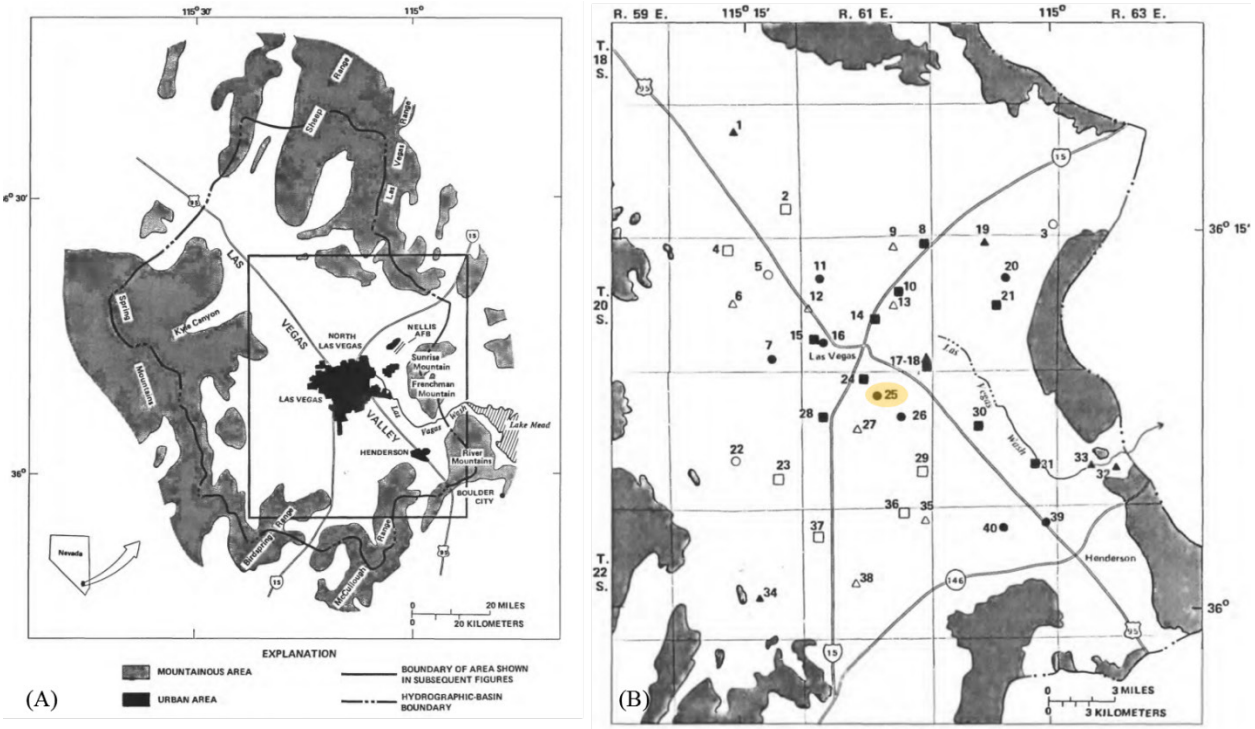


Figure G.1. (A) Las Vegas Valley Basin, (B) Locations of groundwater wells in the valley (Dettinger, 1987). Composition of water from Well No. 25 is selected to formulate the composition of ambient reservoir water.

This water was heated to 50°C in the presence of reservoir rock (quartz and calcite). Heating of this water to 50°C in the presence of quartz and calcite did not change the composition significantly (Figure G.2) because it was slightly supersaturated with respect to both quartz and calcite. During this heating, small amounts of quartz (0.65 mg) and calcite (18.48 mg) precipitated into the reservoir. For all subsequent geochemical modeling tasks, this 50°C is used as the initial water.

## 4. Conceptual Reservoir Model

Initially, the reservoir is assumed to be lithologically and thermally homogeneous unit consisting of calcareous (or calcite cemented) sandstone (with major rock forming minerals such as quartz and calcite). Ambient temperature of the reservoir is 50°C. At the beginning, water from this reservoir is withdrawn to the surface and used for capturing excess heat in the heat exchanger (Figure 3). Once the temperature of the water reached to 250°C, the hot water is designed to inject back into the reservoir. Over time, the injection of hot water will move the thermal front away from the injection well bore and likely create a reservoir with multiple thermal zones with different temperatures. For simplification, the reservoir is divided into 5 temperature zones, ranging from injection temperature (250°C) to ambient reservoir temperature (50°C). A simplified sketch of this zonal reservoir is depicted in Figure G.3.

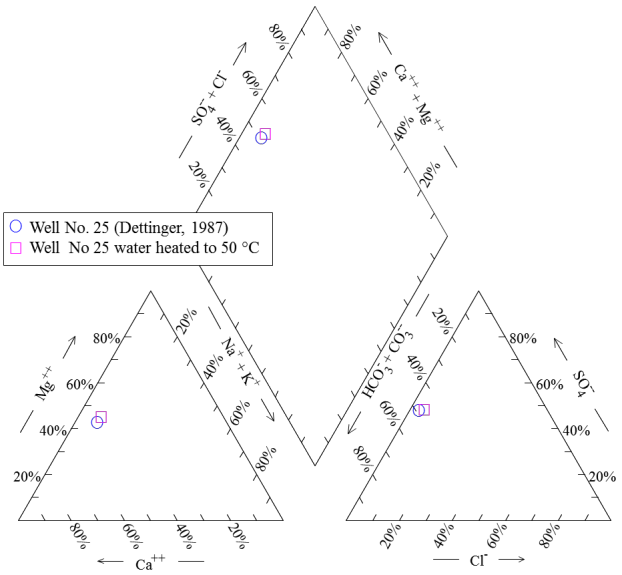


Figure G.2. Piper diagram illustrating compositions of water from Well No. 25 (Dettinger, 1987) and its derivative water at 50°C.

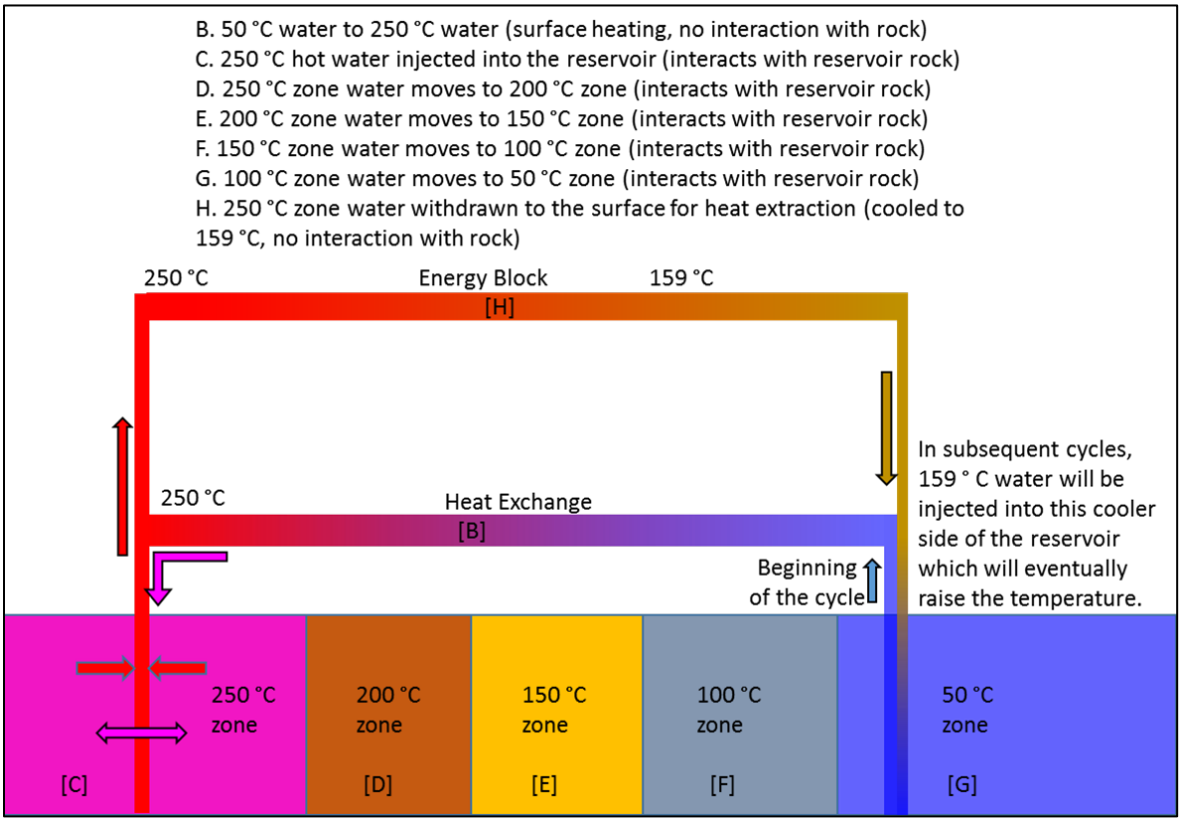


Figure G.3. Simplified conceptual model of the reservoir. Over time, the reservoir is assumed to have several temperature zones. The 50°C zone (ambient zone) as depicted here is likely to have higher temperature as the injection of recycled water at 159°C begins. This scenario is not included in the current simplified geochemical modeling.

## 5. Geochemical Consequences in the Reservoir

Initially, the ambient reservoir water will be withdrawn and heated to 250°C with the excess heat in the plant. This heating of water takes place in the heat exchanger in the absence of rock. The geochemical consequences during this initial heating largely depend on the composition of initial/ambient reservoir water that is used to capture the excess heat. In the current case, it is likely to precipitate 204.5 mg anhydrite/L of water. Other potential minerals to precipitate during this heating phase are brucite, antigorite, and magnesite (Figure G.4B). The composition of evolved water is depicted in Figure G.5.

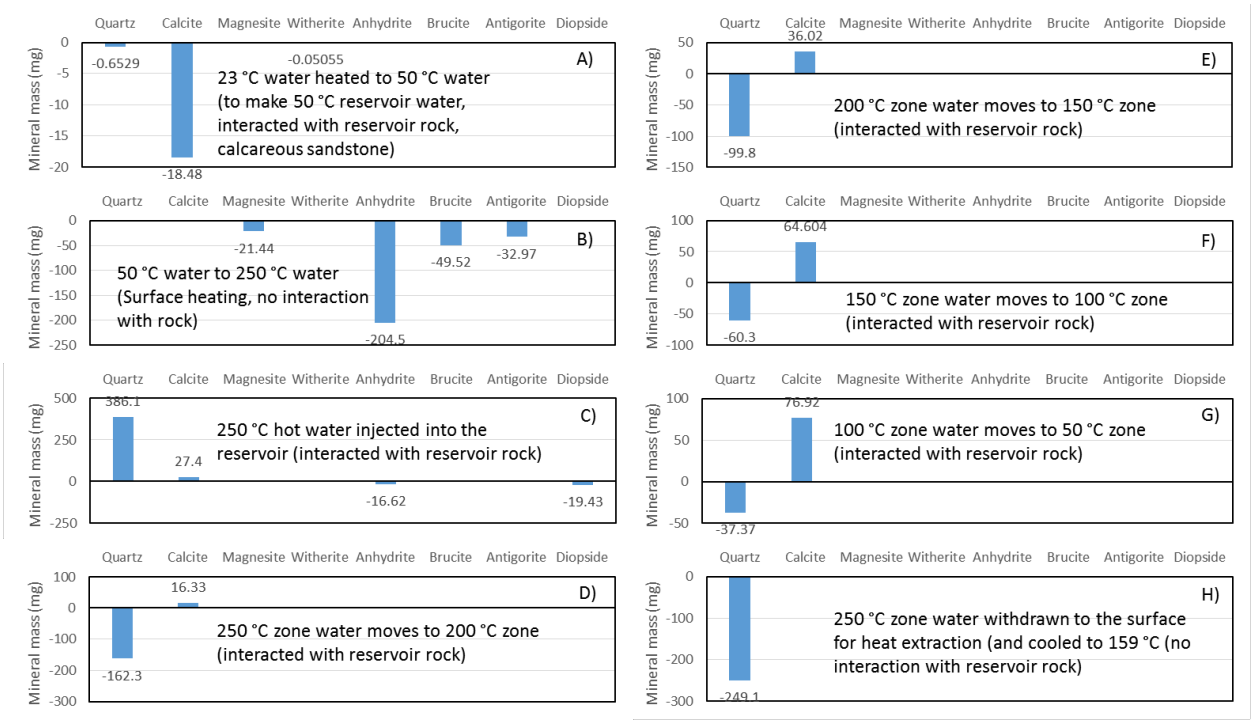


Figure G.4. Likely minerals to precipitate or dissolve as the water moves from one equilibrated geochemical regime to a different one. (A) The Well No. 25 water is being heated to 50°C. This heating helped create ambient reservoir water. (B) Ambient reservoir water is withdrawn to the surface and heated to 250°C in the heat exchanger (in the absence of reservoir rock). (C) The surface heated water (250°C) is injected into the reservoir. The hot water interacts with the reservoir rocks and attains an equilibrium state at 250°C. (D) Water from 250°C enters into the 200°C zone of the reservoir where it attains a new equilibrium state for that temperature. (E-G) Equilibrated water from higher temperature zones subsequently moves to the lower temperature zones and attains successive equilibrium states at those temperatures. (H) Water from the hottest zone (250°C) is withdrawn to the surface for closed system heat extraction in the Power Block (Figure 3), where it eventually cools to 159°C. The given mineral masses are either precipitated (negative masses) and separated from the 1 L of water or minerals in the reservoir (quartz and calcite) are dissolved (positive masses) and added to the 1 L of water as chemical components.

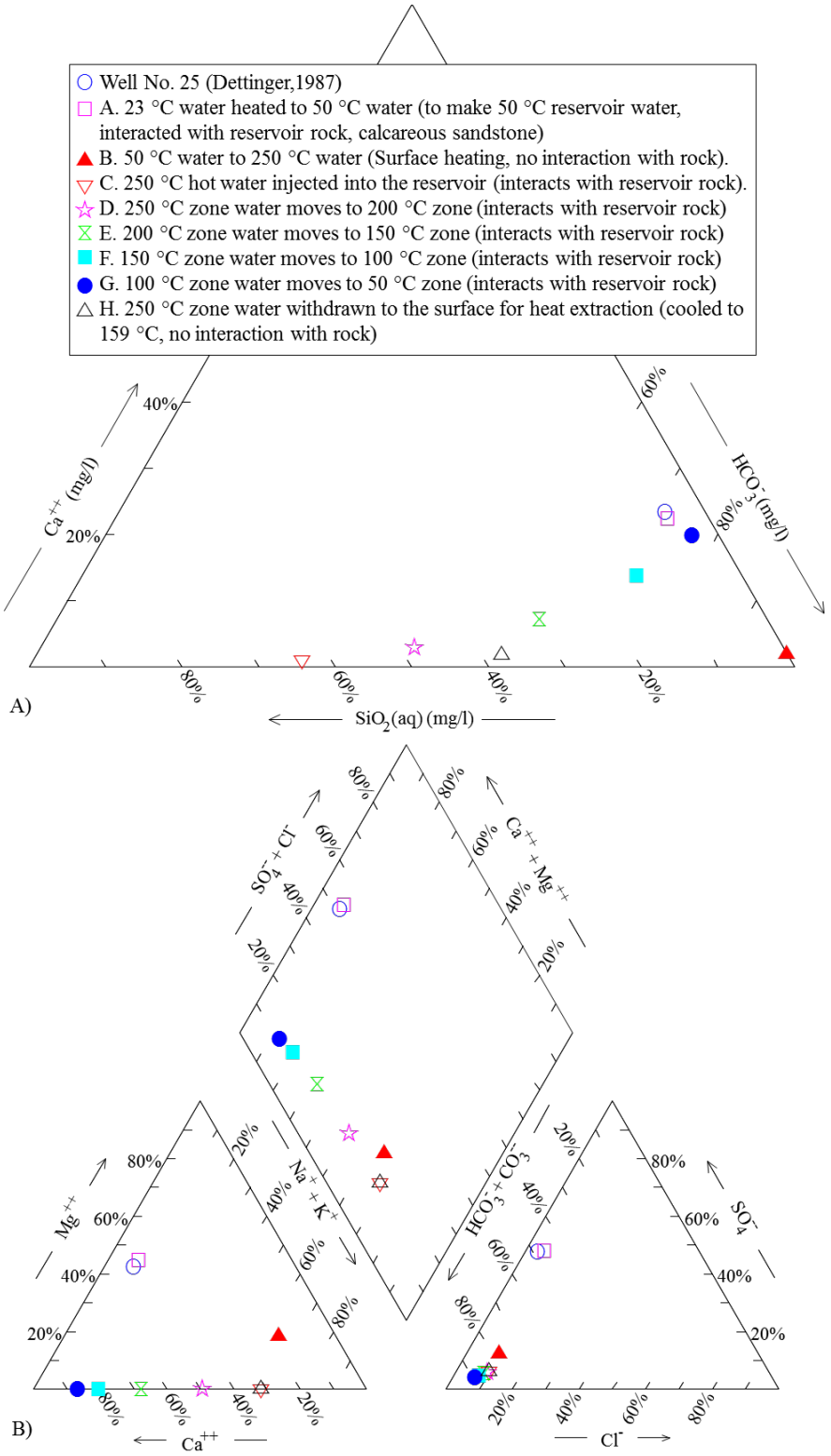


Figure G.5. (A) Ternary diagram showing changes in $SiO_{2(aq)}$, $HCO_3$, and Ca; and (B) Piper diagram showing changes in major ions in the water as it moves through different parts of the plant and reservoir zones.

As the hot water (250°C) injected into the reservoir, it will change the geochemical regime around the near wellbore reservoir. The hot water mixes with the ambient water in the reservoir as well as it starts interacting with the reservoir rock (quartz and calcite). In our simplified geochemical modeling work, we did not include the consequences of mixing of hot water and ambient water in the reservoir. We assumed that a part of the reservoir near the injection well bore eventually reaches to the temperature (250°C) and attains geochemical equilibrium. By the time this hottest part of the reservoir attains the equilibrium, the hot water is likely to dissolve about 386 mg quartz/L of water (Figure G.4C). Over time, this hot water moves further away from the well bore and successively increases the temperature of the reservoir. Each temperature zone eventually attains the geochemical equilibrium. Likely minerals that may precipitate or dissolve in each temperature zone in the reservoir is given in a series of diagrams in Figure G.4. In general, as the hot water moves further away into the lower temperature zone and increases the temperature there, it will lead to precipitation of silica (e.g., quartz) and dissolution of calcite in the reservoir. As a result of this precipitation and dissolution of minerals, the composition of water will evolve as it passes through and attains new equilibrium. The evolution of water over time through these different temperature zones in the reservoir is depicted in Figure G.5. In general, as the water moves from hotter zone to cooler zone, it will become less loaded with $SiO_{2(aq)}$ and progressively becomes enriched in Ca and $HCO_3$ (Figure G.5A).

During high energy demand, water from the hottest part of the reservoir will be pumped to the surface for extraction of heat. The water in the hottest reservoir is loaded with $SiO_{2(aq)}$. As heat is extracted from this hot water (in the Energy Block in Figure 3), it will cool to a temperature of 159°C. Even though this cooling occurs in a closed system, the cooler water has lower solubility for silica, resulting in precipitation of 249 mg quartz/L of water. This potential for precipitation of quartz (silica) can foul the piping and equipment in the Energy Block.

## 6. Summary

This simplified geochemical modeling work indicates that injection of hot water into the geologic formation as a mean to store excess heat is likely to alter the ambient geochemical regime in the reservoir. The geochemical consequences during the initial heating phase on the surface is largely depends on the chemistry of the initial water. Once the heated water is injected into the reservoir, it is likely to dissolve quartz (or other silica polymorphs) and some other minerals (depending on the reservoir mineralogy). As the hot water moves further away from the wellbore, it is likely to create multiple thermal as well as geochemical zones/regimes. Overtime, each thermal zone or geochemical regime may attain equilibrium. However, this equilibrium may not be stabilized for a long time (or never) because of the push-pull nature of the system that is likely to perturb the geochemical state of the reservoir frequently.

Similarly, the withdrawal of hot water from the hottest part of the reservoir for power generation is likely to create additional consequences such as fouling of piping and equipment in the Energy Block (Figure G.3) and on the lower temperature side of the plant. Quartz (or other silica polymorphs) is the most likely mineral to precipitate during this cycle of plant operation. This type of potential fouling is not a new nuisance to geothermal industry (Grassiani, 2000). Geothermal power plant operators in various sites are dealing with this issue by employing various chemical treatments of brines. For example, acid treatment of the brine is one of the commonly suggested method to control kinetics of silica-polymerization by lowering pH of the brine (Henley, 1983). Site specific treatment can be defined and implemented to minimize the potential adverse effects of geochemical consequences of hot water storage and withdrawal.

## References

Dettinger, M.D., 1987. Ground-Water Quality and Geochemistry of Las Vegas Valley, Clark County, Nevada, 1981-83: Implementation of a Monitoring Network. Water-Resources Investigations Report 87-4007, 73 p.

Grassiani, M., 2000. Siliceous scaling aspects of geothermal power generation using binary cycle heat recovery. Transactions-Geothermal Resources Council, 475-478.
Henley, R.W., 1983. pH and silica scaling control in geothermal field development. Geothermics, 12(4), pp.307-321.
Plume, R. W., 1984, Ground-water conditions in Las Vegas Valley, Clark County, Nevada Part I. Hydrogeologic framework: U.S. Geological Survey Open-File Report 84-130, 25 p.